NBSIR 76-1101 (R)

E-(49-1)-3800-4
District Category UC-90g

DEVELOPMENT, TESTING AND EVALUATION OF MHD-MATERIALS

Quarterly Report

for the period April - June 1976

H. P. R. Frederikse, T. Negas and S. J. Schneider

Inorganic Materials Division
Institute for Materials Research
National Bureau of Standards
Washington, D. C. 20234

Date Published: June 30, 1976

PREPARED FOR THE UNITED STATES
ENERGY RESEARCH AND DEVELOPMENT ADMINISTRATION
Under Contract No. E(49-1)-3800

AUTHENTICATED
U.S. GOVERNMENT
INFORMATION
GPO

ABSTRACT

In February, ERDA requested NBS to assist in the analysis and evaluation of channel wall materials after a 95 hour test of the AVCO Mark VI, C-channel. During this quarter, therefore, activities were focused on this task. All work was completed, a report was presented at the 15th MHD Symposium, Philadelphia, PA and a summary report will be transmitted to ERDA.

The Final Report for the Phase I, U-02 test will be completed upon receipt of translated Soviet contributions.

The viscosity of slag from "standard coals" (Illinois #6 and Rosebud) was measured and electrical conductivity measurements are in progress. Based on encouraging electrical and chemical data, an iron-containing, $MgAl_2O_4$ spinel solid-solution served as the basis for the development of several electrode module designs. This material will be tested during U-02, Phase II and in the ANL, U-25 materials screening program.

More recent data suggest that measured potassium pressures over silicate solutions depend on Knudsen effusion hole size and, hence, previous estimates of K_2O solubility in a slag are probably too high.

ZrO_2-based materials containing rare earth oxides from La to Tb readily react with K_2O. ZrO_2/Y_2O_3 materials are more resistant to attack by seed.

A scanning electron microscope-energy dispersive x-ray analyzer facility was installed and is operational for future analysis of materials.

Diffusion couple experiments were conducted to determine optimum methods for data collection and theoretical work is in progress to elucidate diffusion processes in MHD electrode systems.

As part of a continuing program, additional thermophysical/chemical data for alloys were compiled. Based on these properties, together with environmentally imposed MHD requirements and cost estimates, the selection of metals for steam plant components can be facilitated.

Objectives and Scope of Work

The overall objectives of this program are to obtain chemical and physical definition of high temperature materials which have shown promise for use in coal-fired open-cycle MHD power systems. Major problem areas in which investigations will be concentrated are:

1. Characterization of coal slag and its effects on system components and performance at prototype temperatures.

2. Development of electrode materials which provide adequate performance over extended periods of time.

3. Insulating materials which limit thermal losses and are resistant to prolonged thermal and erosion effects.

4. Preheater materials which can withstand the operating modes of separately and directly fired operation.

5. Seed recovery methods from slag which are technically and economically feasible.

6. Phase equilibria and diffusion rates of seed in slag and the corrosive action of combination on system components and materials.

7. Durability of prototype MHD sub-systems.

The program is designed to contribute to the solution of these problems by providing much needed data on candidate materials and by evaluating test samples and structures that have been subjected to real or simulated MHD conditions. The activities are grouped under six tasks:

G. Program Management Coordination (Assisting ERDA in coordination, planning and review of the various MHD-Materials Development Programs).

H. U-02 Materials Testing and Characterization (Coordination of U-02 Test Activities, Phase I).

I. Operational Design Properties (viscosity, electrical conductivity, vaporization).

J. Corrosion by Seed and Slag (phase equilibria, diffusion).

K. Materials Testing and Characterization (test coordination, pre- and post-test analysis).

L. Assessment of Steam Plant Components (corrosion resistance of metals and alloys).

Summary

Task G. Program Management Coordination

- Conducted and participated in ERDA program review meetings and sessions devoted to Phases I, II and III of the U-02 and U-25 Bypass Materials Testing Programs.

Task H. U-02 Materials Testing and Characterization

- All work for this task is complete. A Final Report will be issued after contributions from the Soviet side are translated, received, and meshed with the U. S. input.

Task I. Operational Design Properties

a. Viscosity of Coal Slag

- Analysis of slag from "standard coals" was initied. Viscosity of a synthetic slag simulating Illinois #6 coal slag was measured.

- Viscosity of a bottom-ash from a power plant using "Rosebud" coal was measured and compared with the synthetic variant. The real slag has a viscosity one order of magnitude higher than the synthetic suggesting a considerable difference in bulk composition. This will be resolved by chemical analysis.

b. Electrical Conductivity

- A detailed investigation of the electrical conductivity of the candidate electrode material, $3MgAl_2O_4:Fe_3O_4$ (spinel solid-solution) was completed. This material has a melting point near 1860 °C and could operate within the 500-1700 °C range.

c. Vaporization

- Mass spectrometric-Knudsen effusion measurements of the potassium pressure over simple and complex silicate solutions were performed. Potassium pressures over K_2O/SiO_2 solutions were found to depend on effusion hole size suggesting that equilibrium concentration of K_2O in slag will be lower than previously estimated.

Task J. Corrosion, Processes, Seed-Slag Interaction, Diffusion

- A scanning electron microscope-energy dispersive x-ray analyzer system was installed and is to be utilized for work pertinent to this task and, particularly, to Task K and related materials testing programs.

- Data collection and measurement techniques necessary to determine diffusion coefficients from diffusion couples were developed and will be refined.

- Matrix and diffusion of probability techniques are being used to calculate diffusion parameters for MHD materials. Analysis of perturbation effects from temperature and electric field gradients permits results to be related to diffusion processes in MHD electrode systems.

- Completed a study of subsolidus phase relations in the K_2O-Al_2O_3-SiO_2 system and initiated a study of the K_2O-iron oxide-SiO_2 system.

Task K. Materials Testing and Coordination

- An electrode system utilizing an iron-containing, $MgAl_2O_4$ spinel solid solution, flame sprayed onto a wire alloy mesh was designed. After fabrication this module will be tested during the ANL U-25 electrode screening program. This spinel system but with different design, fabricated by Battelle-Northwest and Westinghouse, also will be tested during Phase II, U-02.

- Completed a comprehensive analysis of AVCO Mark VI, C-channel electrodes operated for 95 hours.

- Analyzed by x-ray diffraction several preheater ceramics tested at FluiDyne Corporation.

Task L. Assessment of Steam Plant Components

- Environment conditions (and hence performance requirements) for components "below" the preheater (and seed condensor) are constantly updated and modified.

- Reports are being analyzed dealing with the potassium (or sodium) corrosion and oxidation resistance of various alloys (stainless steel, Inconel, Hastelloys, etc) in the range 870 - 1000 °C.

NBS Papers and Reports on MHD, April - June 1976

Inorganic Materials Division

Title	Expected Date of Report or Publication
1(a) Final Report U-02 Test (Phase I) W. R. Hosler, editor with contributions from Battelle NW, Westinghouse, and NBS.	Completed draft to Steering Committee, June 1976 (USSR contributions received for translation).
(b) Joint Test of the Electrode System in USSR U-02 Facility, W. D. Jackson, S. J. Schneider, W. E. Young, A. E. Sheindlin, G. P. Telegin, D. K. Burenkov.	15th MHD Symposium, Philadelphia, Pa. May 28, 1976.
(c) Investigations of the Thermophysical Properties of High Temperature Materials for MHD Generator Channel, G. P. Telegin, S. J. Schneider, et al. (et al. not given).	5th European Conf. on the Thermophysical Properties of Materials at High Temperature, Moscow, 5/18/76
2. Chemical Aspects of Materials Containing Cerium Oxide, T. Negas, R. S. Roth, H. S. Parker, C. L. McDaniel and C. D. Olson (preprint available).	Moscow Conference (see above), 5/18/76
3. Spinels for MHD Electrodes, H. P. R. Frederikse, W. R. Hosler, A. J. Armstrong, T. Negas	15th MHD Symposium, Philadelphia, Pa. May 24, 1976.
4. Crystallization and Vaporization Studies of Synthetic Coal Slag Compositions, L. P. Cook, E. R. Plante, T. Negas, R. S. Roth, C. D. Olson	15th MHD Symposium, Philadelphia, Pa. May 24, 1976.
5. Influence of K_2O on the Cerium Oxide-ZrO_2 system, T. Negas, R. S. Roth, C. L. McDaniel, C. D. Olson (preprint available).	12th Rare Earth Research Conf., Vail, Colorado, 7/18/76
6. Oxidation-Reduction Reactions of $CeMO_{4+x}$ (M=Ta or Nb) Phases, T. Negas, R. S. Roth, H. S. Parker, C. L. McDaniel, C. D. Olson (preprint available).	12th Rare Earth Research Conference, Vail, Colo., 7/18/76.
7. Analysis of AVCO Mark VI C Channel Electrodes After Long Duration Test, W. R. Hosler, T. Negas, S. W. Petty	15th MHD Symposium, Philadelphia, PA May 24, 1976.
8. Materials for Open Cycle MHD, Div. 11 of the US-USSR Status Report on MHD Power Generation, S. J. Schneider, H.P.R. Frederikse, T. Negas (ed. M. Petrick, Argonne National Lab.).	1st draft submitted to Steering Comm. June 1976. USSR contributions received for translation.
9. The System K_2O-Al_2O_3-SiO_2. Part 1. Crystal Chemistry of Phases on the $KAlSiO_4$-$KAlO_2$ Join, L. P. Cook, R. S. Roth, H. S. Parker, T. Negas (preprint available).	Submitted to American Mineralogist, May 1976.

Milestones - April - June 1976

Listed below are recent accomplishments based on the projected milestones of the ERDA-NBS MHD contract. It should be recognized that our work scheduling is strongly influenced by the needs of ERDA and associated contractors. For example, programs such as U-02 Phase I and AVCO Mark VI, C-channel, as well as the forthcoming ANL, U-25 Screening Test and U-02, Phase II, require a continuing shift of the duties of our limited staff. Hence, some milestones will change while others will be subordinated to more urgent work.

4(a). Measured the viscosity of "standard" slag from a midwestern and western coal.

11a. Completed an investigation of a portion of the K_2O-Al_2O_3-SiO_2 system.

b. Extended the study of this system by adding CaO.

c. Measured potassium pressures over multicomponent synthetic slags containing the oxides above.

19. Measured the electrical conductivity of promising (new) electrode materials (spinels).

28. Assembled and put into operation a scanning electron microscope-energy dispersive x-ray analyzer system for measuring diffusion and penetration of seed/slag into MHD-components.

39,40. Completed an analysis of AVCO
a) Mark VI C-channel electrodes.
b) U-02 Materials Testing and Characterization, Phase I, is complete.
c) Completed U-02, Phase I Report except for Soviet contributions to be translated.

41. Compiled and analyzed (from data and experience of MHD facility operators) the range of environmental conditions under which steam plant components operate. This analysis will be continually updated as new information becomes available.

42. Assessment of the corrosive attack by potassium compounds in the flue gas and general guidelines for the initial selection of promising alloys resistant to this type of attack has been carried out by making use of Na_2SO_4 data from marine gas turbine research as a best approximation to supplement the relatively little data available on K_2SO_4 and K_2CO_3 attack.

43a. A compilation of data on promising steam superheater tube alloys is well underway.

45a. Reasons have been given for recommending that hot corrosion experimental data be obtained on certain of these alloys under conditions more closely approximating the actual superheater tube environment.

Task G. Program Management Coordination

U.S. - U.S.S.R. Materials Program Activities

S. J. Schneider, (NBS-) ERDA Materials Coordinator participated in several (AVCO, MIT, FluiDyne) program review meetings as well as meetings related to the US-USSR cooperative program on Materials Testing and the ANL, U-25 Materials Screening Test.

On April 14 a meeting of the Materials Working Group, including representatives from ERDA, NBS, Westinghouse, UTSI and Battelle Northwest was held at NBS. Discussions involving materials selection, fabrication and overall design of the module for the Phase II, U-02 test were conducted.

The US-USSR MHD Steering Committee met in Washington, June 7-8. S. J. Schneider participated in discussions leading to tentative plans for the U-02, Phase II and U-25 Bypass testing of materials. Present scheduling suggests that the Westinghouse U-02 Phase II module will be delivered to Moscow, August 10 followed by a test sometime between Sept. 15-25. Phase III testing will be conducted using a U-25-Bypass-dropout section sometime during early 1978. USSR contributions to the Division 11 Materials Status Report and to the U-02 Phase I Report were received during this meeting.

T. Negas, with Dr. B. Rossing (Westinghouse) and Dr. D.P.R. Hasselman (Montana Energy and MHD Res. and Dev. Inst.) attended meetings in Moscow, May 18-22, for discussions concerned with U-02 Phase II testing, U-02 Phase I Final Report, Materials Status Report, and Soviet testing in US facilities.

Task H. U-02 Materials Testing and Characterization (Phase I) (W. R. Hosler)

Pre- and post-test materials analysis and characterization for the U-02 Phase I test have been completed. The Final Report awaits translation of Soviet contributions which, finally, were received June 4. Translation is in progress and the Final Report should be completed by late July 1976. Reproducible copies will be transmitted to ERDA for approval and distribution. A paper was presented at the 15th MHD Symposium, Philadelphia, May 24-25, 1976. This paper, "Joint Test of a U.S. Electrode System in the USSR U-02 Facility", is included in Appendix I of this report. We are grateful for the cooperation, effort, and technical contributions made by personnel from Westinghouse Corp. and Battelle NW for the Final Report, U-02, Phase I test.

This task is considered complete and will be terminated as of June 30, 1976.

Task I. OPERATIONAL DESIGN PROPERTIES

a. VISCOSITY OF COAL SLAGS (W. Capps and D. A. Kauffman, Inorganic Glass Sec.)

Introduction

It has been requested that NBS characterize the slags from the several coals adopted as "standard" coals for forthcoming MHD tests. These coals include Montana Rosebud and Illinois #6. The coals to be used in the joint US-Soviet tests will be American coals that resemble those of special interest to the Soviets. The Soviet coals are Krushnitz and a Siberian coal. The Montana Rosebud coal apparently resembles the Siberian coal closely enough to be used as their "standard". The Krushnitz coal counterpart is not yet known. In comparing the ash analysis for the Krushnitz (according to Dr. Crawford of UTSI) with those in Selvig and Gibson, it appears that there are similar coals from Pennsylvania, Kentucky, Alabama, Illinois, and New Mexico. The proposed characterization consists of 1) the estimation of expected slag compositions in the several parts of an MHD-system based on expected conditions of temperature, etc., 2) the determination of viscosity-temperature relationships of real slags and of synthetic slags of expected compositions, and 3) the determination of the electrical conductivity of these slags.

Slag Preparation and Measurement

Progress to date consists of the following:

1) A bottom-ash sample from a Montana power plant from Montana Rosebud coal was obtained and its viscosity was determined. A piece of this remelted slag was annealed and is being used for conductivity measurements.

2) A synthetic slag was prepared having a composition similar to that of Montana Rosebud given in ECAS Specifications from a NASA study. The viscosity of the melt from the coal ash was an order of magnitude higher than the synthetic slag. The reported analysis of that coal was probably determined under conditions that retained the sulfur. The analysis showed extremely high sulfur content (26.2%). It is possible that the bottom ash did not have such a high sulfur content and that much of the sulfur went up the power plant stack as gases or as flyash. Both the real and the synthetic slags will be analyzed for sulfur.

3) To test this theory, a second synthetic slag was prepared identical to the first but sulfur was omitted. The viscosity was also very low and not too different from the sulfur-bearing counterpart. Sulfur retention may be a critical factor and must be examined by analysis of specimens after viscosity determination.

4) A synthetic slag representing Illinois #6 coal, as given in the ECAS Specs., was prepared and its viscosity was determined. No real Illinois #6 slag has been obtained but is expected from PERC.

Viscosity-temperature curves will be given in the next report when chemical analyses of the samples have been completed.

PLANS

1. Prepare synthetic Krushnitz coal slag and determine viscosity--furnish specimen for conductivity measurement.

2. Have chemical analyses made to determine if real and synthetic slags resemble the analyses in the ECAS Specifications.

3. Obtain and measure viscosity of Illinois #6 slag and compare with synthetic model slag.

b. ELECTRICAL CONDUCTIVITY (W. R. Hosler, A. J. Armstrong, H.P.R. Frederikse)

During this reporting period, a detailed study of the electrical conductivity of a sintered, high density spinel of composition 75 mole percent $MgAl_2O_4$ plus 25 mole percent Fe_3O_4 was conducted; the electrical conductivity of this material was measured from room temperature to 2001 K under three oxygen partial pressures. The electrical conductivity was found to be 3.24×10^{-5} $ohm^{-1}cm^{-1}$ at room temperature and 2.80×10^{-3} $ohm^{-1}cm^{-1}$ at 186 °C (the maximum temperature for use of copper in air). The electrical conductivity at several O_2 pressures from 769 K to 2001 K is shown in Figure 1. As the iron component in this spinel may undergo oxidation at temperatures near 1200 °C (and below) in an oxidizing atmosphere (air), we conducted a long term experiment to explore this possibility. A sample was heated at 1200 °C in air for 117 hours while the electrical conductivity was monitored continuously. Only a small decrease (1%) in the electrical conductivity was observed during this time. Subsequent examination indicated damage to the platinum electrodes but no physical damage to the sample. Under these conditions it appears that the dense ceramic spinel retains adequate electrical conductivity for use as an electrode material.

A paper, "Spinels for MHD Electrodes", was presented at the 15th Symposium on Engineering Aspects of MHD (see Appendix I).

Samples of two slags from western and midwestern "standard" coals have been obtained and are being prepared for electrical conductivity measurements.

Samples of $3MgAl_2O_4/1Fe_3O_4$ spinel and a graded ceramic based on ZrO_2-ceria compositions, to be used in the U-02 Phase II test, will be investigated using the laser thermal gradient apparatus.

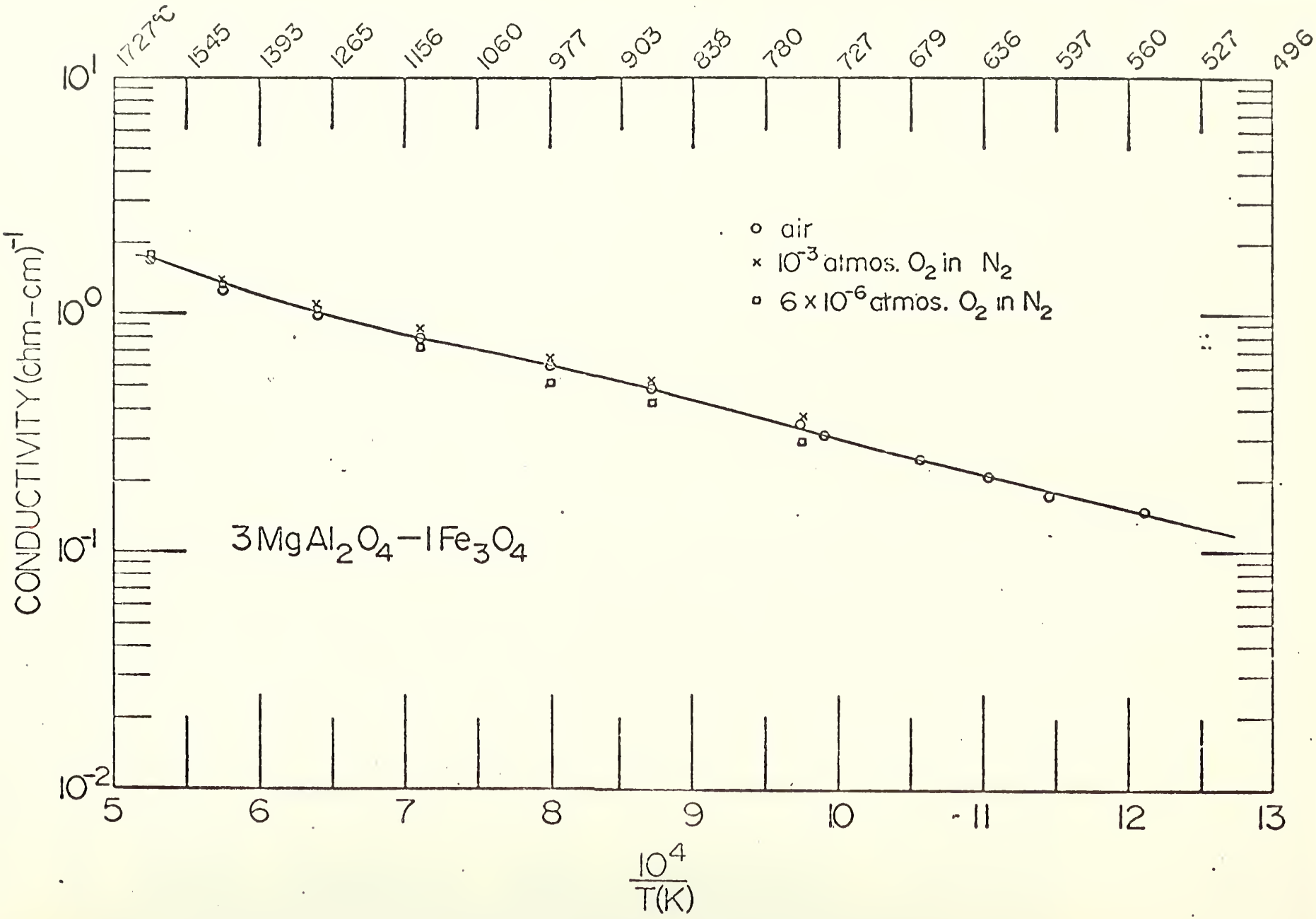

Figure 1. Electrical conductivity of sintered spinel electrode material at elevated temperatures and various oxygen partial pressures.

c. Vaporization Studies (E. R. Plante)

Vaporization studies during the last two quarters have involved measurements of the K(g) pressures produced by the reaction;

$$K_2O(\ell, \text{ dissolved in slag or } SiO_2) = 2K(g) + 1/2O_2(g).$$

Pertinent data, results, and conclusions from studies of two synthetic slag samples were given in a paper by Cook, Plante, Negas, Roth and Olson at the 15th MHD Symposium in Philadelphia (May 24-26, 1976)[1]. A copy of this paper is appended to the present report so that only a summary of these studies is needed here.

Briefly, mass spectrometric-Knudsen effusion measurements were made using Knudsen cells having nominal .5 mm diameter orifices. Use of small effusion holes has the effect of decreasing the sensitivity of the mass spectrometer so that measurements in the liquid range of the slags could be made. The conclusions were that the K(g) pressures over the slags at a fixed wt % K_2O and temperature were significantly higher over the synthetic slags than over solutions containing just SiO_2 and K_2O obtained from previous NBS data[2].

This conclusion would be consistent if the addition of other slag components such as Al_2O_3, CaO, MgO, and Fe_3O_4 had a tendency to destabilize the K_2O-SiO_2 solutions. However, this result would also be possible if the measured pressures depended on the orifice size (1 mm diam.) of the Knudsen cell in the K_2O-SiO_2 solution studies.

To check on this possibility, mass spectrometric Knudsen effusion studies were made on a sample of K_2O-$SiO_2(\ell)$ contained in a Knudsen cell having a .5 mm diameter orifice. The results show that the K(g) pressures are significantly higher than those previously measured using a 1 mm diameter orifice. As an additional check on the influence of the size of the effusion hole on the apparent K(g) pressure, measurements of a K_2O-SiO_2 solution are being made using a 1 mm diameter effusion hole. Initial results confirm that there is an important hole size effect. In addition, the mass spectrometer results show satisfactory agreement at 40 wt % K_2O with previous NBS results.

Two important conclusions can be drawn from these results. First, the thermodynamic estimate for the equilibrium concentration of K_2O in slag is roughly a factor of two too high. Secondly, the failure to achieve equilibrium under relatively ideal Knudsen cell conditions with a sample area/escape area ratio of about 60 can probably be taken as fairly strong evidence that the equilibrium concentration of K_2O in slag will not be attained except possibly for slag which has a long life on the channel walls.

Future Work

Vaporization measurements on selected slags will be continued to determine the effects of various components on the activity of K_2O. Analysis of current data for use in engineering calculations will be attempted.

References

1. L. P. Cook, E. R. Plante, T. Negas, R. S. Roth and C. D. Olson, Crystallization and Vaporization Studies on Synthetic Coal Slag Compositions, 15th MHD Symposium, Philadelphia, Pa., May, 1976.

2. E. R. Plante, C. D. Olson and T. Negas, Sixth International Conference on Magnetohydrodynamic Electrical Power Generation II, 211.

Task J. CORROSION PROCESSES, SEED-SLAG INTERACTION, DIFFUSION

a. Seed-Slag Interaction (L. P. Cook)

An investigation of subsolidus phase relations for a portion of the K_2O-Al_2O_3-SiO_2 system was completed and a paper, "The System K_2O-Al_2O_3-SiO_2. Part I. Crystal Chemistry of Phases on the $KAlSiO_4$-$KAlO_2$ Join", was submitted to the American Mineralogist. Due to the length of this paper only an abstract is included in Appendix I. However, preprints are available upon request. This paper presents a wealth of information for materials specialists involved in slag-seed characterization studies or in thermodynamic calculations of slag/seed interactions. The K_2O-Al_2O_3-SiO_2 system is far more complex than that portrayed by equilibrium diagrams presently available.

In another paper, "Crystallization and Vaporization Studies of Synthetic Coal Slag Compositions" (Appendix I), it is demonstrated that high CaO contents in slag can lead to higher K_2O activity and, hence, less absorption of seed by slag.

Future work will concentrate on the effect of iron oxide on the K_2O-Al_2O_3-SiO_2 system.

b. Seed-Refractory Oxide Reactions (C. L. McDaniel)

Post-test analysis of U-02 Phase I, ZrO_2/cerium oxide electrode materials revealed substantial alteration via reaction with potassium, particularly at the cathode where cerium oxide was reduced during operation. The reactivity of other ZrO_2/rare earth oxide materials with K_2O, therefore, was investigated. All materials containing rare earth oxides from La to Tb readily react with K_2O to form identical corrosion products. ZrO_2/Y_2O_3 and, probably, HfO_2/Y_2O_3 materials are less susceptible to corrosion by K_2O.

c. Diffusion (E. N. Farabaugh, J. R. Manning)

1. Experimental Results

Further work on the diffusion of potassium into MHD materials has been accomplished. A major part of this effort has been in the area of data collection from diffused specimens. Primarily this work was done on an Al_2O_3 ceramic specimen diffused at 1400°C for 96 hours. It has been evident from work done that the simple technique of running a single line scan from either an electron probe or SEM across a ceramic specimen to determine a concentration profile does not give satisfactory results. The profiles obtained by this method are very irregular and do not yield a curve from which a diffusion coefficient can be determined. As the electron beam transverses the specimen in this method, it goes across flat areas and voids. When the electron beam is incident on a void, the proper signal will not get back to the detector. As the beam goes across the diffused area, many of these voids are transversed and the resulting profile is very irregular. In an attempt to produce a smoother curve a diffused specimen surface was polished with a succession of diamond grits down to 3 micron diamond. Again a line scan was run on a polished diffused surface but the resulting curve was still too irregular to allow any calculation of a diffusion coefficient. Next, it was decided to integrate for potassium over the area of a strip of the specimen parallel to the edge from which the potassium diffused. This was done by using an electron probe to raster along a strip approximately 10 microns by 2 mm. (The long dimension of the strip is parallel to the edge of the specimen.) The raster was then moved 100 microns in a direction normal to the edge and another strip was integrated over for potassium counts. This was done completely across the specimen from edge to edge. This data collection resulted in a much better concentration profile, from which one could make an estimate of a diffusion coefficient of the order of 10^{-9} to 10^{-10} cm^2/sec. Since there are not enough data points in the present profile, data will need to be collected in perhaps 20 micron steps rather than 100 micron steps in order to give improved accuracy in the profile shape and obtain a more accurate value of the diffusion coefficient.

In addition to the measurements described above, which were done with an electron probe, our new SEM also was used with its EDX accessory utilizing a rectangular 10×300 micron partial field to measure concentration profiles. A similar technique of stepping across the specimen was used and collection of data representative of a strip of diffused material parallel to an edge was taken at intervals of 100 microns. This data was nearly the same as that obtained by the electron probe on the same material, Al_2O_3 ceramic diffused 96 hours at 1400°C. Then to get a better defined curve, a second traverse was made with data being collected every 10 microns. However, this time instead of a strip, a 10 micron square area was integrated over in several places in the 10 micron×300 micron strip. The areas selected for data collection were those areas in the strip which were either free from voids, or at least had a very small part

of its area occupied by voids. This did not yield a greatly improved profile shape. Irregularities still occurred. Thus, one is led to believe that both voids and non-uniform diffusion of potassium in the ceramic contribute to the sometimes irregularly shaped profile. It appears that the technique of integrating over as long a strip as possible parallel to an edge must be the approach to use if we are to obtain usable concentration profiles. These data collection techniques are currently being worked on, and it is felt that most of the diffusion data can be collected using the new SEM facility with only a minimal reliance on electron probe analysis.

Other diffusion couples have been made. One of the couples was made up of single crystal Al_2O_3 embedded in β-Al_2O_3 powder. The single crystal specimen was rectangular in shape with the edges parallel to $[000\underline{1}]$, $[10\bar{1}0]$ and $[11\bar{2}0]$. Thus proper sectioning of the diffused specimen has yielded samples for which diffusion profiles in the three crystallographic directions can be determined. This couple was heated at 1400°C for 96 hours. This was done so we can compare the results of the single crystal diffusion with diffusion into Al_2O_3 ceramic for which we have our best data and profiles. Although it is recognized that single crystal Al_2O_3 plays no active role in MHD applications, diffusion data on it will give us a base line to work from. These single crystal samples are currently being examined, and we have no data on them yet.

An MgO ceramic diffusion couple, heated at 1400°C for 24 hours was analyzed with the SEM. Just as was the case with the Al_2O_3 ceramic run at 1400°C for 24 hours, only small concentrations of potassium could be found in the specimen and no profile could be determined. The question arises if during the run the potassium in the β-Al_2O_3 pellet was depleted. As a check on this problem, powder from the β-Al_2O_3 pellets on this and subsequent couples which was next to the host material was removed from the pellet. Care was taken that only material which was in contact with some part of the specimen was removed. An x-ray powder pattern was taken of the material showed only the β-Al_2O_3 lines, no Al_2O_3 lines at all. This indicates no significant depletion of the potassium in the β-Al_2O_3.

In the next quarter we plan to further refine our data collection technique, study diffusion in more dense Al_2O_3 ceramic, obtain data on single crystal Al_2O_3, and measure a concentration profile from which a reliable diffusion coefficient can be determined.

2. Theory

Diffusion in MHD channel wall materials, particularly in the electrodes, will be affected by the electric fields and temperature gradients present. It has been shown in previous work at the National Bureau of Standards that an important kinetic force which influences diffusion in such fields and gradients is the vacancy wind force, which arises whenever there is a net vacancy flux. One quantity which must be known to calculate the magnitude of the vacancy wind force is the effective return frequency H of vacancies to the various migrating atoms. Values of this quantity are being calculated for MHD materials.

The frequency H is related to the correlation factor f for diffusion in the absence of driving forces; and the equation $f = H/(2w_2+H)$, where w_2 is the jump frequency for exchange of the particular migrating atom with a neighboring vacancy, can be used to help determine H. Here f is a measure of deviations from random walk diffusion behavior. The kinetic calculation of f in the absence of electric fields and temperature gradients is much simpler than a calculation with one of these driving forces present. Also studies at NBS have shown that f itself is unaffected by driving forces, even though the various components of H are subject to change from these forces. Thus, in the present calculations, it is planned first to calculate H in the absence of driving forces and then to determine the linear perturbations to this result introduced by the electric fields and temperature gradients.

With this approach in mind, various methods of calculating f and hence H in situations which may arise in MHD electrodes have been investigated. In particular, it was concluded that the comparison made between correlation factor calculations for metal alloys and various defects in metals [J. R. Manning, Comparison of Matrix Inversion, Monte Carlo, and Diffusion of Probability Techniques for Calculation of Diffusion Correlation Factors, Proceedings of Conference on Computer Simulation for Materials Applications, Gaithersburg, Md., April 1976, pp. 109-120, Nuclear Metallurgy, Vol. 20] should apply equally well to most systems proposed for use as MHD electrodes, including spinel structure materials (hercynite, magnetite, $MgAl_2O_4$) and fluorite structure materials (CeO_2, stabilized zirconia). It appears that matrix techniques and diffusion of probability techniques can be used with confidence for kinetic calculations of f and H in these materials. Consequently, these techniques are being used for the present calculations. An analysis of perturbation effects from temperature gradients and electric fields then will allow these results to be related to diffusion processes in MHD electrodes.

The diffusion flux J in the x-direction in both electric fields and temperature gradients can be represented by the equation

$$J = -D^* (\partial c/\partial x) + cFD^*/kT$$

where D^* is the tracer diffusion coefficient of the diffusing species, c its concentration, F the driving force from electric fields and temperature gradients, k Boltzmann's constant and T the absolute temperature. In the linear perturbation region, the forces qE from an electric field E and $Q^* \partial \ln T/\partial x$ from a temperature gradient add linearly to the vacancy wind force to yield the net driving force F. Here the effective charge q and the effective heat of transport Q^* are parallel quantities, both being properties of the diffusing ions and the materials they diffuse in, whereas E and $\partial \ln T/\partial x$ are properties of the MHD environment. Thus, q and Q^* are directly dependent on the particular electrode materials chosen, as also is D^*, and these are the key kinetic quantities that will differ from one electrode material to another. Kinetic expressions are being developed for these quantities, starting with calculations of f and H as mentioned above.

Even in originally homogeneous electrodes the cF term creates a diffusion flux which can cause significant changes in the oxygen and metal ion distributions and lead to degradation and failure of electrodes. In graded electrodes where an original concentration gradient is introduced to provide uniform conductivity in a temperature gradient, diffusion effects may make the concentration gradient difficult to maintain. Both the $\partial c/\partial x$ and cF terms can contribute greatly to the diffusion flux in graded electrodes.

Similarities and differences between the diffusion effects from electric fields and temperature gradients as described above were discussed in a talk on "Diffusion in Temperature Gradients and Electric Fields" presented by J. R. Manning as part of the Symposium on Control and Utilization of Defects in Non-Metallic Solids at the Spring 1976 Meeting of the Electrochemical Society. Significant differences can arise both from the non-uniform ion fluxes created by diffusion in a temperature gradient and from the possibility that vacancy concentrations may not be maintained at local equilibrium values during diffusion in a temperature gradient. Nevertheless, because of the similarities, the equations for the diffusion flux J as written above allow electric fields and temperature gradients to be treated in a nearly parallel fashion. Present indications are that these equations provide a good framework for the description of kinetic diffusion processes in MHD electrodes.

Task K. MATERIALS TESTING AND CHARACTERIZATION

a. Phase II, U-02

Plans previously formulated for Phase II, U-02 are being implemented. The test schedule was delayed (by mutual agreement, US/USSR), however, until September 15, 1976. The test also has been scheduled for 100 hours maximum instead of 100 hours minimum duration. Design considerations have not been changed and sample and module preparation by Westinghouse Research and Development Lab. are on schedule. Shipment of the module will be delayed until mid August 1976.

b. Phase III, U-02 Plans

According to the latest plans of the US-USSR-MHD Steering Committee, the Phase III, U-02 materials test will be shifted to a U-25 bypass drop-out section. A cooperative US/USSR effort is contemplated for the design of the electrode system(s). The test will be of 100 hour duration with maintenance (replenishment) and is scheduled, tentatively, for early 1978. At this time, absolutely nothing is known about pertinent engineering parameters and, hence, planning activities cannot be initiated or implemented.

c. Post-test Analysis of AVCO MHD electrodes (W. R. Hosler, T. Negas)

The analysis of the AVCO Mark VI, C-channel electrodes was completed according to the general plan established in the last Quarterly Report. The analysis was based primarily on results from scanning electron microscope involving microprobe and EDAX analysis and elemental x-ray mapping of specific areas as well as x-ray diffraction measurements to determine crystalline phases present. Chemical analyses of pre- and post-test materials also were made as needed. A paper, "Analysis of AVCO Mark VI-C-Channel Electrodes After Long Duration Test", was presented at the 15th Symposium on Engineering Aspects of MHD in Philadelphia, PA (May 24, 1976) and is included in this report in Appendix I. Results will also be published in the near future in the Bulletin of the American Ceramic Society. The numerous photographs in this paper make reproduction (~60 copies) difficult and costly. Original reprints, however, are available on request.

d. ANL U-25 Materials Screening Tests (W. R. Hosler)

The electrode material to be used in fabrication of the US built U-25 channel has not been selected. Argonne National Laboratory is conducting at the Reynolds Facility a screening test directed toward the selection of a suitable material. Electrode systems submitted by a number of organizations will be tested according to a predetermined test schedule and conditions.

It is the responsibility, as designated by ERDA, for NBS to perform post-test analysis on these electrode systems. Results of the analyses are to be reported within 2 to 3 weeks after the samples are received at NBS. As this is a stringent time requirement for a thorough analysis, a special NBS team of specialists has been designated to perform this task as their primary function when the systems are received. Electrode systems will be analyzed using x-ray diffraction, SEM, optical microscopy, and chemical analysis when appropriate. Each system will be handled on an individual basis depending on its condition upon arrival at NBS. After thorough discussions by the team members, procedures to obtain maximum results will be instigated. In addition, it is desirable for the most

meaningful analysis to have information about the electrode system construction and layout in the test chamber together with appropriate test infromation such as temperature at various points, times of different test conditions, unplanned excursions in test conditions or parameters etc. For these considerations, it is desirable to have a NBS team representative at the test to collect the information necessary for the analysis.

Testing was scheduled to begin about June 1. Unforseeable and unavoidable delays have caused a change in the schedule and NBS must be notified when the first test is to begin.

e. NBS Magnesia-Alumina-Iron Spinel Electrode Material (W. R. Hosler, T. Negas)

Spinel solid-solutions of the $MgAl_2O_4$-Fe_3O_4 system appear to be very attractive electrode module constituents. The electrical conductivity of a typical solid solution consisting of $3MgAl_2O_4/Fe_3O_4$ (see Task I) is excellent as the curve remains fairly flat with temperature and is nearly independent of oxygen pressure (see Figure 1). This particular spinel has adequate conductivity down to 500 °C and has a melting point near 1860 °C (reducing conditions) as reported by J. L. Bates, BNW Laboratory. Higher melting temperatures can be achieved by simply decreasing the iron oxide content of the spinel subjected to the highest temperatures (i.e., grading the material). Better electrical conductivity at lower temperatures can also be accomplished by grading the material toward higher iron oxide content. Indeed, one advantage of this material, is that grading laterally to a pure $MgAl_2O_4$ (or MgO plus $MgAl_2O_4$) spinel insulator is possible.

NBS does not have the facilities to fabricate complete electrode modules utilizing these spinels. However, much effort was devoted toward the development of methods and techniques to produce spinel powders which can be fabricated into dense, sintered ceramics or which can be utilized for flame or plasma spraying. This was accomplished through close cooperation and consultation with a firm independent of NBS.

By taking material properties into consideration (i.e., electrical and thermal conductivity, thermal expansion, adaptability for sintering or spraying, etc.) is is possible to suggest an electrode module design. Major problems, however, are not related directly to the material but to problems imposed by environmental parameters. For example, the large heat fluxes for the ANL U-25 Screening Test dictate electrodes having particularly small dimensions (thickness). Large temperature gradients and, therefore, large stresses over small dimensions, therefore, are unavoidable. Joining the thin, conducting ceramic to an effective leadout then becomes a formidable problem. One possible design based on an assumed wall heat flux of 100 W/cm^2, is illustrated in Figure 2. For the leadout, a mesh composed of sintered metal fibers is suggested for two reasons. Flame or plasma sprayed spinel forms a tenacious bond with the mesh which, in turn, helps relieve mechanical stresses created by large thermal gradients and the mismatch of the thermal expansion of the oxide and most metals.

This design (Figure 2) as well as others have been discussed with Argonne National Laboratory, AVCO MHD Lab., Westinghouse, and others. The spinel material will be tested in the U-02, Phase II program scheduled in Moscow

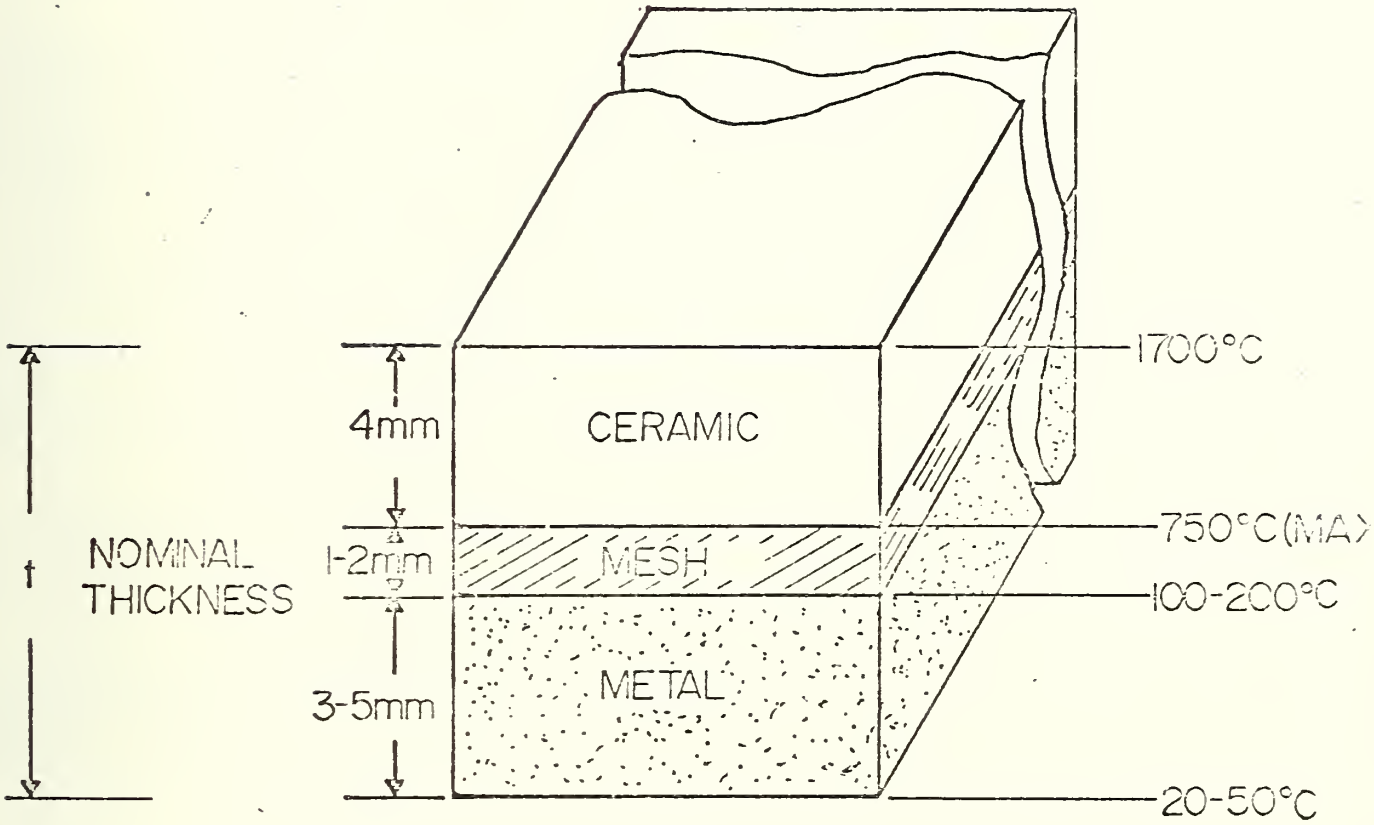

Figure 2. Schematic Design of MHD Electrode.

for September 1976. Fabrication of an electrode system based on Figure 2 is in progress and this module will be tested in the ANL U-25 Screening Tests. As indicated above, appropriate adjustments in composition can lead to higher (and lower) working temperatures and better insulation characteristics. These refinements must await future work.

f. X-ray Examination of Corhart X-317 Ceramics (magnesia spinels) Tested at Fluidyne Eng. Corp. (A. Perloff)

Preliminary SEM work by E. N. Farabaugh on the magnesia spinel ($MgO-MgAl_2O_4$) sample FN-27 done last quarter on the old unit and reconfirmed this quarter on the new SEM unit has shown the elemental composition of the surface material to be primarily Mg, Al, Si, K and Ca plus a small amount of Fe. The interior composition is primarily Mg and Al plus a small amount of Ca.

The X-ray examination of three similar specimens (FN-12, FN-17, FN-30) is in agreement with these findings inasmuch as all identifiable surface phases have been silicates of K, Al, Mg and Ca. The dark coloration of the surface is probably due primarily to the presence of Fe. No specific iron compound could be identified so it is likely that the iron exists in substitution for Ca or Mg (Fe^{+2}) and Al(Fe^{+3}).

The patterns of the internal material of all samples show essentially only MgO and $MgAl_2O_4$ (spinel) as would be expected.

Sample FN-30 (1600°K, 30 hrs.)

The powdered surface material yields a pattern containing moderate amounts of MgO and spinel. It probably, also, contains $Ca_3Mg(SiO_4)_2$ (merwinite) plus a number of other silicates. The most likely candidates include α-$K_2MgSi_3O_8$, K_2MgSiO_4 and $KAlSiO_4$.

Sample FN-17 (1700°K, 30 hrs.)

The powdered surface material pattern shows large amounts of MgO and spinel. The spinel probably exists in two compositions. Slight splitting of high angle lines suggests two spinels, in approximately equal amounts, whose cell sizes differ by $\sim$0.01A.

Many weaker lines are present in the pattern. Most of these lines can be approximately satisfied by assuming a mixture of $KAlSiO_4$, $CaMgSiO_4$ (monticellite), and $Al_6Si_2O_{13}$ (mullite). This identification must be considered only tentative in such a complex pattern.

Sample FN-12 (1800°K, 5 hrs.)

The powdered surface material pattern contains large amounts of MgO and two spinels. The spinel cell sizes differ by about $\sim$0.02A and there appear to be about equal amounts of each spinel.

The remaining weaker lines can be partially identified as probably containing $CaMgSiO_4$ (monticellite) but there still remain a number of weak lines for which no satisfactory identification has been found.

Two slag samples (FN-23 and FN-29) have, also, been examined by x-ray diffraction.

Sample FN-23 (Accumulation from slag tap)

This pattern contains MgO and spinel along with several other materials for which a completely satisfactory identification has not been made to date. Among the possible candidates are compounds resembling $NaAl_{11}O_{17}$ or $NaAl_7O_{11}$ or $KAl_{11}O_{17}$, $Ca_3Al_2O_6$ and assorted potassium aluminum silicates.

Sample FN-29 (Accumulated seed and slag)

This pattern contains a large amount of K_2SO_4, but no MgO or spinel. There are significant amounts of other phases present, but identification has been unsuccessful to date.

g. SEM Installation and Testing (L.P. Cook and E.N. Farabaugh)

A scanning electron microscope [SEM] equipped with energy dispersive x-ray analyzer was installed during this quarter. The instrument has been tested, the majority of specifications have been validated, and it will be accepted pending correction of problem areas by the manufacturer. This will constitute completion of a major milestone, it is hoped, before the end of the quarter. The instrument has been used for about three weeks during which time users have become familiar with its operation, capabilities and limitations. It is thought necessary to discuss briefly the SEM vacuum system, since an expenditure above the price of a conventional system was involved. The ion-pumped system has proved beneficial so far primarily in increased filament life and reduced aperture contamination at high beam currents. Use of the airlock provided has been found to be essential for routine work. This introduces some, but not serious, restrictions on the size of samples which can be exchanged routinely. With the airlock, sample exchange and pump down times at 10^{-6} torr operation are comparable to those for conventional oil-pumped systems, provided exceptionally gassy samples are not used. We have had no difficulty thus far in working with one-inch diameter epoxy-potted electrode specimens. It is expected that the principal value in the ion-pumped system, which has ultra-high vacuum capability of 10^{-9} torr, lies in the extension of the instrument to include certain techniques of surface microchemical examination, such as Auger analysis, windowless energy dispersive x-ray analysis, and secondary ion mass analysis employing a quadrupole mass spectrometer. These and other techniques have immediate application in the more detailed aspects of the MHD materials characterization program. Pending installation of any such accessory equipment as can be purchased it is hoped and expected that the instrument will fullfill all the functions of a conventional high-performance SEM, with the added advantages of an oil-free vacuum. The accompanying illustrations give examples of work done on the instrument during the "shake-down" period.

Figures 3a,b,c,d, and e shows SEM and x-ray map photographs of the border of an inconel cathode (rail-type electrode) run under slagging MHD conditions for ~100 hr in the AVCO facility (1). Segregations of the elements are apparent, and an interesting correlation is shown between Ca and Cr, both of which seem to be concentrated in a zone near the unaltered inconel. In detail, however, there is not a one-to-one correspondence, suggesting the existence of two Cr-rich phases, one without substantial Ca. Similarly an interesting gross correlation between K and Al within voids in the inconel exists - to what extent this has been influenced by the cutting and polishing process is uncertain. Fe and Ni appear to remain concentrated in the inconel despite Cr-depletion.

The new SEM facility was also used in collecting data for determination of potassium concentration profiles in various ceramic materials. Utilizing the EDX accessory and the partial field mode of operation x-ray analysis were made of various regions in the diffused specimen. In this investigation and

also in some limited investigations of a Cohart refractory, the x-ray analysis accessory has proven easy to use and yields reliable and reproducible results. The ability of moving the x-ray detector closer to the specimen by means of a telescoping adjustment provides the capability of obtaining purer spectra and higher counting rates.

Reference

1. W.R. Hosler, T. Negas, and S.W. Petty, 1976, Analysis of AVCO Mark VI C Channel Electrodes After Long Duration Test, Proceedings of the 15th Symposium on Engineering Aspects of Magnetohydrodynamics, Philadelphia.

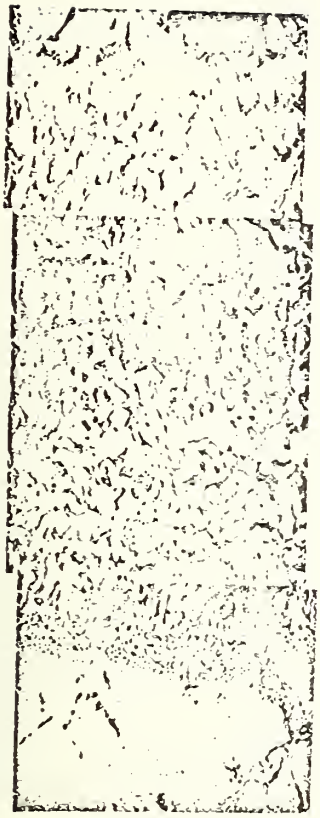

Figure 3a. SEM photograph of a portion of an inconel cathode electrode, rail-type, from AVCO test (see text). Lower part is inconel grading through altered inconel toward the upper part near the slag/metal interface.

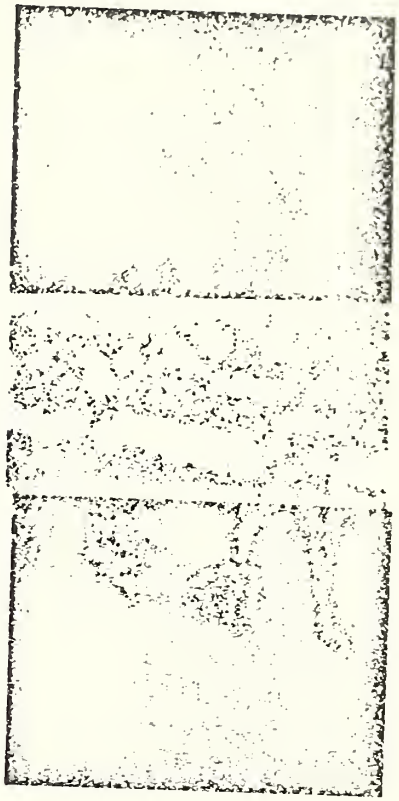

Figure 3b. X-ray map of area in Fig. 3a for Ca.

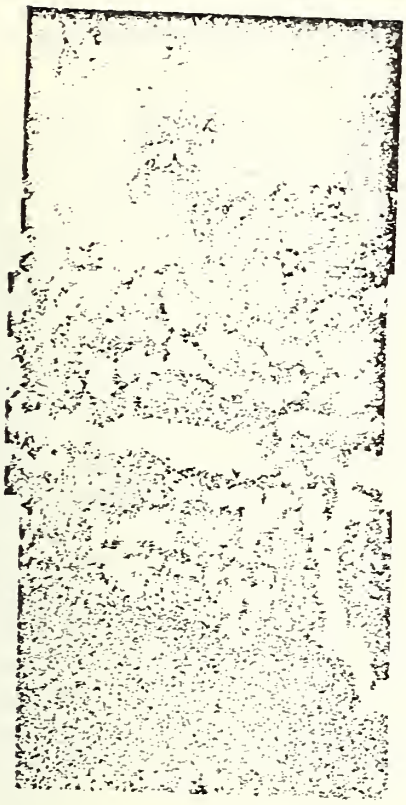

Figure 3c. X-ray map of area in Fig. 3a. for Cr.

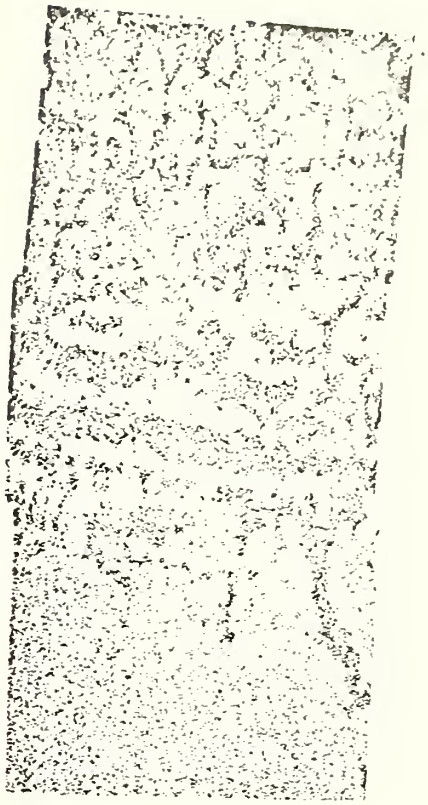

Figure 3d. X-ray map of area in Fig. 3a for Fe.

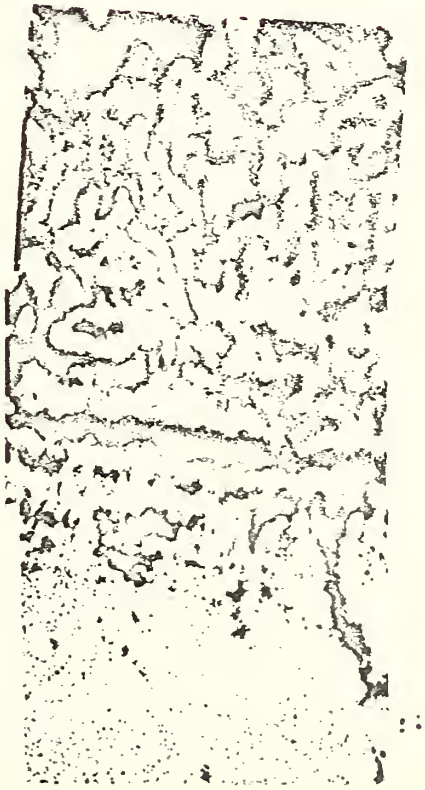

Figure 3e. X-ray map of area in Fig. 3a for Ni.

Task L. ASSESSMENT OF STEAM PLANT COMPONENTS (J. R. Cuthill)

This is the fourth quarterly report since the initiation of Task L as a three year program. The objective of Task L is the selection of commercially available alloys for critical components of the down stream steam plant, notably the boiler tubes and valve seats, after making a judgment as to the anticipated service as more detailed data are made available from computer model system studies, while simultaneously reviewing alloy properties.

In connection with the boiler tubes a principal concern has been the unknown severity of the hot corrosion problem (attack by the K_2SO_4, K_2CO_3, and KCl in the flue gas). With this phenomenon foremost in mind, property data have been collected on alloys that would be expected to exhibit good hot corrosion resistance. This list has again been updated from the previous quarterly report by the addition of Inconel 718 and which is expected to exhibit good hot corrosion resistance. See Tables 1, 2, and 3 which are compositions, mechanical and thermal properties, respectively. (Table 1a is the original table of alloy compositions of which Table 1 is a continuation, and is reproduced here from the second quarterly progress report for convenient reference). It should be noted that only wrought alloys have been tabulated thus far because, although there are many cast alloys on the market with excellent resistance to hot corrosion attack as a result of marine gas turbine research, there seems to be no application for cast components in boiler and hear exchangers subjec ted to the flue gas. (Cast alloys, IN 713C and W152 were included in the original alloy composition table because reference was made to them in a discussion of hot corrosion behavior in the second quarterly progress report). Some of the INCO alloys in that list are comparatively new alloys and Table 4 in this quarterly report gives some price information on them, obtained for us by James R. Hunt, INCO Washington District Manager. Although these alloys appear relatively expensive, superheater tube sections have been installed in commercial power plants, generally as a replacement for stainless steel tubing.

However, it may be that hot corrosion attack will not be the major problem - clogging of the boiler with huge deposits of K_2SO_4 and K_2CO_3, and serious reduction in heat transfer efficiency may be of primary importance. The anticipated amount of these deposits based on STD Corporation's state point calculations will be discussed below.

It appears quite obvious from the litter data on simulation of boiler tubes in downstream MHD steam plants that has been obtained so far, such as the Bruceton tests[1] and the British tests[2] that the low alloy steels commonly used for boiler tubes used in the past, will not hold up. On the other hand the service conditions are complex and the ultimate alloys in respect to hot corrosion resistance may not be needed, because hot corrosion attack is the most severe where the salt is molten on the surface of the metal and this does not appear to be the condition that will exist on the surface of the boiler tubes. Rather, it appears that the surface of the boiler tube will act as a chill surface which will condense out as solid mixtures of K_2SO_4, K_2CO_3, and KCl in varying proportions on the tube service. The deposit would continue to build up and the thermal conductivity through the deposit - covered tube wall will continue to drop until the temperature on the surface of the deposit increases to the melting point of the salts, at which point further

material condensing out as a liquid will sluff off and no further build up will occur. This anticipated behavior is based on calculated state point data from the STD Corp. For a 2000 MW plant the STD data shows 768.6 kg/sec. of flue gas entering the high pressure steam boiler at a temperature of 1445°K (see Fig. 4)*. If the steam temperature inside the boiler tube is in the 1000 to 1050°F range, the outside surface of the metal wall of the boiler tube will be at about 900°K. From the distribution of molecular species at 900°K in the flue gas predicated by the STD Corp. calculation it appears that virtually all of the potassium will precipitate out in the form of K_2SO_4, K_2CO_3 and KCl on the surface of the boiler tubes, with the initial rates of precipitation on the bare boiler tube as follows:

	ppt. during 1st hr.
5 Kg/sec. of K_2SO_4	18 metric tons
9.5 Kg/sec. of K_2CO_3	34 metric tons
0.2 Kg/sec. of KCl	0.8 metric tons

If in actual fact the only potassium salts in contact with the metal are well below their melting points the hot corrosion might not be as severe as it might otherwise be. It has even been reported that the oxidation of Cobalt and Co-Cr alloys is slower with a Na_2SO_4 coating than without[4]. Therefore it is imperative that simulated boiler tube testing be carried out on these new alloys where the flue gas composition, velocity, and temperature is controlled, such as the type of test carried out at Bruceton[5], to permit a determination of the lowest price alloy that will do the job. It is realized that these tests themselves are costly so therefore it would be prudent to do some preliminary screening by conducting "crucible" tests.

Some additional guide lines have been drawn from the recent hot corrosion research in the marine gas turbine area, involving Na_2SO_4. These guidelines are as follows:

1. Alloys that form only Al_2O_3 films for oxidation protection are highly susceptible to hot corrosion attack whereas alloys that form predominately a Cr_2O_3 film, show generally good hot corrosion resistance.

---

*These STD Corp. calculations are based on Montana Rosebud coal. Results of similar computer model calculations have been received from PERC (Bruceton, Pa) but they were carried out on the basis of upper Freeport Seam coal. Also, some preliminary calculations have been received from Argonne.

Recently, a more detailed Baseline system diagram has been presented[3] showing flue gas temperatures at corresponding points in the down stream steam plant that run somewhat higher than those in Figure 4, although the temperature in the combustor is virtually the same. However, with the high pressure steam still remaining in the 1000-1050 °F range the seed condensation problem would be expected to remain similar.

2. Alloys high in Mo that precipitate Mo carbides to impart strength are susceptible to hot corrosion pitting. Tungsten has a similar but less pronounced effect. (See previous quarterly report.)

3. Alloy additions of the rare earths, Y, and La, increase the stability of the protective film resisting hot corrosion attack.

There are other locations and components in the system that are not subject to hot corrosion, but simply to high temperature oxidation in air, such as air ducts in the air preheating system. As a guide to the selection of alloys for such applications, Table 5 is included which lists some representative construction alloys together with the temperature to which they are stated to be resistant to oxidation. In some cases there have been specific rulings under the ASME Boiler and Pressure Vessel Code on the maximum temperature at which the alloy can be used in such applications, and where available, these are given.

Future Plans

Continue compiling data on wrought alloys for heat exchange tubes, hot air ducts, etc. Begin compiling data on hard facing alloys that are hot corrosion resistant, for valve seats, etc., and continue to obtain data from the various MHD contractors to update the assessment of service conditions.

References

1. D. Bienstock, R. J. Demski, and R. C. Corey, Corrosion of Heat-Exchange Tubes in a Simulated Coal-Fired MHD System, J. Engineering for Power, 93 Series A, #2, 1971, pp. 249-256.

2. J. B. Heywood and G. J. Womack, eds., Open Cycle M.H.D. Power Generation, Pergamon Press, 1969, Chapter 10.

3. W. D. Jackson, R. V. Shanklin III, R. L. Lawit, R. A. Stoudt, M. G. Klett, S. T. Demetriades, J. C. Cutting, C. D. Maxwell, and R. F. Schnorr, Development of a Baseline Reference Design for an Open Cycle MHD Power Plant for Commercial Service, Proceedings of the 15th Symposium, Engineering Aspects of Magnetohydrodynamics, Philadelphia, Pa., May 24-26, 1976.

4. D. M. Johnson, D. P. Whittle and J. Stringer, Oxidation of Na_2SO_4-Coated Cobalt Base Alloys, Corrosion Science, 1975, Vol. 15, pp. 649 to 661.

Wrought Alloy Compositions (cont. from previous Quarterly Report)

Resists v. hi-temp oxidation

Resists molten sulphate

Mfgr. Desig.	Cr	Base Alloy Type: Ni	Co	Fe	Al	Carbide formers: Ti	Zr	Hf	V	Nb	Ta	Mo	W	Mn max	Si max	C	Other
INCO CLAD 671/800																	
Inconel 671	48	bal.	-	-	-	.35	-	-	-	-	-	-	-	-	-	.05	
Incoloy 800	21.	32.5	-	46.0	.38	.38	-	-	-	-	-	-	-	.75	.50	.05	.38 Cu,.008 S
Incoloy 800H	21.0	32.5	-	46.0	.38	.38	-	-	-	-	-	-	-	-	-	.06-.1	
Incoloy 802	21.0	32.5	-	46.0	-	-	-	-	-	-	-	-	-	-	-	.35	
Inconel 617	22.	54.	12.5	-	1.0	-	-	-	-	-	-	9.0	-	-	-	.07	
Haynes 188	20-24	20-24	bal.	3.0	-	-	-	-	-	-	-	-	13-16	1.25	.2-.5	.05-.15	.05 .15 La
Hastelloy X	20.5-23	bal.	.5-2.5	17-20	-	-	-	-	-	-	-	8-10	.2-1	1.0	1.0	.05-.15	.02 La,0.2 N
Inconel 718	17-19	50-55	1	bal.	.2-.8	.9	-	-	-	4.25 - 5.5		3	-	.35	.35	.08	.006B, .3Cu

Table 1a

Alloy Compositions

C = cast material
W = wrought material

Resists v. hi-temp oxidation

Resists molten sulphate

Base Alloy Type

Carbide formers

	UNS No.*	Mfgr. Desig.	Cr	Ni	Co	Fe	Al	Ti	Zr	Hf	V	Nb	Ta	Mo	W	Mn max	Si max	C	Other
		Haynes 25	19-21	9-11	bal.	3.0 max	-	-	-	-	-	-	-	-	14-16	1-2	1.0	0.1	
W	S31000	310 S.S.	24-26	19-22	-	bal.	-	-	-	-	-	-	-	-	-	2.0	1.5	.25 max	-
W	S31600	316 S.S.	16-18	10-14	-	bal.	-	-	-	-	-	-	-	-	-	2.0	1.0	.08 max	-
W	S44600	446 S.S.	23-27	--	-	bal.	-	-	-	-	-	-	-	-	-	1.5	1.0	.2 max	.25 max N
C	N07713	IN713C	12-14	bal.	-	2.5 max	5.5-6.5	.5-1.0	.05-.15	-	-	1.8-2.8	-	3.8-5.2	-	.25	0.5	.08.2	.005-.015B
W	N07500	U500	15-20	bal.	13-20	4.0 max	2.5-3.2	2.5-3.2	-	-	-	-	-	-	-	-	-	.15 max	.008 B
		FSX418	-	-	bal.	-	-	-	-	-	-	-	-	-		-			
C		W152	2.10	-	bal.	-	-	-	-	-	-	1.75 total		-	11.0	-	-	0.45	
W		INCO Clad 671/800H																	
W		Inconel 671	50	50	-														
W		Incalay 800	20	32	46														
W		Inconel 617																	

*The Unified Numbering System(11) is a consensus system of alloy idenification covering all commerically produced metal and alloys within the United States. The system was developed and is administered by a committee representing standards organizations, metal and alloy producers, and government agencies including the National Bureau of Standards. The Unified Numbering Systems provide a mean of correlating many and diverse nationally used numbering systems.

Alloy	100 hr rupture strength ksi	yield strength .2% offset, ksi	tensile strength ksi	Elastic modulus $x10^6$ psi	1000 hr Creep rate at 8 kips, % hr	Fatigue strength 10^8 cycles	Impact strength ft-lbs.	Resists oxidation in air up to	Comparative Cost(5)	Boiler Code max. allow stre
Haynes 25	18(1500 F)	34.5(1600 F)	46.6(1600 F)	26.3(1400 F)		12(1800 F) 30(1500 F)	120(1600 F)		$29.10	
INCO CLAD 671/800		69.3(R.T.)(3)	92.5(R.T.)(3)		0.0016(1600 F)					same as for Incoloy 80C
Inconel 671	28(1200°F)		125(R.T.)							
Incoloy 800		61.0(R.T.)	111.6(R.T.)				35(R.T.)	<1150°F(7)		6.6(1200°F)
Incoloy 802	13.9(1200°F)							1500°F(7)		
Incoloy 800H	13.3(1200°F)	14.5(1200°F)	49.7(1200 F)					1150°F(7)		8.4(1200°F)
Inconel 617	65(1200°F)	24.8(1200°F)	82.4(1200°F)				>120(R.T.)	2300°F(7)		12.5(1200°F)
Haynes 188	31(1400°F)	43.6(1200°F)	106(1200°F)		13,000(1400°F)		87(1300°F)(1) 126(1300°F)	2100°F	$27.75(est.)	
Hastelloy X	42(1200°F)	39.5(1200°F)	83(1200°F)		22,000(1200°F)(2)		29(1500°F)	2200°F [1650°F](4)	$16.75	
Inconel 718	85(1200°F)	154(1400°F)	185(1400°F)	24(1400°F)				1800°F		

+Property value corresponds to the temperature given in parenthesis. Haynes 25 data at 1500°F was chosen because the latter is concluded to be the max safe operating temperature for Haynes 25 under MHD conditions (Bureau of Mines, Bruceton). 1200°F approximate the outer wall temperature of the boiler tubes. Data at other temperatures are given when they represent either the only data or the nearest data available.

(1) 87 is transverse and 126 is longitudinal.
(2) psi for 1% elongation in 1000 hrs.
(3) after repeated exposure between 1000 and 1400 F.
(4) Temperature in square bracket is max. Boiler Code approved service temperature at which the alloy can be used.
(5) Price per ft. of welded tubing, 2"O.D x 0.12" wall thickness.
(6) 1000 hr value
(7) Temperature given by mfgr. for boiler tube type application.

Table 3

Thermal Properties

Alloy	Thermal Conductivity watt.cm/ cm^2°C	Thermal Conductivity BTU.in./ ft^2.hr.°F	Mean Coefficient of Thermal Expansion $x10^6$/°F
Haynes 25	.204(600°C)	142(1100°F)	8.2(70-1200°F) 9.4(70-1800°F)
304 S.S.		149(68-932°F)	11.0(68-1600°F)
310 S.S.		130(68-932°F) 99(212°F)	10.9(68-1832°F)
316 S.S.		113(212°F)	10.8(68-1832°F)
446 S.S.		171(68-932°F)	6.5(68-1472°F)
U500		135(1100°F)*	8.2(70-1200°F)
INCO CLAD 671/800H			
Inconel 671		109(70°F)	7.99(78-1200°F)
Incoloy 800H		146(1100°F)	9.6(70-1200°F)
Inconel 617		155(1100°F)	8.0(78-1200°F)
Incoloy 800		146(1100°F)	9.6(70-1200°F)
Haynes 188	.210(593°C)	146(1100°F)	8.6(70-1200°F)
Hastelloy X	.206(600°C)	144(1100°F)	8.6(79-1200°F)
Inconel X-750		138(1100°F)*	8.5(70-1200°F)
Incoloy 802		142(1100°F)	9.5(70-1200°F)

*Estimated from graph

Table 4

COLD DRAWN TUBING, PKL, ANN, RDM, 10,000# QUANTITIES

SIZE

Alloy	2.000" OD .125" AW	2.000" OD .250" AW	2.000" OD .375" AW	2.500" OD .125" AW	2.500" OD .250" AW	2.500" OD .375" AW	3.000" OD .125" AW	3.000" OD .250" AW	3.000" OD .375" AW
	$/Ft.	$/Ft.	$/Ft.	$/Ft.	$/Ft.	$/Ft.	$/Ft.	$/Ft.	$/Ft.
INCOCLAD 671/800H	25.26	42.87	59.71	31.99	55.11	78.08	38.73	67.36	96.45
INCONEL 617	27.03	50.01	69.31	34.40	63.73	89.31	41.20	77.28	109.22
INCOLOY 802	16.52	30.45	42.41	21.00	38.90	54.73	25.08	47.08	67.18
INCOLOY 800	8.18	15.08	21.00	10.40	19.26	27.10	12.42	23.31	33.26

DLH
3/29/76

Table 5

Some Representative Construction Alloys and their Reported Resistance to Oxidation in Air†

Alloy	Major Constituents††	Resistant to Oxidation up to, °F
Plain carbon steels		800 (1)
Low alloy steel		875 (1)
Type 406 S.S.	13 Cr, Fe-base	1400 (2)
" 446 "	26 Cr, Fe-base	1950 (3)
" 304 "	18 Cr, 8 Ni, Fe-base	1550 (4)
" 316 "*	17 Cr, 12 Ni, Fe-base	1500 (4)
" 310 "	25 Cr, 20 Ni, Fe-base	1900 (5)
Haynes 25	20 Cr, 10 Ni, 15W, Co-base	1900
Hastelloy X	22 Cr, 19 Fe, Ni-base	2000 1650 (6)
Haynes 188	22 Cr, 22 Ni, Co-base	2100
Haynes 556***	22 Cr, 20 Ni, 20 Co, Fe-base	2000
Inconel 600	15.5 Cr, 8 Fe, Ni-base	2150
Inconel 601**	23 Cr, 14 Fe, Ni-base	2300
Inconel X750* (formerly designated: Inconel X)	16 Cr, 7 Fe, Ni-base	2000
Inconel 718*	48 Cr, 18 Fe, Ni-base	1800
Incoloy 800A	21 Cr, 32.5 Ni, Fe-base	1150 (7)
Incoloy 617	22 Cr, 12.5 Co, Ni-base	2300 (7)
Incoloy 802	21 Cr, 32.5 Ni, Fe-base	1500 (7)
Incoloy 800	21 Cr, 32.5 Ni, Fe-base	1600 (7)

Notes pertaining to Table 5

† The temperatures listed, unless otherwise noted are generally those stated as such by the producer. However, these values should only be taken as a guide. The detailed oxidation behavior can vary significantly.

†† Other constituents sometimes total 10% or more and play an important role in oxidation resistance and strength.

1. Generally recommended maximum in steam boiler application. Specific temperature varies with the type steel.

2. Scaling temperature in continuous service; 50°F higher in intermittant service.

3. Scaling temperature in continuous service; 100°F higher in intermittant service.

4. Scaling temperature in intermittant service; 100°F higher in continuous service.

5. Scaling temperature in intermittant service; 150°F higher in continuous service.

6. Allowed by the ASME Boiler and Pressure Vessel Code.

7. Recommended by producer/boiler tube type applications.

* Highly resistant to chloride ion-induced stress corrosion.

** Good resistance to sulfidizing atmospheres.

*** Developmental alloy.

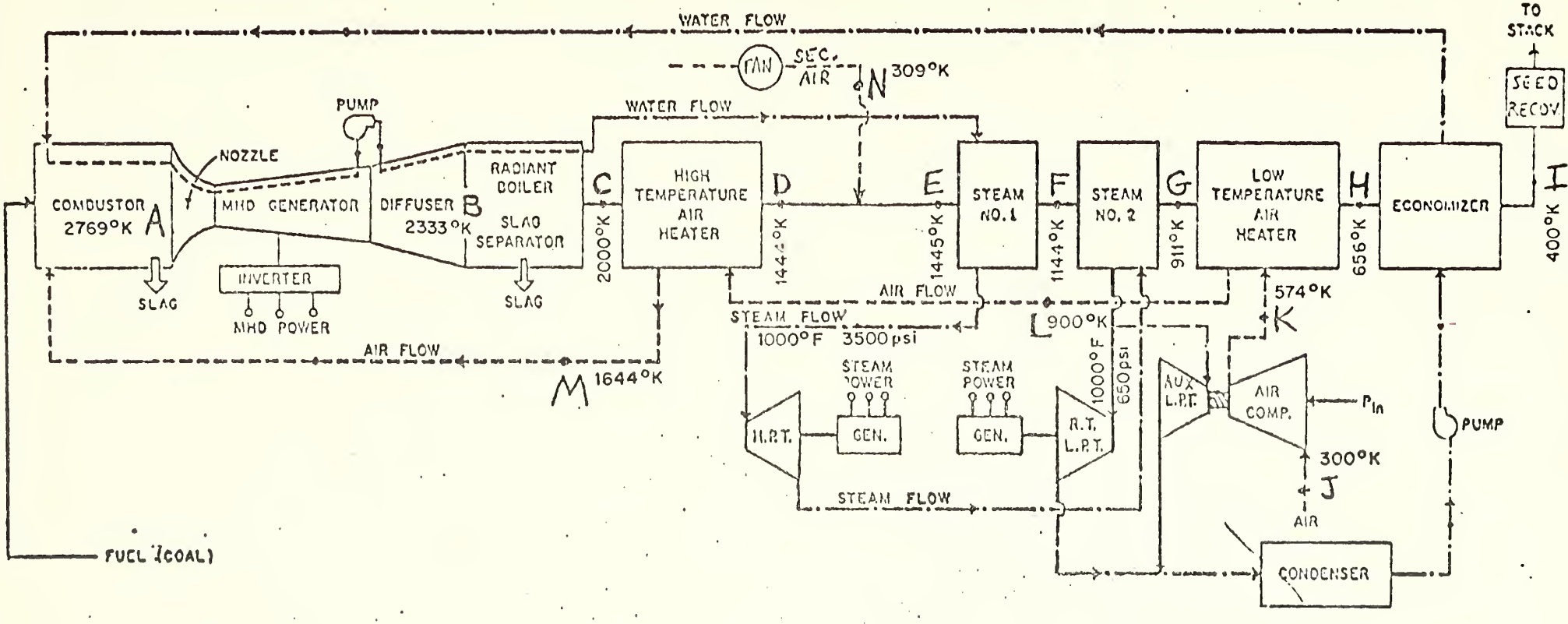

Fig. 4. STD Research Corp state point temperatures with seed condenser after the steam plant.

SPINELS FOR MHD-ELECTRODES *

H. P. R. Frederikse, W. R. Hosler, A. J. Armstrong and T. Negas
National Bureau of Standards
Washington, D. C. 20234

Abstract

Solid solutions of Mg-chromite and Mg-aluminate spinels and magnetite appear to be promising materials for MHD electrodes. This paper presents high temperature electrical conductivity data and discusses some structural and chemical properties of these compounds. The Mg-Al-spinels show good resistance to seed corrosion, while the Mg-Cr-spinels appear to stand-up well in a slagging environment. A third spinel, composed of Fe_3O_4 and Co_3O_4, is a very good electrical conductor and has potential as a lead-out material.

I. Introduction

Recent tests of several promising preheater materials conducted by the FluiDyne Engineering Corporation have indicated that Mg-Cr-and Mg-Al-spinels can withstand the rigors of an MHD environment remarkably well.[1] In these tests the materials were subjected to a slag and seed environment. Two runs of about 100 hours were made during which the sample temperature was cycled periodically reaching a maximum of 1800 K. These results have further encouraged us to explore the possible use of spinels as the basic materials for MHD-electrodes. The question is: can oxide additives be found which change the usually high resistance Mg-spinels into reasonably good conducting semiconductors? Fortunately, this can be achieved rather easily by mixing the insulating spinels with good conducting magnetite (Fe_3O_4, which also has the spinel structure) to form single phase solid solutions.

Spinels are cubic solids with 24 cation sites, 8 tetrahedrally surrounded by oxygen ions, and 16 octahedrally coordinated. Hence, the general chemical formula is $A_8B_{16}O_{32}$. When all the trivalent ions are on the B-site, the spinel is called "normal"; on the other hand when equal numbers of tri- and divalent ions occupy the B position one speaks of an "inverse" spinel.[2]

In this paper we will focus our attention on $MgCr_2O_4$ and $MgAl_2O_4$ spinels, containing up to 30 mole percent Fe_3O_4 in solid solution. The distribution of the cations over the tetrahedral (A) sites and octahedral (B) sites was first discussed by Verwey and his coworkers.[3,4] $Mg(Cr)_2O_4$ and $Mg(Al)_2O_4$ are normal spinels due to the rather strong preference of Al^{3+} and specifically Cr^{3+} for the octahedral B sites. On the other hand, $MgFe_2O_4$ and Fe_3O_4 are inverse spinels, because Fe^{3+} favors the tetrahedral site more than most other ions. Hence, the chemical formulas for the latter two compounds can be written as follows: $Fe^{3+}(Mg^{2+}Fe^{3+})O_4$ and $Fe^{3+}(Fe^{2+}Fe^{3+})O_4$. The large conductivity of magnetite is easily explained; it stems from the electronic exchange between ferrous and ferri-ions on equivalent (octahedral) lattice sites. Using the same reasoning one can understand why pure $MgCr_2O_4$ is an insulator. Verwey et al. have shown that the conductivity of the mixed crystals increases rapidly with increasing iron content.[5] However, iron decreases the melting point of these compounds: $MgCr_2O_4$ melts at 2400 °C, $MgAl_2O_4$ at 2110 °C, while magnetite (Fe_3O_4) has its melting point at 1591 °C, hercynite ($FeAl_2O_4$) at 1780 °C and $MgFe_2O_4$ at 1717 °C.[6,7] The phase diagrams of the systems $MgO-Cr_2O_3-Fe_2O_3$ and $MgO-Al_2O_3-Fe_2O_3$ (Figures 1 and 2) indicate that the spinel fields are quite extensive in both cases.[8] However, the melting temperatures are low and hence compositions rich in FeO_x should be avoided. Iron also tends to raise the volatility and the chemical reactivity. All these chemical facts are reasons for using just enough magnetite to produce solid solutions with sufficient electrical conduction, and at the same time to retain most of the stability of the higher melting spinels.

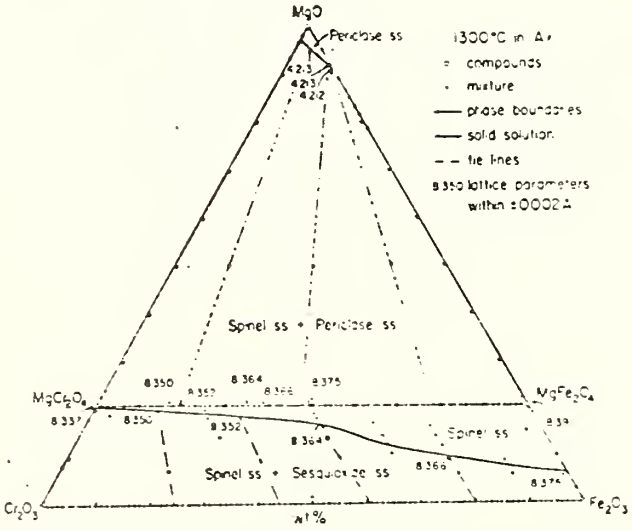

Figure 1. The system $MgO-Cr_2O_3-Fe_2O_3$ at 1300 °C in air. (Ref. 4).

Of course, it is by no means obvious that relatively small amounts of iron oxide will lead to a reasonable degree of conductivity. Let us take as an example a mixed spinel consisting of 1/4 magnetite and 3/4 magnesium chromite. (In terms of hematite the ratio is 1 Fe_2O_3 to 2 $MgCr_2O_4$). The electrical conductivity and cation distribution of this mixture has been discussed by Verwey et al.[5] Because of the strong preference of Fe^{3+} for the tetrahedral position no trivalent iron will be found on the B-sites in this concentration range. On the other hand, the Fe^{2+}-ions can be located either on the A or the B-site leading to the following two extreme distributions:

$$\text{I. } (Fe^{3+}_{1/2}\ Mg^{2+}_{1/2})(Fe^{2+}_{1/4}\ Mg^{2+}_{1/4}\ Cr^{3+}_{3/2})O_4^{2-}$$

or

$$\text{II. } (Fe^{3+}_{1/2}\ Fe^{2+}_{1/4}\ Mg^{2+}_{1/4})(Mg^{2+}_{1/2}\ Cr^{3+}_{3/2})O_4^{2-}.$$

Only spinel II and di- and trivalent iron on equivalent lattice positions (A-site) and hence would show appreciable electronic conductions; spinel I will be an insulator. However, the difference in energy between these two site arrangements is small and an intermediate distribution is far more likely, especially at high temperatures. Such a "half-way" arrangement may have the composition:

$$(Fe^{3+}_{1/2}\ Fe^{2+}_{1/8}\ Mg^{2+}_{3/8})\ (Fe^{2+}_{1/8}\ Mg^{2+}_{3/8}\ Cr^{3+}_{3/2})O^{20}$$

This spinel is expected to be a (semi)conductor because both Fe^{3+} and Fe^{2+} are present on equivalent A-sites (although not in equal amounts).

The above reasoning assumes that the spinel is stoichiometric and fully oxidized. A reducing atmosphere will give rise to a relatively larger Fe^{2+} content, which certainly will enhance the electrical conductivity.

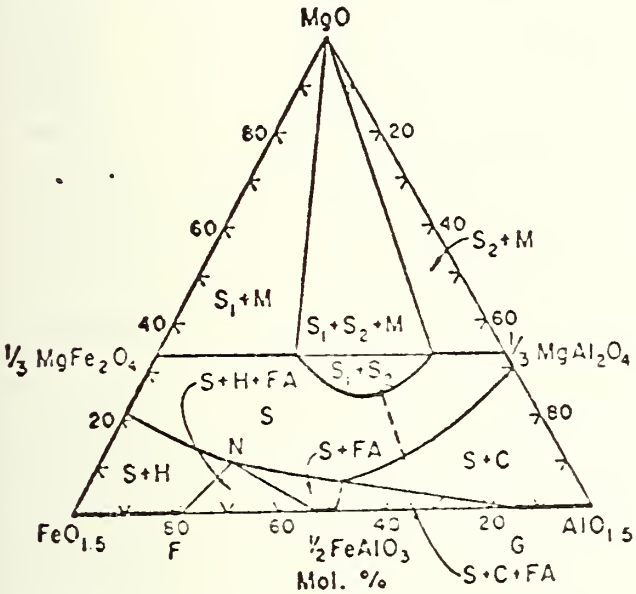

Figure 2. The system $MgO-Al_2O_3-Fe_2O_3$ at 1400 °C. S = broad spinel band, S_1 = $MgFe_2O_4$ ss, S_2 = $MgAl_2O_4$ ss, H = hematite ss, C = corundum ss, M = MgO, FA = $FeAlO_3$ ss. [After W. Kwestroo, J. Inorg. Nucl. Chem. 9, 67 (1959)].

A similar argument can be used to explain the electrical conductivity of spinels formed from magnetite and magnesium aluminate. Although the octahedral site preference energy for Al^{3+} is considerably smaller than that of Cr^{3+}, the other ions Mg^{2+}, Fe^{2+} and Fe^{3+}, strongly favor the tetrahedral site.[9] Hence, one expects that the physical behavior of Mg-Fe-aluminate and Mg-Fe-chromite will be quite similar, including their respective conductivities. The somewhat higher conductivity observed in the chromites may indicate that not only the Fe-ions but also the Cr-ions are present in more than one valence state.

II. Conductivity Measurements and Results

Electrical conductivity measurements were made on a number of Mg-Cr-Fe- and Mg-Al-Fe-spinels in the temperature range between 1000 and 1900 K. The experimental method has been described previously.[10] The oxygen partial pressure was varied between 0.2 and 6 x 10^{-6} atm. Some 10 samples of chromite and aluminate spinels have been investigated of which 6 were obtained from a commercial source and 4 were prepared in our laboratories. Details concerning composition and density are presented in Table I. Beside the chromites and aluminates, the conductivity of one sample of iron-cobalt spinel was also measured. Results of these measurements are presented in Figures 3 and 4.

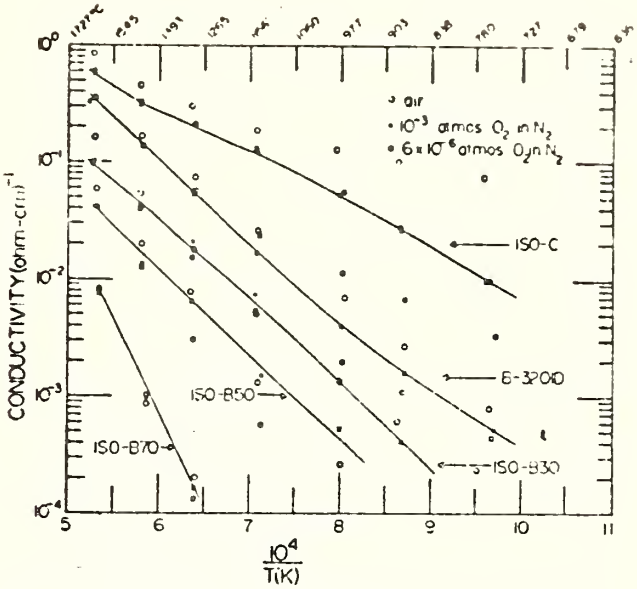

Figure 3. Electrical conductivities of 5 commercial materials containing MgO, Cr_2O_3, Al_2O_3 and Fe_2O_3 as major constituents [see Table I. Data on sample B-3226 D (not shown) are nearly identical to those obtained on sample B-3210 D].

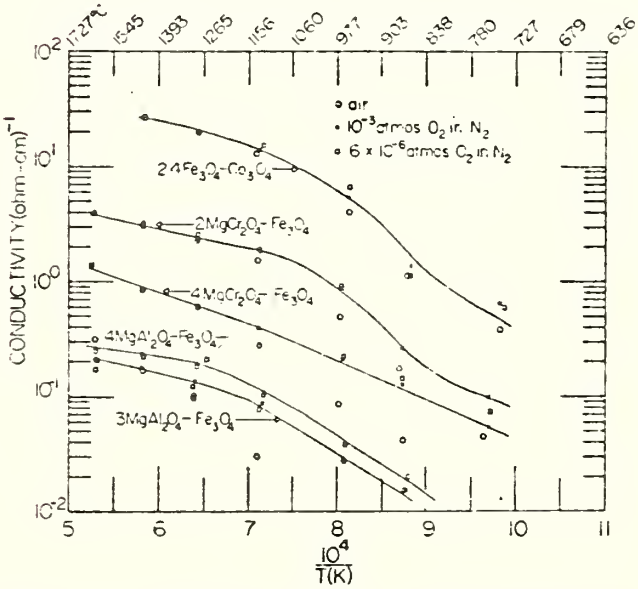

Figure 4. Electrical conductivities of 5 laboratory prepared spinels (see Table I).

Of the commercial materials only the sample labeled ISO-C has an acceptable level of conductivity ($\sigma \gtrsim 10^{-2}$ $ohm^{-1}cm^{-1}$) and a sufficiently small temperature dependence. However, a large excess of Cr_2O_3 in this material is a considerable drawback because of the high vapor pressure of this oxide and its strong tendency to react with potassium. Hence, one expects that the ISO-C materials will deteriorate rather rapidly in a seeded atmosphere at high temperatures.

The single-phase Mg-Fe-chromite (#6) shows excellent conductivity over the entire range between 1000 and 1900 K. This is not too surprising because the iron oxide content is higher than in any of the other Al- or Cr-spinels tested. It should be noted

Table I. Composition of Spinel Samples Studied

	MgO	Cr_2O_3	Al_2O_3	Fe_2O_3	(Fe_3O_4)	Co_3O_4	SiO_2	CaO	porosity(%)
$^{\Delta}$ISO-B70 (w/o)	70	11.7	12.0	5.3					12.3
sp. (m/o)	50+	16.7	26.0	7.3					
$^{\Delta}$ISO-B50 (w/o)	50	20.1	20.0	8.8					6.3
sp. (m/o)	50+	17.7	25.6	7.2					
$^{\Delta}$ISO-B30 (w/o)	30	28.3	28.0	12.7					10.4
sp. (m/o)	50+	17.2	25.2	7.3					
$^{\Delta}$ISO-C (w/o)	5.8	79.3	3.14	4.8					2-8
sp. (m/o)	50	19.8+	28.8	10.4					
$^{\Delta}$B-3201D (w/o)	27.0	38.7	10.4	22.8			0.82	0.27	
sp. (m/o)	50+	25.5	10.2^5	14.2					
$^{\Delta}$B-3226D (w/o)	38	31.7	10.7	18.3			0.96	0.31	
sp. (m/o)	50	24.0	12.5	11.5					
*Chromite #2 (m/o)	42.1_5	42.1_5		15.8					
	$(44.4^5$	44.4^5			11.1)				
*Chromite #6 (m/o)	36.4	36.4		27.2					
	(40.0	40.0			20.0)				
*Aluminate #3 (m/o)	42.1_5		42.1_5	15.8					
	$(44.4^5$		44.4^5		11.1)				
*Aluminate #5 (m/o)	40.0_5		40.0_5	20.0					
	$(42.8^5$		42.8^5		14.3)				
*Fe-Co spinel (m/o)					70.8	29.2			

$^{\Delta}$- These samples were prepared by the A. P. Green Refractories Company. The chemical composition in weight percent is given on the 1st line of each sample. These specimens were not single phase, but a mixture of spinel and excess (cubic) MgO or excess Cr_2O_3 (sample ISO-C). The second line gives the composition of spinels (sp.) in mole percent (+ indicates large amounts of excess MgO or Cr_2O_3).

*- These samples were prepared in the Solid State Chemistry Section of NBS. All samples were single phase spinel. The fact that the mole percentage of MgO is smaller than 50 indicates that these spinels are partially "inversed".

that only above 1500 K the conductivity is independent of the partial oxygen pressure. Below 1500 K a more oxidizing atmosphere - expected to prevail on the anode wall of an MHD channel - will depress the electrical conductivity.

Conductivities of acceptable magnitude are observed also in the Mg-Fe-aluminate spinels. At about 1100 K the conductivity drops below 10^{-2} $ohm^{-1}cm^{-1}$. Hence, it is desirable to combine this spinel with a better conducting material for the lower temperature range.

A prime candidate to perform this function (of "lead-out") is a Fe-Co spinel with the composition 70 m/o Fe_3O_4-30 m/o Co_3O_4 (see Table I). This particular composition melts above 1600 °C and has the spinel structure over a large temperature interval as shown in Figure 5. The electrical conductivity is high and independent of the oxygen pressure down to 900 K. At this temperature the material can be brazed to a metal-alloy lead-out (e.g., stainless steel) without much danger of corrosive decay through oxidation.

III. Conclusions

A number of high temperature spinels appear to hold promise as building blocks for MHD-electrodes. Above 1200 K (and in some cases even 900 K) the electrical conduction in iron-doped Mg-chromite and Mg-aluminate spinels is sufficiently high to carry the current generated in MHD-channels. Fe-Co-spinel seems to have all the properties desired for a good lead-out material. Mg-Al-Fe spinel is recommended for use with clean fuels, because its reactivity with potassium apparently is very small. On the other hand the chromite spinel has shown good corrosion resistance in a slagging environment. A slag layer on top of a chromite electrode would absorb much of the seed, hence lower the potassium activity and thus diminish the possibility of strong K_2O-Cr_2O_3 reactions.

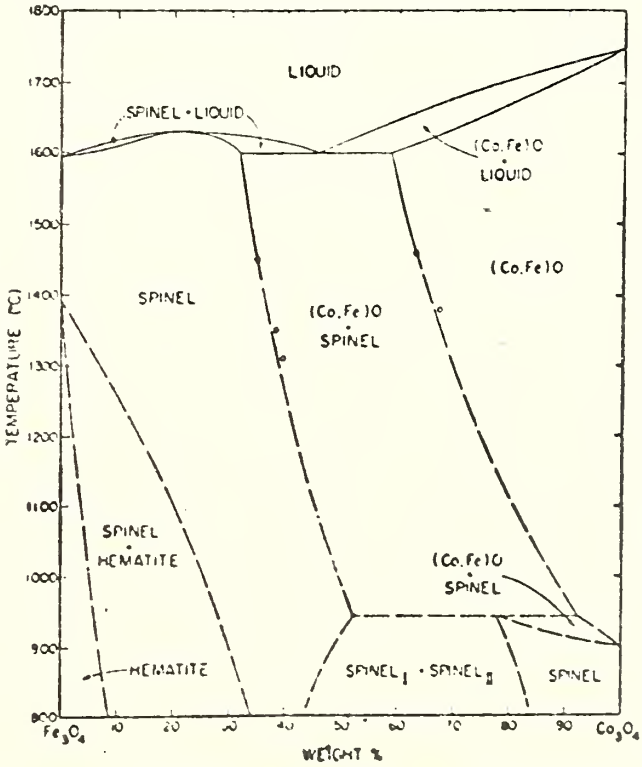

Figure 5. Phase diagram of the system Fe_3O_4-Co_3O_4 in air. (Ref. 11)

References

*Supported by Energy Research and Development Administration.

1. Quarterly Progress Report (to ERDA), Fluidyne Eng. Corp., August 1975.

2. "Introduction to Ceramics", by W. D. Kingery, Publ. John Wiley, New York, (1967), p. 115 and also p. 750.

3. E. J. W. Verwey and E. L. Heilmann, J. Chem. Phys. 15, 174 (1947).

4. G. C. Ulmer and W. J. Smothers, J. Am. Ceram. Soc., 51, 315 (1968).

5. E. J. W. Verwey, P. W. Haayman and F. C. Romeyn, J. Chem. Phys. 15, 181 (1947).

6. L. M. Atlas and W. K. Sumida, J. Am. Ceram. Soc. 41, 150 (1958).

7. J. C. Willshee and J. White, Trans. Brit. Ceram. Soc. 66, 541 (1967).

8. "Phase Diagrams for Ceramists", Ed. by E. M. Levin, C. R. Robbins and H. F. McMurdie, (Publ. by Am. Ceram. Soc., Columbus, Ohio, 1964).

9. Arthur Miller, J. Appl. Phys. 30 (Sup.) 24S (1959).

10. H. P. R. Frederikse and W. R. Hosler, J. Am. Ceram. Soc. 56, 418 (1973).

11. Arnulf Muan, in "High Temperature Oxides, Vol. 5, Part I, Ed. A. M. Alper, Publ. Academic Press, New York, 1970, p. 334.

ANALYSIS OF AVCO MARK VI C CHANNEL ELECTRODES AFTER LONG DURATION TEST*

W. R. Hosler and T. Negas
National Bureau of Standards
Washington, D. C. 20234

and

S. W. Petty
Avco Everett Research Laboratory
Everett, Mass. 02149

I. Introduction and Procedures

The recent AVCO 100 hour test[1] marked a milestone in the U. S. MHD effort to produce energy through MHD. Although a distinct success, problems developed in both the anode and cathode electrode walls as the test continued. Most important are:

1. the degradation of the electrical insulation between the cathode electrode segments together with the erosion/corrosion of the associated copper fin on the downstream side of the insulator gap, Figure 1a, and,

2. the considerable erosion/corrosion of the anode electrode wall.

To investigate possible causes for these main problem areas, sections were removed from the anode, cathode and sidewall anode and cathode in the upstream portion of the channel where the construction was of the Inconel button type, Figure 1b. Corresponding sections also were removed from the channel midsection consisting of rail-type electrodes, Figure 1a. These sections, containing two or more adjacent segments, were examined in detail using optical and scanning electron microscopy (SEM) in conjunction with chemical and X-ray diffraction analyses. After appropriate samples were taken for chemical and X-ray diffraction analyses, the electrode sections were potted in epoxy resin and subsequently sawed to yield cross sections which expose significant areas for optical and SEM examination. Figure 2 shows the dissected electrode sections. Unfortunately, while the slag on the walls remained nearly intact after cool down of the channel (especially on the cathode), during the section removal process much of the slag cracked loose from the metal surface (primarily on the anode). An effort was made to preserve the slag in the same general area above the metal since this interface is a critical area for analysis. Table I lists semiquantitative analyses for several slag specimens from various portions of the MHD system together with the dominant components of the original fly-ash.

II. Results and Discussion

A. Cathode Wall

The problem concerning the degradation of the electrical insulation at the cathode wall is extremely important because the result is a short in the axial, Hall voltage. In turn, this causes electrical stress (overloads) on adjacent electrodes which then are subjected to accelerated degradation leading to premature failure of the generator.

Figure 3 shows a cathode rail wall cross-section and the particular area where insulation degraded. The copper cooling fin is brazed onto the downstream electrode from the insulator gap. Initially, this fin had a rectangular cross section so the copper has eroded/corroded during the test. We believe that the shorting of the insulating gap is caused by one or a combination of several factors. Originally, the area just upstream and downstream from the rail of each electrode was filled with castable zirconia (CaO stabilized) and alumina castable cements, respectively. A striking feature of every section taken is that the alumina cement has been altered and nearly completely replaced by slag saturated with seed. This phenomena is associated with the zone wherein shorting occurs. The narrower, adjacent (upstream) gap filled with zirconia castable remains practically unaffected and is relatively free of seed deposits.

As cold coal slag of the type used at AVCO is a relatively good insulator, the shorting process must be due to other factors. Figure 4, a schematic drawing of the cathode electrode rail assembly, illustrates the area where insulation has degraded. The entire areas, a, b, and c contain potassium as evident from X-ray diffraction and EDX data. Area c, however, has a significantly higher potassium content. Indeed, when exposed to ambient conditions (after cool down), hydration in this area and in area b commences and a solution oozes from the surface. This observation as well as x-ray diffraction data, indicate that zone c and, at least, the lower portion of zone b, are saturated with condensed K_2CO_3. (Fig. 5). X-ray diffraction patterns of "slag" specimens from zones within areas in Figure 4 further demonstrate that there is a potassium concentration gradient (differential) within the slag at the cathode in contrast to slag at the anode. Zone (a) is glassy and has no crystalline phases containing potassium, although some potassium, presumably in solution, is present. Intermediate area (b) contains crystalline, orthorhombic $KAlSiO_4$ as the predominant phase. However, toward the base of area (b), tetragonal and cubic K_2O-aluminosilicates, crystalline phases richer in K_2O than $KAlSiO_4$, clearly are present. These materials have been characterized previously by Cook et al.[2] at NBS. Area (c) represents the zone saturated with potassium so indicated above. The differentiation of potassium at the cathode conceivably could be attributed to temperature gradients. However,

*This research was supported by ERDA.

Table 1. Semi-quantitative spectrochemical analysis of bulk slag materials from several locations in the generator system. Only elements significant to the experiment are listed (wt. %).

	Burner	Upstream Cathode	Upstream Anode	Cathode Exit	Anode Exit	Diffuser	Original Fly-Ash
Al	>13	>13	>13	>13	>13	>13	13.5*
Si	>13	>13	>13	>13	>13	>13	16.7*
K		>13	>13	>13	>13	>13	
Ca	1.5	2	1	1.5	1	1	4.08
Cr	.05	<.05	<.05	0.15	0.15	.05	
Ni	.05	0.2	0.2	0.5	0.2	0.2	
Fe	>13	>13	5-10	5-10	5-10	>13	13
Cu	.15	3	1.5	0.05	1.5	.05	

*Wet Chemical Analysis

anode slags, subjected to similar temperature gradients, are completely different. Crystalline $KAlSiO_4$ is distributed throughout the anode slag but phases richer in K_2O and areas comparable to Figure 4c, do not exist. These data point to one of the possible causes for the shorting at the cathode. As area (c), and probably part of (b), Figure 4, are saturated with potassium, it is possible that ionic conductors consisting of condensed K_2CO_3/KOH solutions could short-out adjacent electrodes. These solutions can exist at temperatures below 1300° to about 370°C. It should be recognized that K_2O-rich solutions can be stable and coexist with crystalline slag components saturated with K_2O.

X-ray diffraction and magnetic susceptibility measurements of "slag" extracted from various areas in Figure 4, reveal that iron also differentiates at the cathode. Area (a) contains magnetite, Fe_3O_4, and bulk magnetic susceptibility data indicate ~15% Fe_3O_4. It is unclear, however, whether Fe_3O_4 is primary or is a product which crystallized during the cool-down process. The region between areas (a) and (b) contain crystalline $KAlSiO_4$ (see above) and, as susceptibility data indicate, ~33% Fe_3O_4. Anode slag yields magnetic data corresponding to ~3% Fe_3O_4 while glassy slag from the combustor yields ~1% Fe_3O_4. These percentages represent lower limits for the iron content calculated by comparing magnetic data for pure Fe_3O_4 with that from the slag specimen. Iron not contributing to the magnetism is excluded. The relative percentage differences for iron are significant and indicate that on the cathode highly conductive, crystalline Fe_3O_4 concentrates between (a) and (b), Figure 4. This differentiation easily could contribute to interelectrode shorting. Concentration of iron may result from crystallization and phase separation in a steep temperature gradient. These concentration gradients also may be influenced by electrochemical reactions involving either transport of or oxidation/reduction of iron cations.

Another manifestation of the differentiation of iron is suggested by the composition of the slag at anode and cathode surfaces. Directly above cathode Inconel buttons, Inconel rails and copper fins, the slag surface consists of a thin (< 0.25 mm), red-brown crust. X-ray diffraction data reveal that, hematite, Fe_2O_3, is the dominant crystalline phase associated with this zone which presumably was subjected to the highest temperatures. Below this zone, and in areas between metal components, reduced iron oxide, Fe_3O_4 dominates (e.g., area (a), Figure 4). It might be supposed that the upper surface of the slag at the cathode oxidized during cool-down. This hypothesis is negated by the absence of the Fe_2O_3-rich crust at the surface of the slag between rails and, indeed, its absence at the surface of most anode slag (see below). Thus, a contradiction is apparent. Given a fixed oxygen activity (e.g., 10^{-6} atm) and a temperature gradient, reduced Fe_3O_4 and oxidized Fe_2O_3 (primary or secondary in origin) should exist within the high and low temperature regions of a slag, respectively. We observe precisely the opposite type of differentiation. We speculate that electrochemical reactions and current transport processes within the molten slag may control the oxidation state of iron. Anode slag on the other hand contains Fe_2O_3 in regions well below the surface. However, the slag at the sidewall, rail anode, which has not degraded totally (see below) does contain a thick crust (>0.25 mm) containing Fe_2O_3. This crust occurs above and between metallic components.

Just below the plasma/slag interface and between the copper fin of the downstream electrode and the rail of the upstream electrode, region (a), Figure 4, the molten (glassy) slag layer thickens and lies in a trough along the entire rail. This periodic contour is obvious in the full cathode wall photographs taken of the disassembled channel. We believe that these areas contribute to the observed shorts for several reasons. Molten slag containing iron is a good conductor. Generally, this is a projected problem in any coal-fired MHD channel because the conductivity provides a path for current leakage along the wall. However, if the molten slag layer remains thin above the insulator the effective axial resistance is high. Thickening of the molten slag layer at this region (a), Figure 4 is precisely where it is not desired.

As evident from Figure 3, the cathode copper fin is eroded on the upstream side. This fin is at approximately 20 volts positive potential with respect to the upstream adjacent electrode. X-ray diffraction and EDX data reveal concentrations of copper upstream from the fin possibly resulting

from corrosion of the copper via electrolytic processes. In effect, the area in Figure 4 may represent a miniature electrochemical cell containing dissimilar electrodes, copper and Inconel. The copper at positive potential could degrade according to, $Cu \rightarrow Cu^{+}_{(slag)} + e^{-}$. At negative potential, processes including, $K^{+} + e^{-} \rightarrow K$, $Fe^{3+} + e^{-} \rightarrow Fe^{2+}$, and $Ca^{2+} + 2e^{-} \rightarrow Ca$ could balance the reaction. We note, further, that copper degrades precisely within the area where interelectrode shorting occurs.

A second possibility is that the Faraday current in the form of arc discharges is concentrated on the upstream edge of the cathodes by the JxB force on the arcs. This hypothesis is corroborated by: a) the unmarked condition of the inconel buttons in the cathode design of Figure 1b indicating an absence of current activity and b) the unmarked condition of the downstream side of all cathodes which one would expect should show arc tracks or copper deposition if interelectrode arcs or electrochemical activity were occurring.

An interesting observation that may be of significance to very long term operation of a generator and which may relate to the discussion above was made from an analysis of the cathode rails by SEM. Figure 6 is a SEM micrograph montage of a typical cathode rail electrode. Although this wall withstood the test very well compared to the anode, some corrosion is evident both at the slag-metal interface and the undercut rail surfaces. The Inconel shows trans-granular cracks which are penetrated by calcium and, more deeply, by potassium. Chromium from the Inconel is associated with these penetrations. The SEM micrograph, Figure 7a, of a typical zone and the pertinent X-ray maps for Ca, Figure 7b, and for Cr, Figure 7c, demonstrate this phenomenon. Nickel is not present within areas of alteration and, indeed, at the underside of the rails, alteration has proceeded under the original nickel plate. The chemistry of the Inconel alloy at the slag interface is altered by potassium and calcium which preferentially react with chromium. These reactions alter the Inconel from a non-magnetic alloy to a ferromagnetic material. Potassium and calcium as metallic species in the alloy are unlikely and probably exist as K_2CO_3/KOH and $CaO/Ca(OH)_2$ phases or are associated with chromium oxide compounds such as K_2CrO_4 and $CaCrO_4$. Significantly, corresponding Ni-containing compounds do not exist.

Although the cathode rail wall degrades via trans-granular cracking and penetration of calcium and potassium, we cannot define, unequivocally, the processes or mechanisms involved. The fact that the rail degradation occurred rather uniformly on the underside as well as the top surface would seem to rule out a significant correlation with the main Faraday current which appeared to favor the upstream copper as it did in the button design. The significant difference in the inconel operating temperatures (rail $\approx 2000^{\circ}F$ vs button $\approx 1000^{\circ}F$) may account for the fact that the rails sustained potassium/calcium attack while the buttons did not. It is suspected, however, that this attack is electrochemical in nature and could, therefore, have some tie-in with the main current transport mechanism. Reactions could also be enhanced by localized heating from micro-arc discharge through a thin, cold slag layer near the metal. The top and downstream side of the copper fin are not eroded/corroded suggesting that substantial current was not present in this area for the rail wall design.

Figure 8 shows a cathode button wall cross section. Here, again, conditions similar to the cathode rail wall prevail and result in interelectrode degradation. In this case, however, it is clearly evident that most of the Faraday current was carried by the copper. SEM micrographs show little damage to the Inconel buttons in contrast to the rails but the copper is highly eroded both on the top and the upstream edge where the current erosion is similar to that observed in the rail electrode. Figure 8 demonstrates particularly well, the thickening of the molten slag layer in the critical area above the insulator. The rectangular dark area is the Inconel button. The other dark-area to the left is the molten (glassy when cooled quickly) slag area.

The erosion/corrosion of the Inconel rails on the cathode wall is not extensive for this length of test. Current transfer through the thin, cold, coal slag layer just above the Inconel is assumed to be primarily by arc column transport with possibly small components of electronic conductivity associated with Fe^{3+}/Fe^{2+} ratios, and ionic conductivity associated with cations and oxygen. As an arc column is propagated through the dielectric layer and continued through the slag/metal boundary, material around the arc column may melt and vaporize filling the column with ionized gases. The arc root at the cathode metal (Inconel) could melt a local area. Since the electrode is negative with respect to the plasma stream, metal ions in the vapor would be driven toward the cathode thus minimizing erosion through vaporization. At the same time, if the oxygen activity is low at the cathode metal/slag interface rapid oxidation of the molten metal components would be minimized. Any oxygen ion transport through the slag layer is away from the metal cathode. This arc or spark erosion process parallels closely that observed in the well-known process of electro-discharge machining. On the cathode, the polarities are such that the arc is not favorable for metal removal. However, surface cracking has been observed[3] in experimental electro-discharge machining and this might be the source of the transgranular attack shown in Figure 7a. The suggested current transport processes through the slag layer are speculative. Arc "tracks" through the cathode slag could not be detected.

B. Anode Wall

Erosion/corrosion of the anode metals is very severe. Figure 9 shows a cross section of a rail anode wall which was eroded almost entirely. Similar to the cathode, the anode is completely covered with slag during operation of the generator and it may be assumed that the current transfer through the cold slag layer near the metal surface is, again, primarily via arc columns. The arcs continue to the slag/metal boundary and may provide the source for localized, intensive heating which contributes to melting and vaporization of the metal surface. In contrast to the cathode, ionized metal vapor would be repelled from the anode (positive with respect to the plasma) and transported by the arc column. The activity of oxygen may be high at the anode as a result of

several factors. Oxygen ions may be transported through the molten and solidified but porous slag. The concentration of oxygen or hydroxyl ions also could be enhanced at the anode by the electric field. Oxygen gas would be evolved if these species were discharged at the anode metal/slag interface. Metals, therefore, could be subjected to destructive oxidation accelerated by localized heating and melting due to micro-arcing.

Another mechanism for anode corrosion is indicated by the SEM micrographs shown in Figures 10 a and b. On the rail wall, the Inconel is eroded away (Figure 9) so that erosion mechanisms cannot be assessed. On the anode rail sidewall, however, rails remain and it is evident that their shape is similar to the original but reduced in size. Erosion appears to occur not only on the rail top but around the rounded edges and toward the neck. The SEM micrographs indicate that there are essentially three zones near the slag interface. The innermost zone is Inconel. The intermediate zone is vessicular and consists of Inconel ridges (lighter areas, Figure 11a) and irregular cavities rich in chromium and iron. This suggests that the nickel is oxidizing preferentially. The outer zone (Figure 11b) has a granular microstructure and consists of nickel, chromium and iron. We suggest that this area represents an oxidized scale which ultimately spalls and dissolves in the slag. The mechanism for this degradation must be related to active oxidation of the metal by chemical reaction with oxygen and/or to electrochemical corrosion reactions. It is unclear, however, whether the corrosion observed for the sidewall anode rails is the dominant process leading to destruction of the anode wall, in general. If destructive oxidation dominates, one would expect to find metal oxide components of Inconel in the slag adjacent to the anode electrodes. We searched for these components in the anode slag but could not find significant amounts. However, if the slag is exchanged frequently, metal components would not be present in the newly formed slag. As the total mass ratio of metal removed to coal slag fed to the channel during the 100 hour run is small, a dilution effect is operative. Previous analysis of AVCO cathode and anode slag under different conditions did show 1 to 5 wt% of nickel in localized spots in the anode slag.

Our interpretation of the erosion processes at the anode are based to a large extent on speculation. It is difficult to elucidate possible mechanisms without further investigation of the anode electrodes while an experiment is in progress using instrumentation aimed directly at the problem.

There is considerable evidence, however, from operation with previous Mark VI channels that the recession rate of anode metal is very temperature dependent and, in fact, slag covered inconel anodes operating at less than 1000°F metal temperature showed negligible erosion after 110 cumulative hours of operation in the VI B channel.

III. Conclusions

Several conclusions are inferred from the results of this investigation. It may be beneficial to design an electrode system for a slagging generator in a configuration such that the axial temperature along the wall is nearly constant. Single metal alloy construction would be the simplest and least susceptible to electrochemical effects in the interelectrode gap. High density ceramic insulation, having good thermal conductivity should be used to prevent seed penetration, erosion/corrosion by plasma and slag flow, and to avoid large temperature gradients in the axial direction. Chromium-containing metal alloys for the cathode may not survive extensive attack by potassium and calcium during long term generation of power. At the anode, the selection of a metal depends on what degradational processes dominate. Erosion via micro-arcing combined with destructive oxidation require the use of a metal with a high melting point, good thermal conductivity and high resistance to oxidation. For extended anode durations, it may be necessary to utilize a conducting oxide which is compatible with coal slag. It seems evident that optimal designs for anodes and cathodes will be considerably different and the engineering and materials selection process must recognize this fact.

In this paper, we illustrate several erosion/corrosion processes and demonstrate some remarkable differences in the chemistry of slag at anode and cathode walls. Mechanisms to explain these observations are complex and multiple in nature and need to be "unraveled" by thorough research. Experimentation using test-rigs, high temperature electrochemical cells, etc. could provide invaluable data concerning the nature of the current and mass transport processes occurring at every interface within a cathode and anode wall. Without these data, selection of materials and wall design is subjective and wed to the trial-and-error process.

References

1. Petty, S., Solbes, A., Enos, G. and Dunton, A., "Progress on the Mark VI Long-Duration MHD Generator." 15th Symposium on Engineering Aspects of MHD, Philadelphia, PA, May 1976.

2. Cook, L., Roth, R. S., Parker, H. S. and Negas, T., to be published in American Mineralogist.

3. Williams, R. O., "Elements of Electro-Discharge Machining, Technical Activities Seminar, Sept. 30-Oct. 10, 1957, Cincinnati, Ohio.

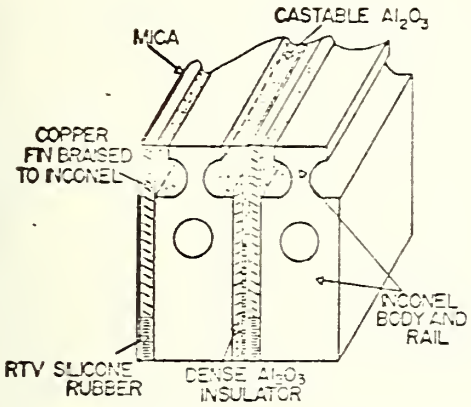

Fig. 1a Rail wall design. Plasma flow from left to right for cathode, right to left for anode.

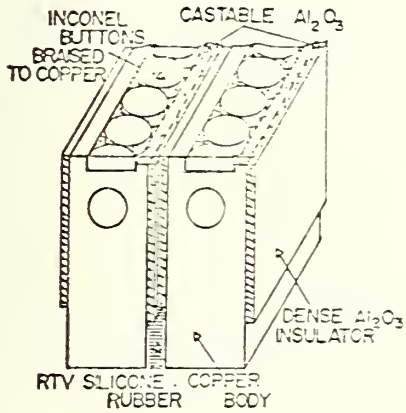

Fig. 1b Button wall design. Plasma flow from left to right for cathode, right to left for anode.

Fig. 2 Sliced electrode sections.

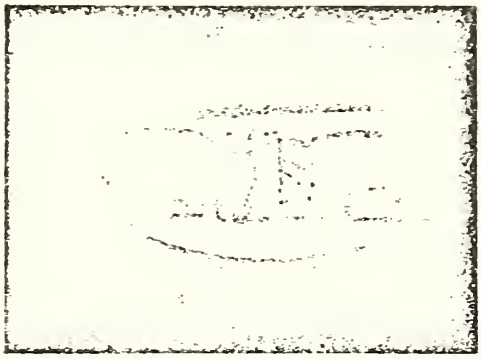

Fig. 3 Cathode rail wall cross section.

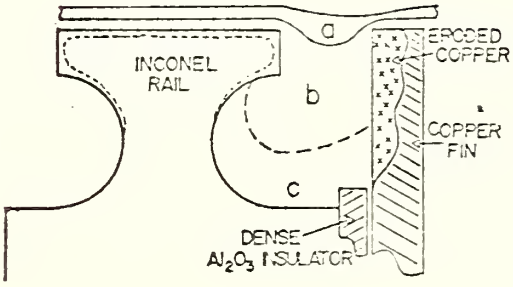

Fig. 4 Schematic diagram of cathode area between rail wall and copper fin. a. molten slag, b. solidified slag, c. high concentrations of K and Ca.

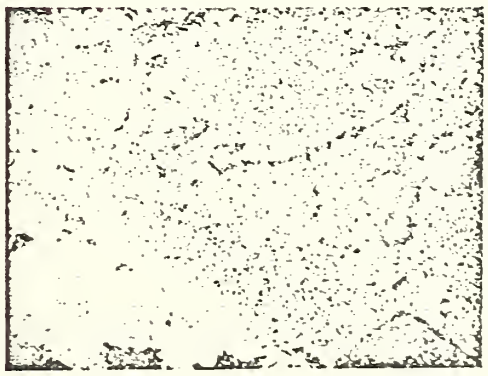

Fig. 5 SEM map of K in area c of Fig. 4. (30X).

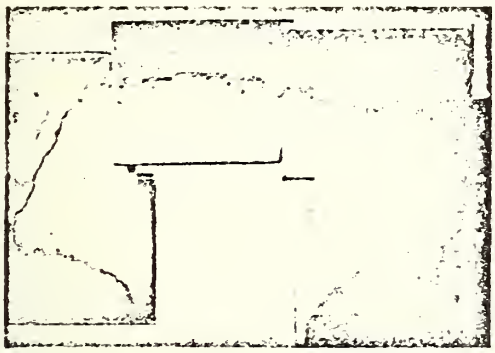

Fig. 6 SEM montage of cathode rail. (30X).

Fig. 7a SEM micrograph of damage to cathode Inconel rail. (150X).

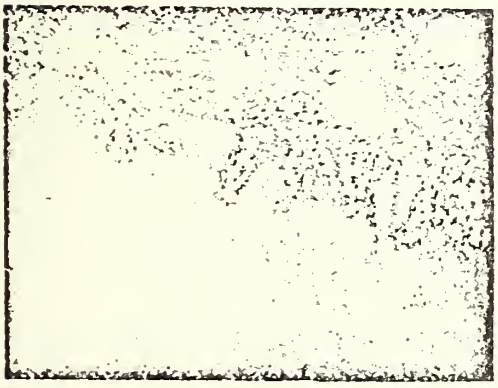

Fig. 7b SEM map for Ca of area in Fig. 7a. The white dots indicate Ca concentrations.

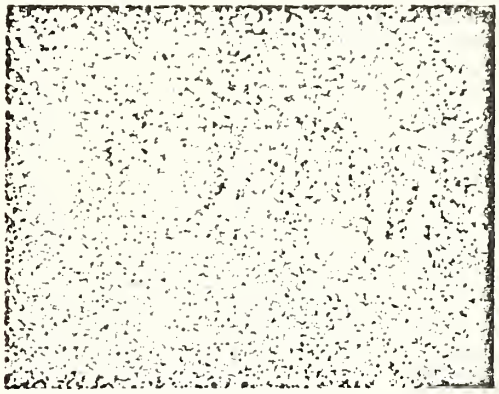

Fig. 7c SEM map for Cr of area in Fig. 7a. The white dots indicate Cr concentrations.

Fig. 8 Cathode button wall cross section. Rectangular dark area is Inconel button. Dark area to left of Inconel is glassy slag.

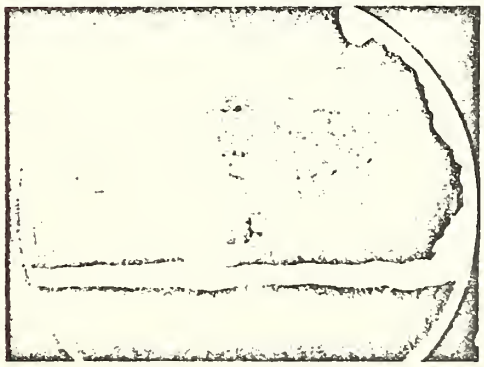

Fig. 9 Anode rail wall cross section. Inconel rail nearly eroded away.

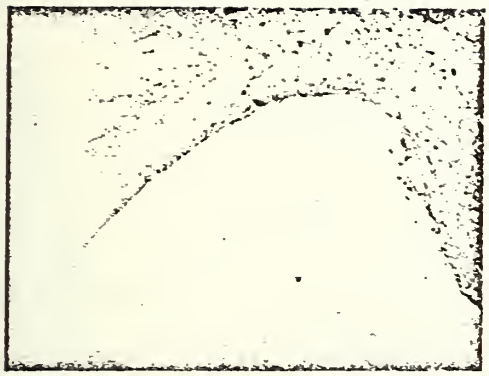

Fig. 10a SEM micrograph of anode sidewall rail. Slice taken near channel corner. (30X).

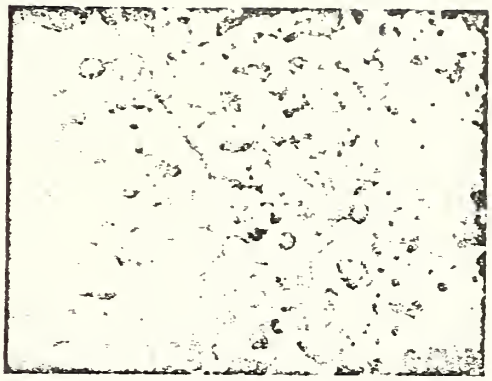

Fig. 11a SEM micrograph of intermediate zone of Fig. 10b. (3000X).

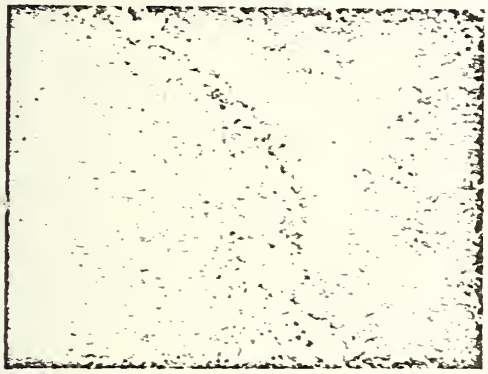

Fig. 10b SEM micrograph of metal-slag boundary of Fig. 10a showing three general areas. (750X)

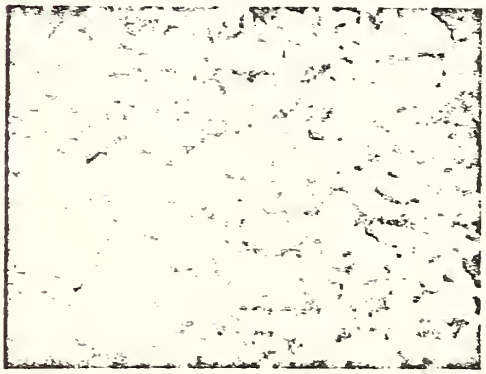

Fig. 11b SEM micrograph of outer zone of Fig. 10b. (3000X).

THE SYSTEM K_2O-Al_2O_3-SiO_2. PART 1. CRYSTAL CHEMISTRY OF PHASES ON THE $KAlSiO_4$-$KAlO_2$ JOIN

L. P. Cook, R. S. Roth, H. S. Parker, and T. Negas

National Bureau of Standards
Washington, D.C. 20234

ABSTRACT

Orthorhombic $KAlSiO_4$ synthesized at 950°C (a=9.057(2)A, b=15.642(2)A, c=8.582(2)A transforms above 1485°C to another orthorhombic phase having a larger unit cell (a=18.110(3)A, b=15.600(3)A, c=8.560(2)A. Nonstoichiometry of the high temperature orthorhombic phase is suggested by analysis of x-ray powder diffraction data. Evidence is presented for the reversibility of this sluggish transition. An excess of $KAlO_2$ appears to increase the rate of the reverse reaction to produce orthorhombic $KAlSiO_4$ with falling temperature.

A body-centered tetragonal tridymite-like phase $K_{1+x}Al_{1+x}Si_{1-x}O_4$ with $x < 0.1$ and unit cell dimensions a=8.943(1)A, c=5.221(1)A has been found to be stable at the expense of orthorhombic $KAlSiO_4$ and cubic $KAlO_2$-silica solid solution in the range 1400-1600°C.

Experiments suggest that the compound previously reported to be $K_2Al_2SiO_6$ is really a f.c.c. solid solution $K_{1-x}Al_{1-x}Si_xO_2$ with $x \cong 0.25$. This compound is the limiting end-member of the cristobalite-like solid solution series at 1600°C.

CRYSTALLIZATION AND VAPORIZATION STUDIES ON SYNTHETIC COAL SLAG COMPOSITIONS

L. P. Cook, E.R. Plante, T. Negas, R.S. Roth, and C.D. Olson
National Bureau of Standards
Washington, D.C. 20234

Abstract

Insight as to the chemical behavior of coal slags accumulating on the walls of MHD systems can be gained by examining the results of high temperature experiments on K_2O-CaO-Al_2O_3-SiO_2 mixtures. An increase in CaO content may increase a_{K_2O} appreciably for certain compositions. Potassium aluminate - silica solid solutions, some of which are relatively water soluble, occur over a significant range of silica-poor and Ca-rich compositions at 1400°C.

Two synthetic slags, with compositions falling close to an observed distribution of coal ash analyses, have been studied with the mass spectrometer using the Knudsen effusion technique. One slag having initially 15 wt% CaO yielded a higher K pressure at 10 wt% K_2O than a K_2O-SiO_2 solution containing 30 wt% K_2O. A second slag with relatively high SiO_2 and Al_2O_3 and 15 wt% K_2O gave a K pressure above that of a K_2O-SiO_2 solution with 20 wt% K_2O.

I. Introduction

The interaction of seed, as K_2O, with slag, leads to a number of important problem areas in the development of open cycle, coal fired MHD electric power generation. These include corrosion by the slag phase in contact with the electrode-insulator structure and seed recovery.

Significant effort has been made in recent years in the development of thermodynamic models, whose function is to predict equilibrium concentrations of K_2O in the slag phase as a function of temperature. Apparently, the consensus is that such models overestimate the amount of seed captured by the slag.[1,2]

Previous efforts at NBS[3] have involved measurements of the K(g) pressure over K_2O-SiO_2 solutions and phases in the K_2O-Al_2O_3 system. These data have been used in modeling slag[1] with the result that the amount of seed absorption predicted by the model is less than that predicted by an ideal solution model. Thermodynamic data for two component systems provide useful insights into the seed-slag interaction problem but its use in realistic models confronts the thermodynamicist with a severe challenge. Obviously, the most serious problem with thermodynamic models for seed, coal-slag interaction results from our almost total ignorance of what the effect of each of the four or five slag components is on the activity of the K_2O component.

II. Chemical Variation in Coal Slag

Inspection of analyses listed in U.S. Bureau of Mines Bulletin 567[4] shows extensive variation in coal ash compositions; however, most of this variability is due to fluctuation in Fe and Ca content. Atomic Si/Al ratios are less variable, as would be expected if these elements originate largely in the clay fraction of the mineral matter - for example, Si/Al in illites[5] typically varies from 1.2 to 1.4. Twenty-eight recalculated coal ash analyses originally reported by Selvig and Seaman[5] and discussed by Selvig and Gibson[4] are shown in Figure 1. These analyses, from different horizons within a bed of Pennsylvania coal, illustrate the sort of variability which can occur. Figure 1 shows a marked concentration at $Si/(Al + Fe^{+3}) \approx 1.5$, while exhibiting a wide variation in content of CaO + MgO + FeO.

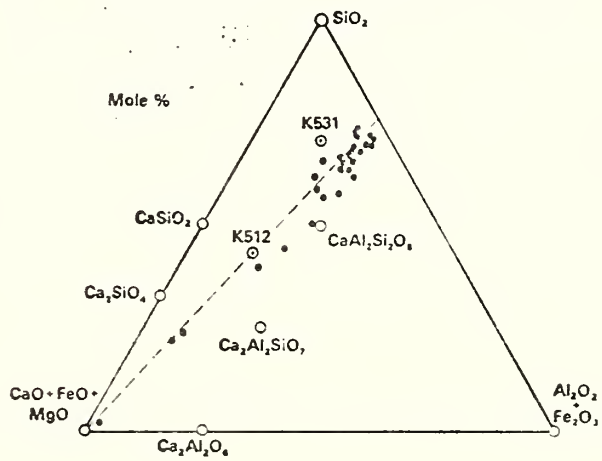

Figure 1. Recalculated analyses of synthetic slags K512 and K531 (circles with dots) and coal ash from Pennsylvania coal (dots), shown in relation to compounds in the system CaO-Al_2O_3-SiO_2 (open circles). Dashed line shows $Si/(Al + Fe^{+3}) = 1.5$.

It is desirable to discuss briefly the manner of treating compositionally complex coal slags, for this leads to three or four component models which serve as a starting point for certain experimental studies. To recalculate the analyses as shown in Figure 1, it has been necessary to make several assumptions. Si, Al, Fe, Ca and Mg are the dominant cations; alkalies are present in subordinate amounts of at most a few weight percent and have been ignored, along with TiO_2, P_2O_5, and SO_3 (not appreciably soluble in most silicate phases). All iron in the "natural" slags was reported in the original analyses as Fe_2O_3. Although this depends to a large extent on bulk chemistry, a more realistic approximation to Fe^{+3}/Fe^{+2} would be 0.20 at a temperature of 1400-1600°C and an oxygen partial pressure of 10^{-3} atm in a silicate melt.[7] An assumption of this sort does not involve an appreciable error in representation of bulk

chemistry for slags in which SiO_2, Al_2O_3 and CaO are major constituents. The Fe^{+3} recalculated in this way was combined with Al_2O_3, assuming ideality of substitution in the silicate phases present. MgO and FeO change the important qualitative aspects of the liquidus and subsolidus relationships little if substitution for CaO occurs in amounts up to 15 mole % FeO[8] and 5 mole % MgO[9]. For this reason, mole percent CaO + MgO + FeO have been combined in Figure 1 providing, it is felt, a more realistic yet simplified representation of slag bulk chemistry than would the neglect of MgO and FeO. Compositions of synthetic slags (Table 2) used in vaporization studies described below are also plotted in Figure 1, and it is apparent that they fall nearly within the distribution of the "natural" slags.

Compositions within the system $CaO-Al_2O_3-SiO_2$ provide the most useful starting point as a model system in the experimental study of equilibrium relations - to which of course K_2O must be added for MHD simulation. As Figure 1 and most of the other analyses given by Selvig and Gibson[7] indicate, K_2O-free compositions may be approximated as being made up of some combination of SiO_2, $Ca_2Al_2SiO_7$, $CaAl_2Si_2O_8$, $CaSiO_3$ and Ca_2SiO_4, as well as, for more CaO-rich compositions, CaO-rich calcium aluminates.

III. The MHD Environment

The open cycle coal-fired MHD systems currently under development[10,11] contain several post-combustion components where seed/slag interaction may occur: generator channel, diffuser, radiant boiler, and preheater. Within each, different conditions prevail, which are dependent upon the specific operation and design parameters of a given installation; the temperatures which are discussed in this section are therefore to be regarded as a first order approximation. Plasma passing through the generator, including entrained slag droplets, will approach the combustion temperature of 2400-2600°C. Wall temperatures within the generator at the plasma/slag interface are much lower, near 1300-1400°C.[12] The temperature of plasma entering a radiant boiler section could approach 2100°C, while that leaving might typically be 1700°C. Preheater entrance and exit temperatures would thus be approximately 1700 and 1300°C respectively, while plasma entering a seed condenser at 1300°C would be cooled to 1000°C or below at exit.[11]

Superimposed upon these MHD temperature regimes is the partial pressure of potassium, P_K, which depends upon the percentage of seed added, as well as the temperature.[3] P_{O_2} similarly shows a strong dependence upon temperature for a given equivalence ratio, but it may be expected to be within the 10^{-2} - 10^{-5} atm range at generator wall surface temperatures,[13] subject to modification by transverse MHD effects.

Principal seed/slag interaction will occur upstream of the condenser section. In combustion systems containing appreciable amounts of sulfur, some of the seed condenses as K_2SO_4 and can be recovered by washing the slag and fly ash with water. The condensation temperature of K_2SO_4 in a combustion system free of slag seeded with sufficient K, as K_2SO_4, to provide a potential atomic concentration which is 1 wt% of the combustion products, is estimated to be about 1325°C.[14] At temperatures above 1325°C slag can still dissolve appreciable amounts of potassium as K_2O. Condensation of K_2SO_4 in the MHD system should therefore be viewed as a mechanism of recovering seed which has not yet reacted with slag.

From the standpoint of significant seed/slag interaction, two temperature regimes must be considered for each section - that of the plasma, and that of the wall accumulations. Interactions within the plasma of the generator channel will have the dominant effect on material passing directly through the system due to higher temperatures - given short residence times, it is doubtful if substantial reequilibration will occur further downstream, except possibly in the preheater. The wall accumulations, on the other hand, are characterized by longer residence times, of length sufficient for appreciable equilibration. Alkali penetration, especially, is expected to reach equilibrium values in the hotter portions of this temperature regime (estimated at 1300-1400°C). Material is eventually removed from walls by run-off or spall-off.[11,12] Results from one test facility[11] suggest that wall accumulations may be separated from plasma-entrained droplets in the seed/slag separator deposits on the basis of particle size. These results indicate that roughly 50% of the coal ash + seed accumulated on walls downstream of the combustor, and 50% passed through the system into the separator without first being deposited on the walls. Obviously, less K_2O will be absorbed by slag carried directly along with the plasma while the material deposited on the walls at 1400°C and below has potential for significant K_2O absorption.[3] The quench experiments described below and their discussion have application primarily to wall slag accumulations. The potassia vaporization studies have application to higher temperature plasma/slag interaction in addition.

IV. Quench Experiments on $K_2O-CaO-Al_2O_3-SiO_2$ Mixtures

Quench experiments were conducted in sealed platinum capsules at 1300-1400°C as summarized in Table 1 below. Starting materials were crystalline single-phase compositions weighed out in a dry box, calcined at the appropriate temperature, and characterized by x-ray diffraction. Products were maintained at temperature in a Pt-wound quench furnace, as monitored with an NBS-calibrated optical pyrometer or a Pt/Pt 10% Rh thermocouple calibrated against the melting points of palladium and gold. Runs were quenched in water, opened,

Table 1. Quench Experiments in the System $K_2O-CaO-Al_2O_3-SiO_2$.

Composition (mole fraction)	Temp. °C	Duration hr	X-ray Examination of Results
$(KAlSiO_4)_{.5}(CaAl_2Si_2O_8)_{.5}$	1395±10	12	glass (dominant) + α-Al_2O_3 (trace)
$(KAlSiO_4)_{.5}(\beta\text{-}CaSiO_3)_{.5}$	1396±10	12	glass (dominant) + orthorhombic $KAlSiO_4$
$(KAlSiO_4)_{.5}(Ca_2Al_2SiO_7)_{.5}$	1394±10	12	orthorhombic $KAlSiO_4$ + $Ca_2Al_2SiO_7$
$(KAlSiO_4)_{.5}(\gamma\text{-}Ca_2SiO_4)_{.5}$	1397±10	5	orthorhombic $KAlSiO_4$ + α_L'-Ca_2SiO_4 [a]
$(K_2Si_2O_5)_{.5}(CaAl_2Si_2O_8)_{.5}$	1368±10	36	$KAlSi_2O_6$ (dominant) + orthorhombic $KAlSiO_4$ + glass
$(K_2Si_2O_5)_{.5}(Ca_2Al_2SiO_7)_{.5}$	1391±10	14	orthorhombic $KAlSiO_4$ (dominant) + α_L'-Ca_2SiO_4 [a]
$(KAlO_2)_{.5}(CaAl_2Si_2O_8)_{.5}$	1395±10	12	orthorhombic $KAlSiO_4$ + glass
$(KAlO_2)_{.5}(\beta\text{-}CaSiO_3)_{.5}$	1384±10	6	$E_{1-\alpha}(Al_{1-\beta}Si_\beta)O_2$ (dominant) + $E_{1-\alpha}Al_{1-\alpha}Si_{1-\alpha}O_4$ + γ-Ca_2SiO_4 [b]
$(KAlO_2)_{.5}(Ca_2Al_2SiO_7)_{.5}$	1397±10	11	$E_{1-\alpha}(Al_{1-\beta}Si_\beta)O_2$ + $Ca_2Al_2SiO_7$
$(KAlO_2)_{.5}(\gamma\text{-}Ca_2SiO_4)_{.5}$	1395±10	12	$E_{1-\alpha}(Al_{1-\beta}Si_\beta)O_2$, $\alpha < 0.2$ + γ-Ca_2SiO_4 [a] + unidentified phase (trace)

[a] Ca_2SiO_4 was poorly crystallized and gave diffuse x-ray powder patterns, making identification of the polymorph present tentative.

examined for evidences of melting, and analyzed by x-ray diffraction.

Examination of results leads to the conclusion that $KAlSiO_4$ and Ca_2SiO_4 coexist at 1400°C. Results further show that $K_{1-x}(Al_{1-x}Si_x)O_2$ solid solutions coexist with $K_{1+x}Al_{1+x}Si_{1-x}O_4$ and Ca_2SiO_4 and that $KAlSiO_4$ and $KAlSi_2O_6$ coexist with liquids in the plane $KAlO_2$-SiO_2-CaO.* Taken together, these observations strongly suggest that the plane $KAlO_2$-SiO_2-CaO is a true ternary system over most of its extent. This contention is supported by isolated observations of other workers, as well.[15] For MHD applications this is helpful, for it means that the effect of adding CaO to compositions rich in $KAlSiO_4$, a compound shown to be a constituent of MHD fly ash and thought to be responsible for tying up a large fraction of the unrecoverable K_2O,[16] can be demonstrated within the model system K_2O-CaO-Al_2O_3-SiO_2. Referring to Figure 2, if CaO is progressively added to compositions near $KAlSiO_4$, three-phase fields A, B and C are successively encountered. If a slight excess of Al_2O_3 is present, a_{K_2O} is fixed at progressively higher values within each three phase field. Within the two-phase field $K_{1-x}(Al_{1-x}Si_x)O_2$ - Ca_2SiO_4, a_{K_2O} increases continously from the value of B to that of the three phase assemblage C.

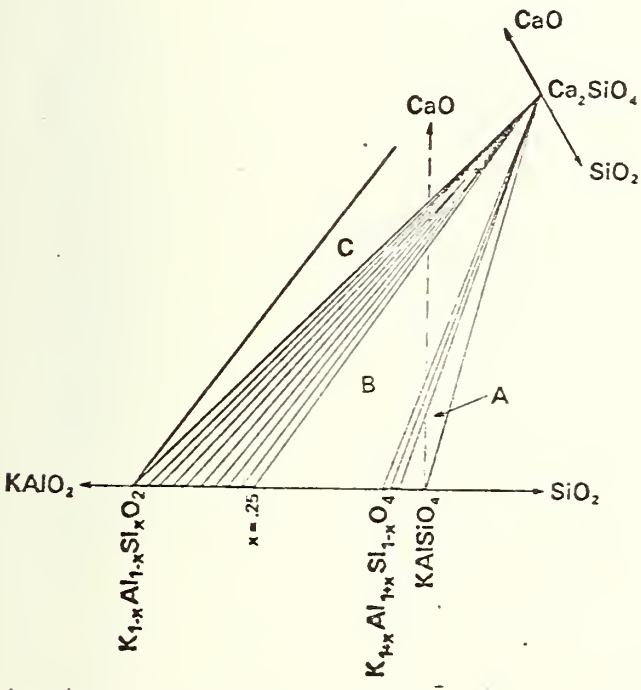

Figure 2. Effect of adding CaO to compositions rich in $KAlSiO_4$ and near the ternary plane $KAlO_2$-SiO_2-CaO.

Other experiments in Table 1 demonstrate the relative stability of $K_{1-x}(Al_{1-x}Si_x)O_2$ solid solutions with $Ca_2Al_2SiO_7$ and the existence of a [relatively] low melting region of Ca-rich liquids between $KAlSiO_4$ and $CaSiO_3$ and between $KAlSiO_4$ and $CaAl_2Si_2O_8$. These experiments indicate a strong partitioning of K between K_2O-Al_2O_3-SiO_2 solids and CaO-Al_2O_3-SiO_2 solids and liquids. Again, this may be significant for MHD applications. The importance of slag bulk chemistry can be shown in determining: a) melting properties, b) absorption of K_2O, c) tendency to form solid compounds which are insoluble ($KAlSiO_4$) or relatively soluble in water ($K_{1-x}(Al_{1-x}Si_x)O_2$) as the case may be.

The addition of other components may alter these effects. FeO should expand the liquid region at any given temperature as well as affecting other slag properties such as viscosity and electrical conductivity.[17] It is expected that for a given FeO content, addition of CaO will still raise a_{K_2O} for most bulk compositions. This must be demonstrated more conclusively than can be done with the two synthetic slags studied in this paper, however.

V. Vaporization of Potassia From Synthetic Slags

NBS has an active program on characterization of the viscosity of slags and the effects of various components thereon. To carry out these measurements, large samples of complex, homogeneous, synthetic slags have been prepared.[18] These slags are well characterized with respect to composition except for the content of dissolved gases which they can absorb since the preparation and measurement is carried out in contact with the atmospheric environment. Also, the oxidation state of the iron oxide dissolved in the slag is unknown.

The object of the vaporization measurements is to measure the activity of K_2O in the liquid slag solution. The primary vaporization process is

$$K_2O \text{ (dissolved in slag)} = 2K(g) + 1/2\ O_2(g)$$

The activity of K_2O in the slag phase is defined as

$$(P_K^2 \cdot P_{O_2}^{1/2})_{slag} / (P_K^2 \cdot P_{O_2}^{1/2})_{K_2O(\ell,\ pure)}$$

These data can then serve as a measure of the activity of K_2O in the liquid slag solution. If data is available over a range of temperatures and compositions, calculation of the K_2O concentration in the slag phase in equilibrium with specified K(g) and O_2(g) pressures in the plasma phase is possible. In the present paper, however, we will compare only the measured K(g) pressures measured over two different synthetic slags with the K(g) pressures previously measured over K_2O - SiO_2 solutions at NBS.[3]

Ideally, measurements should be made under conditions where the slags are entirely liquid and the amount of K_2O loss should be kept to a minimum so that the sample composition remains essentially constant. In practice, some of the measurements extended into the region where crystallization of some of the slag components is possible. Since the slag contains some dissolved gases, sample sizes were kept small (100 mg) to avoid having the sample ejected from the crucible by evolution of gas when the slag becomes fluid. At higher temperatures, fractional loss of K_2O from the sample is appreciable and concentration changes are important. The specific data points are therefore primarily of qualitative significance.

*Further details will be submitted for publication in American Mineralogist.

Measurements were made using a modulated beam, mass spectrometer. The slag sample was contained in a platinum Knudsen cell having a 0.5 mm diameter orifice. Temperatures were read in the orifice of the effusion cell with an optical pyrometer through a prism, window, and the modulation disk. Temperatures were corrected for the reflection of light at the prism and window and for the 50% transmission of the modulation disk. Ion currents due to mass peaks of interest (primarily K^+ and O_2^+) were measured on a lock-in amplifier. Ions were generated by electron bombardment of neutrals at 20 volts. The modulated beam system measures only that signal in phase with the reference signal which is generated by a light and photodiode on either side of the modulation disk.

The pressure of K(g) was determined from the relationship

$$P_K = k_K \cdot I_K^+ \cdot T$$

where k_K is an instrument constant for K of mass 39, I_K^+ is the ion current and T is the absolute temperature. The value of k_K was evaluated from the vaporization of a known amount of K_2O from the slag solution at known temperature and periods of time. The assumptions required in order that this calibration procedure be valid are that the only significant vaporization products from the slag phase are K(g) and O_2(g) having a formal stoichiometry of K_2O and that this accounts for all of the observed weight loss. The ratio of P_K/P_{O_2} over the slag solutions was compared with that obtained from similar mass spectrometric measurements performed in this laboratory on $KAlSiO_4$(s) and K_2O-SiO_2 solutions. In contrast, the ratio for the slag solutions was less than expected below 1200°C and greater than expected above 1200°C. During most of the measurements the O_2 pressure was about twice the value expected for a solution in which the vaporization of K_2O controlled the O_2 pressure. It is presumed that "Fe_3O_4" in the slag is responsible for this behavior. No attempt was made to account for the excessive O_2 pressure in making the calibrations. The potassium pressure is dependent on the oxygen pressure to only the 1/4 power so doubling the O_2 pressure would decrease the K pressure only by 20%. Vaporization of species from the slag such as Fe(g) and SiO(g) were negligible throughout the temperature range of these studies.

Data have been obtained on two synthetic slags having the initial compositions shown in Table 2. The choice of slag K512 was made in part to test the idea that slags high in calcia would have a relatively high K_2O activity while slag K531 was selected in order to determine the effect of relatively high SiO_2 and Al_2O_3 content.

Table 2. Initial Compositions of Synthetic Slags (wt%).

Component	K512	K531
SiO_2	30.00	48.00
Al_2O_3	11.25	20.00
Fe_3O_4	11.25	8.00
CaO	15.00	2.40
MgO	7.50	1.60
K_2O	25.00	20.00
	100.00	100.00

Potassium pressures for the K512 and K531 slags are shown in Figures 3 and 4. In each figure, the measured K(g) pressures are plotted along with curves representing the K(g) pressure over solutions of K_2O in silica with indicated weight percentages of K_2O as previously determined at NBS.[3] Each figure shows the concentration range of the slag for an experimental sequence during which temperatures were generally increased from one constant temperature to another. An exception to this procedure occurred for the data ranging from 15.9-10.5 wt% K_2O in Figure 3 for which the temperatures were decreased between measurements after a maximum temperature of about 1500°C was obtained. The different concentration ranges were obtained during evaporation of the same sample. The concentration ranges indicated were obtained from the mass calibrations and integrated ion intensities. Data points connected by a vertical line were obtained at a fixed temperature. Increase or decrease in pressures is indicated by an arrow on the vertical line.

Both slag samples show significantly higher K pressures than would be expected for slags having the same K_2O concentration but containing only K_2O and silica. The K pressures over slag K512 are higher than those over a 30 wt% K_2O-SiO_2 solution until the K_2O composition has decreased to only 10 wt% of the sample. The K pressures over slag K531 while not as high as those over the K512 slag are higher than those over a 20 wt% K_2O-SiO_2 solution when the K531 slag contains only 13 wt% K_2O. The implication of these results

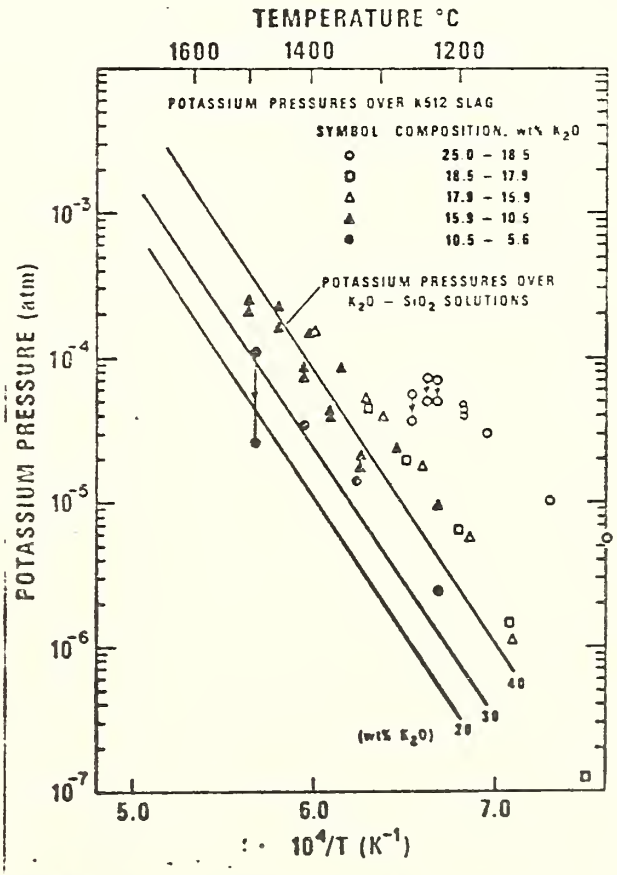

Figure 3. Potassium pressures as a function of $10^4/T$ and varying composition over K512 slag.

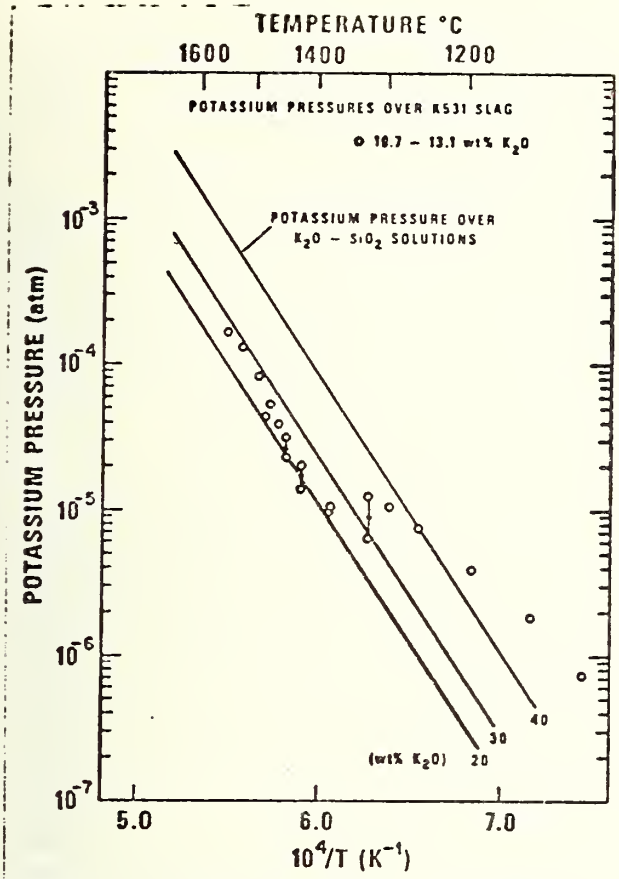

Figure 4. Potassium pressures as a function of $10^4/T$ and varying composition over K531 slag.

is that simple seed-slag calculations in which one uses data for pure K_2O-SiO_2 solutions to model the interaction will predict a concentration of K_2O in the slag solution which is 2 to 3 times greater than that which would actually be obtained. The idea that high calcia content in a slag will increase the K_2O activity by reducing the SiO_2 activity appears to be correct.

Comparison of K pressures over slags K512 and K531 with each other are probably quite valid but comparison of these pressures with pressures over K_2O-SiO_2 solutions must be considered more tenuous because of the possibility of systematic errors between the two different experimental techniques. These latter comparisons must be considered tentative until tested experimentally.

The data presented in Figures 3 and 4 show some unexpected effects. Samples placed in the effusion cell were coarsely ground. The pressures measured initially over these samples are significantly higher than the pressures measured later after the slags had become sufficiently fluid to flow into a molten pool. Thus in Figure 3, the initial series of points show relatively high pressures until they go through a maximum at about 1250°C. In this pressure range the rate of loss of K_2O would not be expected to be sufficiently high to cause the large decrease in pressure because of a concentration change. Likewise, the data in Figure 4 show a noticeable decrease in pressure at about 1350°C. It is noteworthy that the K531 slag is about 250 times as viscous as the K512 slag.[10] The temperatures at which the pressures decrease is believed to be the softening point of the slags.

Two possibilities exist to explain this behavior. First, if some crystallization of the slag had taken place, the glassy phase might have a much higher K_2O concentration than the bulk composition. When the slag became sufficiently molten, the crystallized phase might redissolve in the melt leading to a decrease in the K_2O concentration. The second possibility is that the decrease in pressure is a consequence of reducing the sample area. If this is the case then the pressures measured over the liquid melts do not represent equilibrium saturation pressures and the rate of transport of K and O_2 from the slag to the vapor phase above the slag is kinetically controlled even under the relatively ideal conditions of a Knudsen cell. This would probably mean that present thermodynamic estimates of seed-slag interaction are too pessimistic. This effect needs to be examined carefully to determine which or what combination of these possibilities is responsible for this behavior.

An additional factor bearing on whether or not equilibrium is attained was noted. During vaporization of the K531 slag it was observed that the K^+ and O_2^+ ion currents were not constant but increased for short periods by as much as a factor of two from their nominal values at a temperature of about 1450°C. This behavior had been observed previously in this laboratory during measurements on the vaporization of K_2O-SiO_2 melts. At that time it was assumed that it was due to sample inhomogeneity. The K531 sample however had undergone a great deal of stirring and homogenization during its preparation and use in viscosity measurements so an inhomogeneous sample would not be expected. A common property of the K_2O-SiO_2 melts and the K531 slag is their relatively high viscosities. Since both of these samples had been melted in an air environment they would be expected to be saturated. When heated in vacuum, air can be released. An attempt to observe release of dissolved gases was made by monitoring mass peaks such as H_2O^+, N_2^+, K^+, O_2^+, and CO_2^+ by making simultaneous measurements of two of the peaks on the A.C. (chopped) channel and D.C. (unchopped) channel of the spectrometer. The result was that simultaneous increases in the K^+ and O_2^+ signals could be observed regardless of which channels they were monitored on while increases of N_2^+, CO_2^+ or H_2O^+ were not observed when increases in O_2^+ or K^+ took place. However, in D.C. spectrometry there are relatively large background signals at these mass positions so that increases might be difficult to observe. In A.C. spectrometry, the H_2O^+, N_2^+, and CO_2^+ mass positions have very small signals and any pressure burst would be averaged out by the relatively large time constant of the amplifier. A rough calculation shows that over 99% of the gas released by a bubble of sufficient size to initially raise the partial pressure of the trapped gas to 10^{-4} atm in the Knudsen cell would have effused from the cell within .3 sec.

Presumably, if a bubble could form on the surface of the slag it would disturb the slag layer when it burst. The ensuing disturbance would bring a fresh layer of slag to the surface which would have a higher surface concentration than the undisturbed surface layers. Evaporation

of the fresh K_2O surface layer would give rise to the observed increases in the K and O_2 pressures. This again would be evidence that equilibrium pressure measurements are not being obtained.

Verification of the observations thus far made is important. If equilibrium measurements have not been obtained on the K512 and K531 slags, it is likely that previous measurements of the activity of K_2O in K_2O-SiO_2 solutions are too low because of unsaturation effects. Experimental investigations of these possibilities will be attempted by decreasing the size of the effusion orifice to see if pressure increases at fixed temperatures and K_2O concentration can be observed.

VI. Conclusions

Experiments on K_2O-CaO-Al_2O_3-SiO_2 mixtures demonstrate partitioning of K_2O between K_2O-Al_2O_3-SiO_2 solids and CaO-Al_2O_3-SiO_2 solids or CaO-rich liquids. Addition of CaO to $KAlSiO_4$-rich compositions causes a corresponding increase in a_{K_2O}. Potassium pressures over two synthetic slags were compared to K pressures over K_2O-SiO_2 solutions having similar K_2O concentrations and were found to be significantly higher. One slag with a relatively high calcia content had a K pressure higher than K_2O-SiO_2 solution with 30 wt% K_2O when the K_2O component had decreased to 10 wt% of the sample. The second slag with a relatively high SiO_2 and Al_2O_3 content showed a K pressure above that of K_2O-SiO_2 solution with 20 wt% K_2O when its K_2O content was about 13 wt% K_2O. Vaporization phenomena which might be ascribed to non-equilibrium behavior were observed. Further studies to investigate these effects are planned.

VII. Acknowledgements

We would like to express our appreciation to Dr. W. Haller of the Inorganic Glass Section for an enlightening discussion on the vaporization behavior of glasses and to Webster Capps who provided the slag samples. This work was sponsored in part by ERDA, Office of Fossil Fuels.

VIII. References

1. F. E. Spencer, J. C. Hendrie, Jr., and D. Bienstock, Sixth International Conference on Magnetohydrodynamics Electrical Power Generation, Washington, D.C., June 1975, II, 181.

2. L. W. Crawford, K. E. Tempelmeyer, J. Martin, and J. Muehlhauser, Ibid II, 51.

3. E. R. Plante, C. D. Olson, and T. Negas, Ibid II, 211.

4. W. A. Selvig and F. H. Gibson, Bureau of Mines, Bull. 567 (1956).

5. W. A. Deer, R. A. Howie and J. Zussman, Rock-Forming Minerals, Volume 3 (Sheet Silicates) (1962).

6. W. A. Selvig and Henry Seaman, Carnegie Inst. Technol. Mining and Metallurgical Advisory Boards, Min. and Met. Investigations, Coop. Bull. 43 (1929).

7. E. M. Levin, C. R. Robbins and H. F. McMurdie, Phase Diagrams for Ceramists, (1964) 60.

8. Ibid., 204.

9. Ibid., 210.

10. H.P.R. Frederikse, T. Negas and S. J. Schneider, Development, Testing and Evaluation of MHD-Materials, Quart. Rept. Oct-Dec 1975.

11. University of Tennessee Space Institute, Development Program for MHD Direct Coal-Fired Power Generation Test Facility, Quart. Prog. Rept. Nos 1,2; Month. Tech. Prog. Rept. July, August, September 1975.

12. D. B. Stickler and R. DeSaro, Sixth International Conference on Magnetohydrodynamic Electrical Power Generation, II, June 1975, 31.

13. E. M. Levin, S. J. Schneider, and E. R. Plante, 13th Symposium on Engineering Aspects of Magnetohydrodynamics, March 1973, IV.5.1.

14. C. L. McDaniel and E. R. Plante, 14th Symposium on Engineering Aspects of Magnetohydrodynamics, April 1974, IV.6.1.

15. T. I. Avdeeva and A. A. Novolodskaya, Izv. Sibirsk. Otd. Akad. Nauk SSSR. Ser. Khim. Nauk 2, 82 (1964).

16. C. Karr, P. Waldstein, J. J. Kovach, J. Inst. Fuel 47, 177 (1974).

17. Theodor Myslivec, Sb. Ved. Pr. Vys. Sk. Banske Ostrave. Rada Hutn. 20, 39 (1974).

18. S. J. Schneider, W. Capps, H.P.R. Frederikse, W. R. Hosler, D. A. Kauffman, E. M. Levin, C. L. McDaniel, T. Negas and E. R. Plante, NBSIR 74-543 (1974).

JOINT TEST OF AN U. S. ELECTRODE SYSTEM IN THE U.S.S.R. U-02 FACILITY

W. D. Jackson
Energy Research and Development Administration, (U.S.A.)

S. J. Schneider
National Bureau of Standards, (U.S.A.)

W. E. Young
Westinghouse Research Laboratory, (U.S.A.)

A. E. Sheindlin, G. P. Telegin and D. K. Burenkov
Institute for High Temperatures, (U.S.S.R.)

Abstract

The first (Phase I) joint U.S.-U.S.S.R. test of U.S. electrode materials was carried out in Moscow between September 25 and October 1, 1975 in the U.S.S.R. U-02 MHD facility. The test procedure followed closely a predetermined work plan designed to test five different zirconia based materials in cathode and anode electrode wall modules under MHD operating conditions. The electrode materials were: (in Mol %) $88ZrO_2:12Y_2O_3$, $82ZrO_2:18CeO_2$, $50ZrO_2:50CeO_2$, $25ZrO_2:75CeO_2$ and $20ZrO_2:78CeO_2:2Ta_2O_5$. Each of the five electrode materials had four different current densities established between the anode and cathode during the experiment which lasted a total of 127 hours; 100 hours under MHD power operational conditions.

Fourteen electrode pairs performed satisfactorily during the entire test. Five pairs failed early in the life test and the sixth pair failed in the last several hours. Failure was not due to the electrode materials, however, but due to lead-out melting caused by Joule heating in the platinum wires.

Extensive pre- and post-test materials characterizations were made to determine the effect of the MHD environment on the electrodes and insulators. Measurements included: thermal diffusivity, thermal expansion, chemical composition, microstructure, electrical conductivity, phase composition, closed and open porosity, pore size distribution, and radiography. Results indicate that there was extensive attack by the seed on the cathode wall causing chemical reactions and phase changes of the electrode materials. There was also seed penetration through cracks and pores in both insulator and electrode.

I. Introduction

As part of the U.S.-U.S.S.R. Cooperative Program on MHD, a series of joint tests are planned in the facilities of both countries to aid in the development of high temperature electrode systems and materials. Between September 25 and October 1, 1975 the first of these experiments was conducted in the U.S.S.R. U-02 facility on a section of a MHD generator consisting of U.S. designed anode and cathode modules and U.S.S.R. supplied insulating walls. The main objective of the test was to evaluate the behavior and performance of the electrode system and to establish the characteristics of the various materials of constructions (particularly electrodes and insulators) during long term operation under real MHD conditions.

The entire test, from conception to completion, was carried out on a joint basis with several organizations* in both countries participating in the various activities necessary to mount, conduct and analyze the experiment. The Materials Ad Hoc Working Group, with approval of the Standing Steering Committee on MHD, planned the overall experiment, formulated test objectives and criteria and generally provided guidance for the entire activity. The Energy Research and Development Administration (ERDA) sponsored U.S. activities with Westinghouse Research Laboratory having the responsibility for module design and construction and the National Bureau of Standards and Battelle Northwest Laboratory performing pre- and post-test materials characterization. The Institute for High Temperatures in the U.S.S.R. provided the U-02 facility for the test and in addition performed complementary materials characterization studies. The actual test carried out on the U-02 followed a predetermined work plan and was monitored by a joint working group consisting of six U.S. and six U.S.S.R. specialists, some of whom were always present at the facility.

---

* The following persons also participated in the planning of the work, the conduct of the actual experiment and/or aided in the preparation of this report:

From the U.S.:

G. Rudins (ERDA)
R. J. Wright (Westinghouse)
B. R. Rossing (Westinghouse)
J. L. Bates (Battelle-Northwest)
W. R. Hosler (NBS)
E. Farabaugh (NBS)
A. Perloff (NBS)
T. Negas (NBS)

From the U.S.S.R.:

V. V. Kirillov	IVTAN
O. B. Zamyslov	IVTAN
V. I. Zalkind	IVTAN
A. B. Ivanov	IVTAN
V. G. Gordon	IVTAN
D. A. Vysotskii	IVTAN
Yu. L. Dolinskii	IVTAN
A. I. Romanov	IVTAN

A complete report describing the entire test results and conclusions will be published separately. The purpose of this paper is to present a synopsis of the experiment including significant details on the electrode system design and construction, test conditions, materials performance and preliminary conclusions.

II. Electrode System

Module Design

Plasma property values needed for the design of the electrode system were derived from typical working conditions of the Soviet U-02 MHD facility. The fuel is natural gas containing by volume 97% methane, 2% ethane, and 1% inerts. Combustion occurs with an oxidant which is moist air with 1% moisture by weight and enriched with oxygen to the extent of 40% mole concentration in dry air. Seeding is accomplished by a 50%K_2CO_3 and 50% water mixture (total 1% by weight). At the entrance to the channel the design plasma conditions were: temperature - 2600K, static pressure - 0.80 atm and mass flow - 0.75 kg/s. Design heat fluxes at the channel entrance and exit were 30 W/cm^2 and 18 W/cm^2 respectively for the electrode walls.

The internal dimensional envelope of the channel as given by the facility operator specifies a height of 0.260 m and a width of 0.064 m yielding a constant cross-sectional flow area of 0.0166 m^2. For practical purposes the velocity in the channel was considered constant. With steichiometric combustion the plasma has an average density of 0.1 kg/m. Thus from continuity of mass the average channel velocity is 450 m/s. The magnetic field has a strength of 1.5 T which is constant over the length of the channel. The average plasma conductivity and mobility are 10 mhos/m and 0.7 m^2/Wb, respectively. The Hall parameter has a numerical value near unity (~ .95).

The MHD channel is the Faraday type. Figure 1 illustrates the pre-test cathode wall of the electrode system. In each of the electrode walls there are twenty separate electrodes with the pitch between electrodes being 24 mm. The electrodes proper were 12 mm long, 6 mm deep and 62 mm wide and have platinum lead-outs. Each electrode was individually housed in an insulator made of magnesium oxide. Electrode pairs were connected to separate loads; voltage between electrodes was estimated to be 15V. Channel insulating walls which separate the two electrode walls were designed and constructed by the Institute for High Temperatures of the U.S.S.R. Academy of Sciences. They consisted of hexagonal MgO blocks braised to a copper base.

The electrode modules were isolated from the channel support structure by a phenolic mounting material. In addition the heat sink of each electrode wall was sub-divided into five individual segments. Each heat sink consisted of a water-cooled (one inlet and one outlet) copper block which had been coated with an electrical insulating paint. All exterior surfaces of the heat sink were painted except where the magnesium oxide joined to the heat sink.

Preparation of Materials

The two electrode (anode and cathode sections) walls were made up of five separate segments each having four electrodes of the same material. The groups of electrode materials were (see Figure 2 for identifying number code):

I group = 88%ZrO_2:12%Y_2O_3 (mol %)
II group = 82%ZrO_2:18%CeO_2
III group = 50%ZrO_2:50%CeO_2
IV group = 25%ZrO_2:75%CeO_2
V group = 20%ZrO_2:78%CeO_2:2%Ta_2O_5

The requirements of good resistance to both thermal stress damage and seed attack demand careful control of microstructure and microchemistry for both electrodes and insulators. Thermal stress damage resistance can be increased by the presence of such crack arresting microstructural features as pores, microcracks, and second phases. In single phase materials this can be accomplished by use of a wide variation in grain structure and a moderate level of porosity. Seed resistance is achieved by low and/or closed porosity and low levels of impurities (absence of secondary phases at grain boundaries). Both electrodes and insulators are thus fabricated by making dense high porosity grain, followed by sizing, pressing and refiring. The fabrication details for both electrodes and insulators are detailed in the following discussion.

High purity, reactive powders were used as starting materials for the electrodes. These materials, ZrO_2, CeO_2, Y_2O_3 and Ta_2O_5, were purchased from commercial sources and are claimed to be greater than 99.9% pure with less than 100 ppm of either Fe_2O_3 or SiO_2. The particle size (average) of the ZrO_2, Y_2O_3, CeO_2 and Ta_2O_5 powders were 1.5, 4.5, 6 and 11 microns respectively. A slurry was prepared consisting of distilled water, 1200 g of oxide powder and organic binder (a mixture of polyvinyl alcohol and polythylene glycol). This slurry was milled in a rubber lined ball mill filled with yttria stabilized zirconia balls and introduced into a spray drier to form a free flowing, homogeneous powder. These powders were, in turn, pressed at 30,000 psi into 300 to 400 g bars and subsequently fired for 14 hours at 1500°C.

The sintered bars were then crushed into fine particles using a laboratory crusher. Any iron contamination was removed by magnetic separation and leaching with acid solutions (to less than 30 ppm). The particles were subsequently sized by screening into three size fractions, a course (-30 +70 mesh) fraction, a medium (-70 +325 mesh) fraction, and a fine (-325 mesh) fraction. Additional fine (-325 mesh) material was produced by jet milling course grain material. The average particle sizes for the crushed -325 mesh and the jet milled powders were 15 and 6 microns, respectively. The three size fractions were mixed together in the ratio of 52 coarse to 15 medium to 33 fine. Polythylene glycol was used as an organic binder in pressing this granular mixture. Samples 14 mm x 35 mm x 8 mm were pressed at 15,000 psi on a double action press and fired at 1600°C in air. Linear shrinkages during this heat treatment was less than 2.0%. The final porosity of the five electrode compositions varied from 14.6 to 19.9%. The electrode was then machined to the desired dimensions using diamond grinding tools.

The electrodes were metallized using a commercial platinum paste. Four individual thin coats

were brushed on and fired. During the application and firing of the last three coats a platinum screen was also attached to the metallized surface. Finally a platinum (0.020") wire lead-out was welded to the platinum screen.

The magnesia insulators were purchased from a commercial source. A high purity fused grain of magnesia was sized and hot pressed to produce a body containing approximately 15% porosity. The processing parameters in producing this material are regarded as proprietary by the manufacturer. The hot-pressed blocks which were 152 mm x 152 mm x 36.5 mm were heated in air to remove any graphite pickup and then cut into blocks 1-2 mm larger than the desired insulator dimensions. These blocks were machined into the desired insulator dimensions and shapes.

Finally open spaces between the electrode and insulators in the module assembly were filled with a commercial zirconia phosphate cement. A calcia-zirconia cement also was used to fill voids in other parts of the channel not related to the electrode system.

Instrumentation

Thermocouples and voltage probes were located at various positions within the two electrode walls. Figure 2 is an open schematic of cathode and anode showing materials, identification digits and location of instrumentation. Three electrodes on the anode wall each had two platinum 13% rhodium-platinum thermocouples buried along the electrode centerline. As referenced from the channel entrance these were the first, fourth and seventeenth electrodes. Five electrodes had chromel-alumel thermocouples positioned at the interface between the ZrO_2 phosphate cement and MgO insulator. On the anode wall these thermocouples were the second, tenth and eighteenth electrode positions. On the cathode wall these thermocouples were in the sixth and fifteenth electrode positions. In addition there were sixteen chromel-alumel thermocouples positioned in the colder regions of both the anode and cathode walls. A single voltage probe was located at the center of the electrode at the first, ninth and seventeenth electrode positions on the anode wall and at the eighth and sixteenth electrode positions on the cathode wall. These voltage probes were used to determine the resistance of the lower half of an electrode.

On the cathode wall the fourth electrode position had an access hole for line of sight measurement of electrode surface temperature by an optical technique. This arrangement allowed the surface temperature of the fourth electrode on the anode wall to be measured directly. Just prior to entering the channel the plasma temperature was measured by the sodium line reversal method. Voltage probes also were located laterally and longitudinally on the top insulating wall to measure Hall and Faraday potentials. Thermocouples were buried at various depths in the MgO of the top insulating wall near the entrance, midpoint and exit of the channel.

III. Test Procedures, Operating Conditions and Electrode System Performance

The testing of the electrode modules in the U-02 facility followed a predetermined work plan. This plan or test procedure was divided into four primary phases:

Phase I (18 hours duration)

- pre-start tests of the electrode modules;
- heating of the system and selection of thermal conditions (no seed);

Phase II (6 hours duration)

- study of the electrical characteristics of the modules at the full working conditions;

Phase III (94 hours duration)

- operating life test at the full working conditions;

Phase IV (9 hours duration)

- cooling down the system (no seed);
- post-run tests and dismantling the channel.

The pre-start tests showed that the hydraulic and electrical characteristics of the section corresponded to the design specifications. In particular, the average insulation level between adjacent elements of the working section was equal to 50 kohms at an applied test voltage of 500 V.

Before igniting the combustor the system was heated by air electrically preheated to 250°C. Next the combustor was operated at the maximum possible turndown ratio which would support stable operation of the combustion chamber. The average temperature rise as read by the thermocouples mounted in the electrode modules was 50°C/min.

After a 30-minute hold period the combustion chamber was then gradually brought up to operating conditions (ϕ = 1). Oxygen enrichment then allowed the channel to be brought to life test conditions. The operating conditions of the loop for conducting the life tests of the electrode modules were established at values to achieve temperatures on the 4th anode between 1700°C and 1775°C. These were maintained during Phase II and Phase III of the experiment with an accuracy of ±5%. The following describe the working conditions:

Plasma temperature, K	2573
Total mass flow rate, kg/s	0.75
Static pressure, atm	0.83
Content of potassium in plasma	1.0 wt. %
Magnetic field	1.7 T

The hot surface temperature of Group I electrodes as measured by an optical pyrometer was 1710°C. The temperature of the electrode as measured by a thermocouple at a depth of 3 mm from the hot surface was 1180°C.

During Phases II and III three short duration excursions in the plasma temperature took place. The temperature change as measured by the in-depth electrode thermocouples was 360°C during 2 1/2 minutes in the first case and approximately 425°C during 5 minutes in the second case and 140°C in

2 minutes in the last case.

The loop was cooled during Phase IV according to the schedule in the reverse order of the warm-up period (Phase I).

Analysis of the thermal data revealed that the thermal flux on the electrode walls increased gradually in the course of preheating and then, with a few exceptions, was sufficiently stable or, at any rate changed within a fairly narrow range during the life tests (Phase III). There was however a gradual reduction of thermal flux by 20 to 25% during the period between the 39th hour and the 111th hour of the experiment. The average thermal flux during this period in the cathode module was 1.96×10^5 kcal/m^2- hour (23 W/cm^2) and in the anode module 1.94×10^5 kcal/m^2-hour (22.9 W/cm^2). Furthermore the thermal flux was not uniform along the electrode walls; the smaller thermal flux occurs where the thermocouples and the probes are located. Evidently, part of the heat is lost along the thermocouples and the probes. Also, it is possible that the thermal flux was reduced due to the loss of air seal and the leakage of cold air into the system.

Thermal flux data as well as the readings from the thermocouples placed inside the electrodes and in the MgO units, made it possible to estimate surface temperatures on the rest of the electrode units. These estimates established that the temperature of electrode units of the first cathode module exceeded the temperature of the first anode module by 50 to 100°C. Thus, surface temperatures were in the range between 1,750 and 1,800°C. Taking into consideration the reduction of thermal flux along the channel (which agrees sufficiently well with the calculated data) the surface temperature of the electrode units was evenly reduced in the downstream direction. The fifth cathode module had a gas side temperature between 1,650 and 1,700°C.

Also of interest is the change of temperature on the surface of the electrode when current passed through the electrode. During the 17th hour of the experiment, when the electrodes were for the first time under a load, the temperature of electrode 2101 (at the depth of 3 millimeters) increased by 40°C under a current of 5A (.73 A/cm^2) and at the beginning of the duration run by 80°C with 7.8A (1.12 A/cm^2). The Joule heating of composition V (anode 2517) was not very great; between 20 and 30°C at J=7.8A.

During the first 34 hours of the duration test the temperatures of the electrodes remained constant and the change with time of readings from the same thermocouples did not vary greatly, (as a rule no more than + 20°C). However, beginning with the 34th hour of the duration test (57th hour of the experiment) a temperature increase of 20 to 40°C.in one hour was indicated by all thermocouples readings. Subsequently, a slow increase occurred in temperature of the anode wall elements by some 20 to 40°C during the next 12 hours, upon which the electrode temperatures once again stabilized.

During the life test (Phase III) the electrodes of each material group were operated at four levels of current density: 0A/cm^2, 0.24 - 0.33 A/cm^2, 0.5 - 0.7 A/cm^2 and 1.2 A/cm^2. The operation of electrodes under current was attained by loading them with controlled resistance with an electrical load coefficient at K = 1 (open circuit), K = 0.2, to 0.5; K = 0 (short circuit) and K = (-0.2 to -0.3) (stagnation operating mode with additional current to electrode pairs from separate external voltage source).

The electrode couples numbers 9 and 17 (50% ZrO_2:50%CeO_2 and 20%ZrO_2:78%CeO_2:2%Ta_2O_5 i.e., compositions 3 and 5) had currents at 8.5A and 8.3A (1.18 to 1.2 A/cm^2); the electrode pairs numbers 2, 10, 14, 18 (compositions 1, 3, 4, and 5) had currents from 3A to 4.8A (0.43 to 0.68 A/cm^2); electrode couples numbers 3, 6, 11, and 18 (1, 2, 3, and 4 compositions) had currents of 1.6A to 2.18A (0.23 A/cm^2 - 0.31 A/cm^2). The deviations from the average values did not exceed 15 to 18%. These fluctuations could be explained on the basis of random changes in the thermal parameters of the loop, which were maintained to within ±5%. In addition to the random fluctuations mentioned above, a gradual reduction was observed in the applied voltage necessary to maintain the currents at the assigned level (from 30 to 60 volts down to 10 to 20 volts). Such a change could have little connection with anode-cathode resistance drops (current leaks could have accounted for about 0.5A by the end of the duration test). To a great extent this could have been caused by the drop of the effective internal resistance of the channel, due to the increase during the second half of the life test of the surface temperature on the anode wall (and judging by the decrease of thermal flux, a possible increase in possibly the cathode wall temperature as well). This could have led to a reduction of electrical resistivity of the near electrode boundary layers of the plasma.

During Phase III (life tests) discontinuities in electrical contacts were observed in six loaded electrodes (identified as due to platinum lead-out failures). The failing electrode pair and time to failure were:

Composition & Electrode Pair Mol %	Failure Time From Start (3rd Phase)	Current Density A/cm^2 (Nominal)
82ZrO_2:18CeO_2 1207-2207	7 min.	.65
82ZrO_2:18CeO_2 1208-2208	7 min.	1.10
88ZrO_2:12Y_2O_3 1101-2101	1 hr. 20 min.	1.10
25ZrO_2:75CeO_2 1415-2415	1 hr. 45 min.	.65
25ZrO_2:75CeO_2 1416-2416	2 hr. 20 min.	1.10
20ZrO_2:78CeO_2: 2Ta_2O_5 1517-2517	92 hr. 40 min.	1.10

The life test data basically indicates that the electrical parameters were stable and were within the set limits. The small deviations observed had a definite qualitative explanation. Overall, the electrical and thermal characteristics of the electrodes tested showed them capable of adequate performance on all the electrode pairs, with the exception of those which suffered distruction of the platinum current lead-outs.

IV. Materials Characterization**

Extensive pre- and post-test materials characterizations were made to determine the effect of the MHD environment on the electrode system as a whole as well as on individual electrodes and insulators. Pre-test measurements were used to obtain design information and to establish a base for comparison of post-test results. Pre-test examinations included measurements on: thermal diffusivity, thermal conductivity, chemical composition, microstructure, electrical conductivity, phase composition, porosity and pore size distribution.

Following the test and immediate examination visually, the modules were packed and shipped back to the United States where they were disassembled in such a manner to allow for extensive post-test examination. These analyses involved phase composition and chemical reactions, electrical conductivity, metallography, electron microprobe studies and radiography of current lead-outs.

The following describes some (not all) of the more significant results of the pre- and post-test analysis.

Pre-Test Analyses

Thermal Diffusivity: The thermal diffusivities of the MgO insulator and electrode materials were measured using a laser pulse technique from room temperature to 1750°C. The results for electrode materials are indicated in Figure 3.

Thermal Expansion: The thermal expansion of MgO insulator and electrode materials were measured from about 60°C to 1500°C using an alumina push rod dilatometer. Table 1 lists the coefficient of expansion for the various materials.

Chemical Composition: The compositions of the MgO and electrodes were determined by emission spectrochemical analyses (precision ±5%). The MgO contained less than 170 ppm total impurities. The compositions of the electrodes are given in Table 2.

Microstructure: The electrode and insulator samples selected for metallography were vacuum impregnated with resin and polished for microstructural details. A brief description is as follows:

(MgO) Normal to the hot pressing direction the pores were irregular in shape and uniformly distributed around the MgO particles with no apparent orientation. In contrast, in the direction parallel to the hot pressing direction, the pores appear smaller and are longer in one direction than the other. The smaller width is parallel to the hot pressing direction. The grains were very dense but show evidence of deformation. The average grain size is 10 μm with some grains as large as 0.02 cm. The pore size varied up to 5 μm across.

($88\%ZrO_2:12\%Y_2O_3$) The microstructure of the yttria stabilized electrode sections from the center and edge were essentially the same. However, they differed in color (off white to gray). The larger grains were round or oval in shape and contained a large number of very small pores uniformly distributed throughout. The size of the grains varied up to 65 μm. The edges of the large grains were irregular, indicating sintering between the oxide fines. Sintering was also extensive in the fines between the larger grains.

($82\%ZrO_2:18\%CeO_2$) The microstructure from the center and end of the electrode was essentially the same. A second phase was observed in some selected areas. The size of the large grains varied up to 0.065 cm.

($50\%ZrO_2:50\%CeO_2$) The electrode was mottled with a light yellow background and light gray areas. The middle was substantially darker than the end. The darker areas do not appear to be associated with any particular area. A possible second phase may also be present. The electrode contained a number of microcracks. The size of the large grains was as large as 0.065 cm.

($25\%ZrO_2:75\%CeO_2$) This high ceria-containing electrode was multi-colored, with large areas of yellow, tinted with green, which were interlaced with gray. These areas of different color were related to specific microstructures. Both sections contained a substantial number of cracks which ran parallel to the length of the sample. The large grains were approximately 0.065 cm or less in diameter.

($20\%ZrO_2:78\%CeO_2:2Ta_2O_5$) This electrode material was uniformly mottled with yellow-green background and very dark green spots. These dark green areas were directly related to the large crystallites of the material, while smaller particles are light green. The regular surfaces of the porosity in the areas which bind the larger particles together suggest the presence of a liquid phase during sintering. Some large and small cracks lace the electrodes, especially in the center section. The large grains were 0.065 cm or less in diameter.

Phase Composition: Table 3 lists pertinent x-ray diffraction data for the insulator and electrode materials. Phases present are characteristic of reaction products formed at elevated temperatures under relatively oxidizing conditions. Anode and cathode materials are identical.

Electrical Conductivity: The electrical conductivities of the electrode materials were determined using a d.c. four probe method in various oxygen partial pressures. Figure 4 illustrates typical values for 10^{-3} atm PO_2.

Post-Test Analyses

Physical Description: After completion of the test in Moscow, the electrode section was removed from the U-02 channel. Extensive photographs were

** Characterization activities are being carried out by both U.S. and U.S.S.R. sides. Because these measurements are not fully completed the pre- and post-analysis are based on primarily U.S. results. U.S.S.R. results are expected to conform to that reported here, although some firm conclusions may differ in degree since they depend upon interpretations of difficult experiments.

taken at this time of the electrode section before disassembly and after the electrode sections were removed from the insulating walls.

Immediately after the test visual inspection of the modules revealed:

(Condition of Joints) The joints between the module and the nozzle and diffuser did not leak during the test. However, seed penetrated into these joints to a depth of 10 to 15 mm. The Al_2O_3 spacers in most areas either swelled or reacted with seed. This effect was more evident on the cathode wall. Heavy seed concentration was noted in all joint areas.

(Electrode Condition) The electrodes showed traces of erosion, corrosion and cracking. Erosion and corrosion was greater on the cathode than on the anode. The electrodes exhibited swelling and spalling which was substantially greater on the cathode. The ZrO_2:Y_2O_3 compositions appeared to be less degraded. Electrodes under current exhibited greatest swelling.

(Inter-electrode Insulator Condition) The MgO insulators, in general, were eroded at the joints between the insulators to a depth between 1-3 mm with the cathode side being more affected. The insulators were cracked longitudinally near the centers of the insulator. This condition was present in both anode and cathode walls. The greatest destruction occurred near electrodes working at maximum current.

(Insulation Walls Condition) The general appearance of the insulating walls remained unchanged for the most part. Differences in color were noted.

Microstructure

Each sub-module was sliced (using a diamond saw and ethylene glycol as coolant) perpendicular to the electrode surface and lengthwise, parallel to the plasma flow. Three slices, each approximately 5 mm thick, were removed from each sub-module for various studies. Figures 5 and 6 show a composite of anode and cathode slices.

The highest concentrations of potassium were associated with the cathode side of the channel, especially in that portion of the materials which were at operating temperature of approximately 700 to 1300°C. In the MgO, cement, and in some electrodes, the potassium is associated with the lower density, porous areas which surround the large oxide particles. Potassium is also found in cracks. It appears that the transport of potassium in the oxide is directly related to the open porosity associated with the low density structure of the materials. Little potassium is found on or near the plasma surface of the MgO or cathode. Some potassium was found on the anode surfaces.

The MgO insulator exposed to the plasma had recrystallized to depths as much as 0.4 cm. Although not observed in all electrode pairs, the recrystallization of the MgO generally consisted of three different structures.

(1) Dense band near the surface which varied in width from 0.02 to 0.10 cm. This layer was 3 to 5 times wider on the cathode side than on the anode. This layer also contained a second phase composed principally of zirconia and calcia. However, on the downstream electrodes, this phase also contained increasing amounts of cerium.

(2) Columnar type grains extended to depths between 0.7-0.18 cm. (The depths were approximately the same for the cathodes and anodes.) These long grains were associated with a high porosity at the grain boundaries. On the cathode side, a second phase was found at the grain boundaries. This phase is thought to be a CaO stabilized ZrO_2 which contained more CeO_2 in the MgO downstream.

(3) Equiaxed grain growth occurred to a depth from the surface of approximately 0.3 to 0.4 cm. This recrystallization appears as a densification of the low density fines which surrounded the larger particles, in a decrease in the number of pores, and in an increase in pore size.

The erosion, degradation and recrystallization of the MgO appeared to be more severe on the MgO which was on the upstream side of the electrode. Perhaps associated with this effect, is the apparent increased reaction between the MgO, the cement and the upstream side of the electrode. This effect appeared to be more pronounced on the anode than on the cathode.

The cracking of the MgO appeared similar for all electrode assemblies. Cracks fanned out from the corners initiating at the machined recesses in the insulator. In most insulators, these cracks were found ~0.6-0.7 cm from the surface. Most of these cracks contained potassium.

The microstructure of each electrode pair was unique but some general conclusions may be made. The surface of most electrodes had recrystallized into a dense layer often with large spherical pores. This layer varied in thickness (0.02-0.1 cm) from electrode to electrode. With the exception of the 1103 cathode, the surface contained at least one and up to three phases, with the concentration of these second phases highest at the plasma surface. These second phases on the cathode were principally zirconia containing varying amounts of calcium and cerium. On the anode surface, more than one phase was found and in addition to the zirconia-calcia-ceria phase, phases high in alumina were present. Potassium was also found in some phases.

The phase compositions at the center of the electrodes also varied, and often contained more than one phase. Similarly, the electrode near the platinum current lead-out also was contaminated.

The cement between the electrode and insulation acted as a major sink of potassium concentration and possible path of seed transport into the MgO and electrode. The highest concentration of potassium in the cement was found in the cathodes and increased with current density. Total degradation of the cement occurred. Conversely, the cement associated with the anode remained intact, but contained ~10% potassium associated totally with the low density portion of the cement.

The Al_2O_3 spacers reacted with the potassium, but did not appear to react in any other way with the other materials. The higher temperature top edge of the sintered Al_2O_3 plate appeared to

form porous β-Al_2O_3.

Radiography of the lead-outs revealed that several failures occurred through the melting of the platinum wires. These failures do not appear to be due to chemical attack. It is suggested that in assembly, a scratch or bend was put into the lead wire in a region which was not surrounded by ZrO_2 cement. Joule heating developed and without the cement to carry away the heat, the platinum lead melted.

Electrical Conductivity: Since most electrode sections were cracked and eroded to some extent, it was impossible to remove each half electrode in its original condition. Measurement of electrical conductivity requires a sample of sufficient size to permit attachment of electrodes. Only those anode electrodes, 2102, 2205, 2206, 2207, and 2208 could be used for post-test electrical data.

It is difficult to reproduce in the laboratory measurement apparatus, the exact conditions that were present in the test facility plasma. The conductivity measurements are bulk measurements taken with the entire sample at the same temperature and in a particular atmosphere of oxygen partial pressure. No alkali seed was present in the measuring apparatus. It would seem likely that during the measurement, the condition of the sample could be considerably different from that actually existing while it was exposed to the test plasma.

However, the conductivity results do indicate that no permanent damage had been done to the anode electrodes measured since the pre- and post-test data are very similar. While the series of samples containing $82ZrO_2$:$18CeO_2$ have the lowest electrical conductivity of any material tested, its mechanical resistance to fracture on the anode is the greatest since all anode electrodes of this series were removed intact.

Phase Composition and Chemical Reactions: When the module was received, dismantled, and dissected, a visual observation of the electrodes immediately suggested significant alteration of the CeO_2 containing ZrO_2 materials at the cathode wall. These materials were severely bloated, fragmented, and banded, generally into three zones distinguished by white (top - 1-3 mm in thickness), yellow (1-3 mm below surface), and yellow to olive-green (bottom), colorations. These zones are not of constant thickness within an individual electrode, nor similar in thickness in electrodes of identical starting composition, but with varying current density. Generally, the discolored bands increase in thickness toward the outer MgO spacers. That the zones of discoloration are indicative of phase changes of original materials and of reaction with potassium seed was considered obvious. The bloating or swelling of cathode materials probably occurred during and after cool-down. Almost the entire cathode wall is saturated with seed, mostly as condensed K_2CO_3. This includes the underlying MgO blocks which were cracked extensively. When exposed to moisture, K_2CO_3 (as is well known) expands 40-60% (and ultimately dissolves) by hydrating. This expansion, abetted by the mismatch in the cohesion among zones of dissimilar phases and alteration products, and hence, dissimilar mechanical properties, most likely caused the swelling. Indeed, it is unlikely that the electrodes experienced bloating during operation as protruding material would have been swept away by the gas stream.

Numerous specimens were selected carefully from within each zone of discoloration of every electrode. The $88ZrO_2$:$12Y_2O_3$ electrodes are not zoned, but samples representative of the top, middle, and bottom portions were also taken. All specimens were investigated by x-ray diffraction powder analysis using filtered Cu-radiation.

The outstanding characteristics of all cathode CeO_2-containing materials are their; a) alteration through phase transitions, and/or b) reaction with potassium seed. A detailed account of phase transitions and chemical reactions in ZrO_2:CeO_2 materials is beyond the scope of this report. Several typical examples, displaying the alteration of the cathode materials, however, are given in Table 4.

Anode materials show little evidence associated with alteration by potassium seed. The distinct color zoning, typical of cathode electrodes, is not obvious although a faint yellowish discoloration is apparent at the bottom of some electrodes.

Generally, the hot surface material of anode electrodes tends to be monoclinic, cubic and/or tetragonal phases with smaller unit cells than the original bulk material. This suggests that the surface phases are richer in ZrO_2 and were formed via vaporization of cerium oxides. For example, the ZrO_2:CeO_2 compositions initially rich in ZrO_2 (82%ZrO_2:18%CeO_2, 50%ZrO_2:50%CeO_2) also show the formation of some monoclinic ZrO_2 on the surface. The crystallinity of surface materials is generally poorer (i.e., finer particles or more disorder) than the original materials, which is an additional indication of decomposition. Many of the samples have small amounts of a spinel phase (most probably $MgAl_2O_4$) on the surface.

MgO insulators (cathode and anode) were also investigated for potential chemical/phase changes by x-ray diffraction. Apart from the extensive amount of seed (as K_2CO_3 and/or K_2CO_3 hydrate) found beneath the cathode electrodes within the MgO, insulators exposed to the plasma were altered chemically at their surface. Surprisingly, x-ray lines corresponding to a cubic, spinel-like material are present in the typical MgO pattern. Virgin material does not contain this phase. If this material is a spinel, the small, cubic cell parameter suggests that it is $MgAl_2O_4$. This phase is also present in trace quantities at the surfaces of many of the anode materials and probably of cathode materials. If $MgAl_2O_4$ is the phase present, then Al_2O_3 somehow must have been transported via the vapor phase to react with available MgO. This may be important since it should be recognized that a chemical reaction leading to the formation of a new chemical species could have a degrading effect on the original mechanical/electrical properties of a virgin material.

Although this portion of this report is concerned only with the documentation of phase/chemical characterization of electrode materials, several related questions remain open to interpretation

and further study. Given that alteration of materials preceeded at the cathode at an accelerated rate with respect to the anode, how does seed reach, penetrate and react with materials? Is the difference in reactivity of cathode and anode with seed due to better sealing or higher working temperatures at the anode? If not, are alterations at the cathode accelerated by electrochemical means? It appears unlikely that seed as K(g) is the dominating factor, otherwise anode and cathode materials should reflect nearly identical chemical reaction phenomena. Possibly, $K^+(g)$ attracted from the plasma to and/or formed at the cathode surface (and attracted) according to $K(g) \rightarrow K^+(g) + e$ is the controlling factor. $K^+(g)$ at the anode necessarily would be repelled except, perhaps, for open circuit materials.

V. General Conclusions

Some general conclusions can be drawn even though the behavior of materials subjected to U-02 conditions is complex and analyses of results are difficult:

1. The effects caused by seed penetration are more pronounced at the cathode wall. In general, cathode degradation is substantially greater than at the anode.

a. All CeO_2:ZrO_2-based cathode materials within cooler zones show new phases typical of reactions with seed. Reaction intensity is more evident for current-carrying materials.

b. Within the ZrO_2-cements and MgO insulators below cathode materials, large quantitites of seed, condensed at K_2CO_3 and/or hydrate, are present.

c. Reaction with seed at the anode electrodes is significantly less pronounced and, generally occurs within localized interior zones.

2. Bloating of cathode materials apparently was caused by hydration and expansion of condensed seed during and after the cool-down period.

3. Contrary to the Y_2O_3-stabilized ZrO_2 materials, and the anode materials, CeO_2:ZrO_2 cathode materials appear to have been subjected to reduction *in situ* followed by complete to nearly complete reoxidation during shut-down. The phase transitions due to reduction are manifested particularly by the presence of monoclinic ZrO_2, together with certain additional phases.

4. Surface x-ray analysis, particularly of CeO_2:ZrO_2-anode materials, show depletion of CeO_2. The Ta-containing electrodes also show Ta-depletion.

5. Phase transitions leading to alteration of the microstructure of virgin cathode materials may have enhanced seed penetration. Cements also provide good avenues for seed penetration.

6. MgO insulators (anode and cathode), especially where exposed to the plasma, show compounds with Al_2O_3 and cubic zirconia from x-ray diffraction data. These may contribute to the alteration and the degradation of the erosion resistance of virgin materials.

7. Lead-out failure in electrode pairs was not caused by chemical attack, but rather by Joule heating and eventual melting. Evidence for presence of KCl within lead-out tubes indicated K-penetration within this area.

8. Electro-chemical effects probably enhanced degradation of the electrode materials. However other factors also were influential and the overall damage to the materials probably was caused by a combination of events.

9. ZrO_2:Y_2O_3 materials at the cathode show evidence for partial destabilization of cubic zirconia. Presently, it is unclear whether this process is related to seed reactions or electro-chemical phenomena.

10. Even though extensive degradation of materials occurred, the electrode system generally performed satisfactorily. It may be possible through improved microstructures to control the degradation and thereby permit the operation of these systems for longer times.

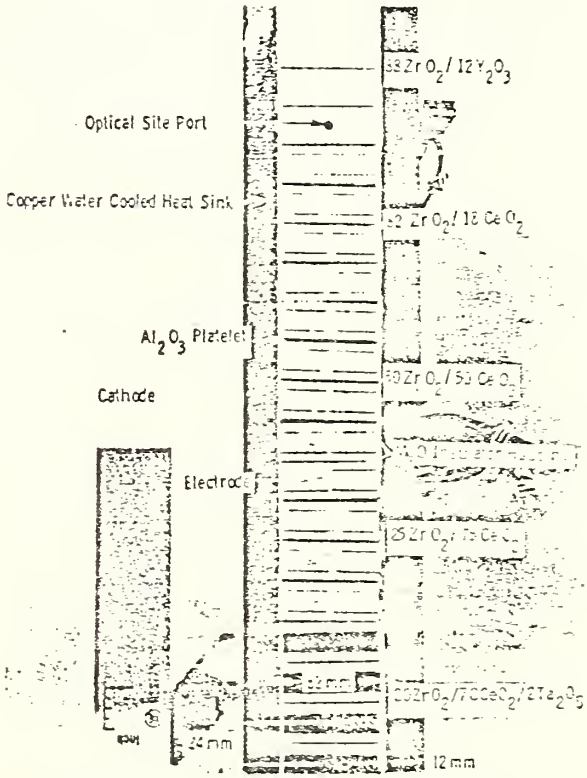

Figure 1. Plan View of Cathode Wall

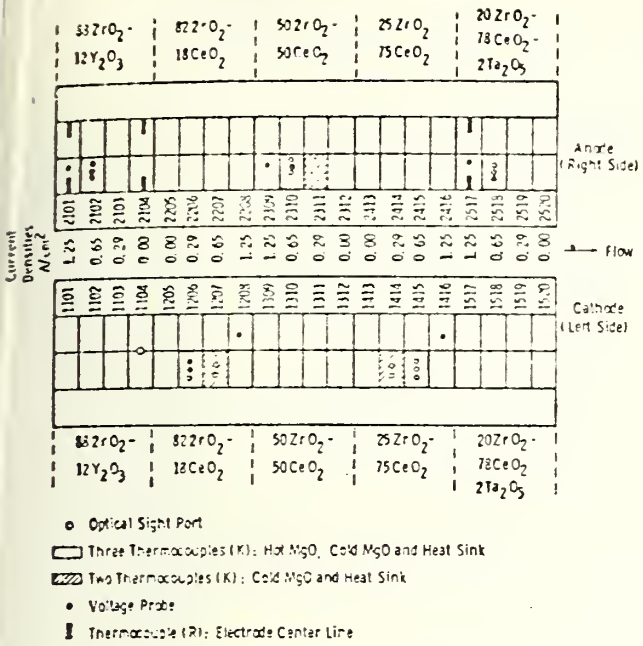

Figure 2. Open schematic of cathode and anode showing materials identification digits and location of instrumentation

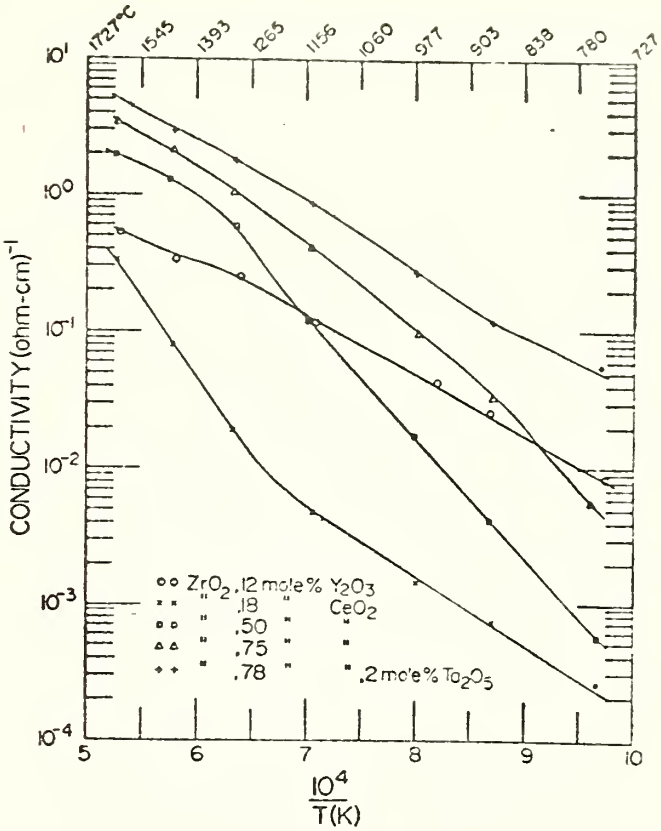

Figure 4. Electrical Conductivities of Electrode Materials at 10^{-3} atm Po_2

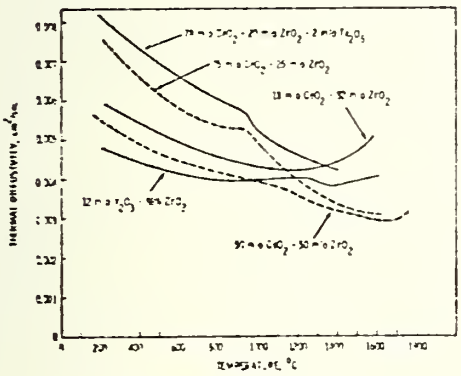

Figure 3. Thermal Diffusivities of Electrode Materials (Pre-Test)

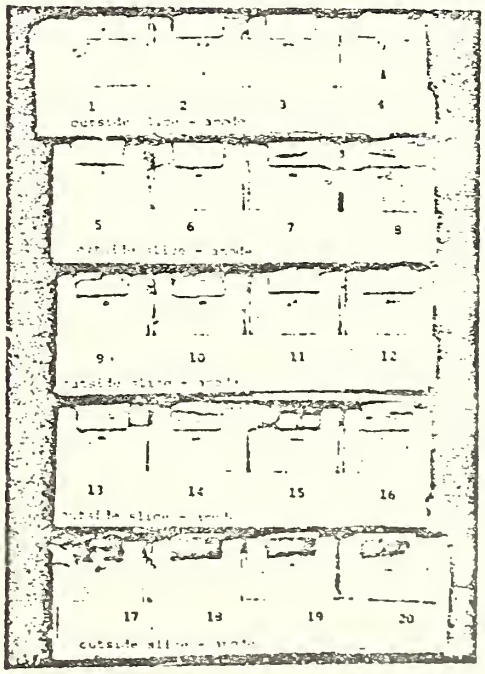

Figure 5. Anode Sections After Test

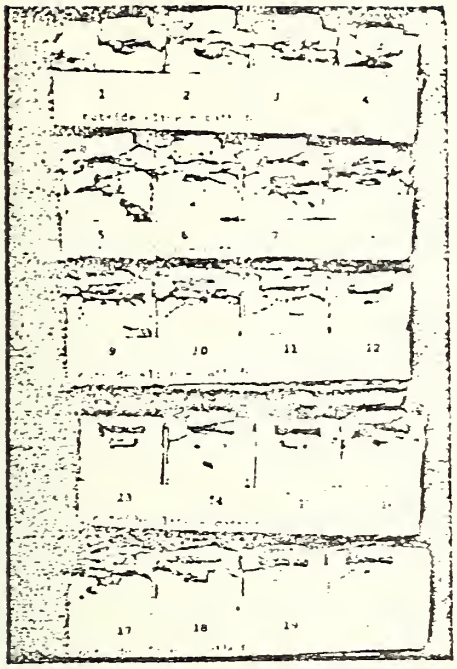

Figure 6. Cathode Sections After Test

TABLE 1

THERMAL EXPANSION OF MgO AND ELECTRODES

Material	$\alpha/°C(10^{-6})$*	
	Argon	Air
MgO	15.6 15.5	14.0
$12\%Y_2O_3:88\%ZrO_2$	12.3	10.9
$18\%CeO_2:82\%ZrO_2$	13.1	11.5
$50\%CeO_2:50\%ZrO_2$	13.6	12.2
$75\%CeO_2:25\%ZrO_2$	14.5	13.2
$78\%CeO_2:20\%ZrO_2:2\%Ta_2O_5$	14.9	13.6

* $\alpha = \frac{\Delta L}{L}$ where L = length

Differences in values probably due to stoichiometric changes caused by different oxygen pressures

TABLE 2

COMPOSITION OF ELECTRODE MATERIALS

Nominal	Measured*			
	ZrO_2	Y_2O_3	CeO_2	Ta_2O_5
	Mol %			
$12\%Y_2O_3:88\%ZrO_2$	88.8	11.2		
$18\%CeO_2:82\%ZrO_2$	78.8		22.2	
$50\%CeO_2:50\%ZrO_2$	46.2		53.8	
$75\%CeO_2:25\%ZrO_2$	19.6		80.4	
$78\%CeO_2:20\%ZrO_2:2\%Ta_2O_5$	16.5		82.2	1.3

*Determined by x-ray fluorescence techniques (results accurate to ±5%)

TABLE 3

PRE-TEST PHASE COMPOSITION (X-RAY ANALYSIS)

ANODE AND CATHODE MATERIALS*

Composition	Major Phases	Minor Phases
MgO	cubic a = 4.212Å	None
$12\%Y_2O_3$ $88\%ZrO_2$	f.c.c. a = 5.151Å	None
$18\%CeO_2$ $82\%ZrO_2$	tet a = 5.15Å c = 5.24Å	Trace of cubic (?)
$50\%CeO_2$ $50\%ZrO_2$	tet a = 5.26Å c = 5.30Å	f.c.c., a = 5.15Å
$75\%CeO_2$ $25\%ZrO_2$	f.c.c. a = 5.342Å	None
$78\%CeO_2$ $2\%Ta_2O_5$ $20\%ZrO_2$	f.c.c. a = 5.352Å	f.c.c., a = 5.37Å

*f.c.c. = face centered cubic (Fluorite)
tet = tetragonal; all compositions are white in color with exception of that containing $2\%Ta_2O_5$ (green)

TABLE 4

U-02, Phase I, Post-Test

POST-TEST PHASE COMPOSITION (X-RAY ANALYSIS) FOR CATHODE MATERIALS

Initial Bulk Composition (mol %)	Relative Position of Material Analyzed	Results Phases Present and Comments[1/]
$82ZrO_2:18CeO_2$ #1205 Open Circuit	upper 1-2 mm white material	Nearly pure mono ZrO_2 + f.c.c. solid-solution + cubic and/or tetragonal solid-solution
	white surface	Mono ZrO_2 + poorly crystalline f.c.c. and/or tet solid-solutions
	yellow interior zone	Mono ZrO_2 (strong) + (C_1), (strong), + a trace phase (P)
	yellow, olive-green bottom	Mono ZrO_2 + (P)-Phase (very strong)
$82ZrO_2:18CeO_2$ #1208 $1.25A/cm^2$	white zone, top	Mono ZrO_2 + two or more f.c.c. solid-solution phases
	yellowish interior zone plus small portion of white zone	Mono ZrO_2 + strong (C_1)-phase, $\underline{a}$=5.26A
	yellowish interior zone plus yellow-green bottom zone	Mono ZrO_2 + (C_1)-phase + (P)-phase
	yellow-green bottom zone	(P)-phase strong + Mono ZrO_2 + (C_1)
$50ZrO_2:50CeO_2$ #1312 Open Circuit	yellow interior	Almost pure (C_1)-phase $\underline{a}$=5.26A + trace mono ZrO_2
	yellow-green bottom	(C_1)-phase strong + additional cubic phases with similar but slightly larger $\underline{a}$ + trace (P)-phase
	top white zone + yellow zone	(C_1)-phase, + cubic solid-solution, + trace of a third cubic phase
$50ZrO_2:50CeO_2$ #1307 $1.25A/cm^2$	yellowish interior	Nearly pure (C_1)-phase, ($\underline{a}$=5.26A) + traces of mono ZrO_2 and a second cubic phase
	yellowish-green bottom	(P)-phase (very strong) + (C_2) $\underline{a}$=5.38A phase (strong) + small amount (C_1)-phase
$25ZrO_2:75CeO_2$ #1414 $.5A/cm^2$	white (top) zone	Two f.c.c. solid-solutions. Major phase, $\underline{a}$=5.35A; minor phase has larger $\underline{a}$
	yellow-brown bottom	Two f.c.c. phases. Major phase $\underline{a}$=5.38A, nearly that for pure CeO_2 ($\underline{a}$=5.42) (P)-phase also present
	dark yellow bottom	At least three cubic phases. Major phase $\underline{a}$=5.34A
$25ZrO_2:75CeO_2$ #1416 $1.25A/cm^2$	white (top) zone	f.c.c. a~5.34-5.35A + f.c.c. with slightly smaller $\underline{a}$
	white + yellowish zones	At least three cubic phases
	yellow-green bottom	At least three cubic phases + (P)-phase. Major phase has $\underline{a}$~5.38A (similar to pure CeO_2)

1/ (C_1)-phase refers to a pyrochlore type phase;;(P)-phase is (K, Ce, Zr-oxide) perovskite; (C_2) phase similar to pure CeO_2; f.c.c. = face center cubic (Fluorite); Tet = Tetragonal; Mono = Monoclinic.

NOTE: Compare results (phase assemblages and cell dimensions) with that given in Table 3 to assess change in starting materials. Color changes are indicative of chemical changes.